



Prof. Sadhan K. De

CERTIFICATE

This is to certify that the thesis entitled 'Chemical and Scanning Electron Microscopic Studies on Failure Properties of Rubber' which is being submitted by Mr. N.M. Mathew, M.Sc., L.P.R.I., for the degree of Doctor of Philosophy to the Indian Institute of Technology, Kharagpur, is a record of bonafide research work carried out by him under my supervision and guidance.

Mr. Mathew has worked on this research problem for about three years. In my opinion the thesis has fulfilled the requirements according to the regulations and has reached the standard necessary for submission. The results embodied in the thesis have not been submitted for the award of any other degree or diploma. Seven research papers from this thesis have been published/accepted for publication in International Journals.

Sadhan K. De
(Sadhan K. De)
1983

ACKNOWLEDGEMENT

I wish to express my profound gratitude to Prof. Sadhan K. De, Rubber Technology Centre, Indian Institute of Technology, Kharagpur for kindly suggesting the problem and for his valuable guidance and encouragement throughout the course of these investigations.

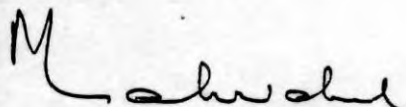
I am very grateful to Prof. D. Sen, Head of the Rubber Technology Centre, Indian Institute of Technology, Kharagpur for providing me with all laboratory facilities. I am also grateful to the authorities of the Rubber Board and the Rubber Research Institute of India, Kottayam, for granting me study leave, which enabled me to undertake this work.

I gratefully acknowledge the help rendered by Prof. B.K. Dhindaw, Metallurgical Engineering Department, Indian Institute of Technology, and Dr. A.K. Bhowmick, Institute of Polymer Science, University of Akron, Ohio, during the early part of these investigations. I am also thankful to Mr. R. Bhar, Regional Sophisticated Instruments Centre, Bose Institute, Calcutta for his cooperation in making the scanning electron microscopic observations.

My sincere thanks are also due to my colleagues in the Rubber Technology Centre, Indian Institute of Technology, Kharagpur and in the Rubber Research Institute of India, Kottayam, for their cooperation and useful discussion.

The encouragement and cooperation from my wife, without which this work could not have been undertaken, are gratefully acknowledged.

Finally I thank Mr. Ajay Kumar Maity for typing the manuscript and Mr. G. Bose for the drawings.

A handwritten signature in dark ink, appearing to read 'N. M. Mathew', with a stylized initial 'M' and a long horizontal stroke.

N. M. Mathew

PREFACE

Although a number of theoretical studies have been reported on the various aspects of failure of rubber, the nature of the failure surfaces and the chemical changes associated with failure still remain largely unexplored. In this thesis the various types of failure of rubber have been studied by scanning electron microscopy and by chemical characterization. A sound knowledge about the mechanism of failure will help in developing products which will last longer.

The subject matter of the thesis has been presented in seven chapters.

The introductory chapter consists of a brief review of earlier works in this field and the scope of the present work.

The experimental techniques are described in Chapter II.

Chapter III consists of scanning electron microscopic studies on tear and tensile fracture of rubber vulcanizates.

Chapter IV deals with thermooxidative aging of natural rubber vulcanizates and its effect on network structure and fracture mode. Studies on ozone cracking of natural rubber and natural rubber/EPDM rubber blend are also reported in this chapter.

Fatigue resistance of natural rubber and natural rubber/polybutadiene rubber blends has been studied by chemical methods and by scanning electron microscopy. The results of these studies are given in Chapter V.

In Chapter VI studies on the mechanism of abrasion of natural rubber/Polybutadiene rubber blends under different test conditions are reported.

Chapter VII consists of the results of the studies on the network changes in rubber vulcanizates under simulated service conditions.

GLOSSARY OF TERMS

| | |
|-------|--|
| BR | Polybutadiene rubber |
| CBS | N-cyclohexyl-2-benzothiazole sulfenamide |
| Conv. | Conventional |
| DCP | Dicumyl Peroxide |
| EPDM | Ethylene propylene diene rubber |
| EPR | Ethylene propylene rubber |
| EV | Efficient vulcanizing |
| FT | Fine thermal |
| HAF | High abrasion furnace |
| IPPD | N-isopropyl, N'-phenyl p-phenylene diamine |
| MBTS | Dibenzothiazyl disulfide |
| NR | Natural rubber |
| PENA | Phenyl- β -naphthylamine |
| PBT | Poly(butylene terephthalate) |
| phr | Parts per hundred rubber |
| pphm | Parts per hundred million |
| rpm | Revolutions per minute |
| SBR | Styrene butadiene rubber |
| SEM | Scanning electron microscope |
| SRF | Semi-reinforcing furnace. |

CONTENTS

Page No.

CHAPTER I

| | |
|-----------------------------------|----|
| INTRODUCTION | 1 |
| Failure properties of rubber | 4 |
| Structural changes during failure | 19 |
| Microscopic studies | 20 |
| Scope of the present work | 28 |

CHAPTER II

| | |
|-------------------------|----|
| EXPERIMENTAL TECHNIQUES | 31 |
|-------------------------|----|

CHAPTER III

SCANNING ELECTRON MICROSCOPIC STUDIES ON :

| | |
|------------------------------|----|
| A. TEAR FRACTURE OF RUBBER | 57 |
| B. TENSILE RUPTURE OF RUBBER | 64 |

CHAPTER IV

CHEMICAL AND SCANNING ELECTRON MICROSCOPIC STUDIES ON :

- | | |
|--|-----------|
| A. THERMO-OXIDATIVE AGING OF RUBBER | 71 |
| B. OZONE CRACKING OF RUBBER | 92 |

CHAPTER V

- | | |
|--|------------|
| A. CHEMICAL AND SCANNING ELECTRON MICROSCOPIC STUDIES ON FATIGUE FAILURE OF NATURAL RUBBER VULCANIZATES | 98 |
| B. SCANNING ELECTRON MICROSCOPIC STUDIES ON FLEXING AND TENSION FATIGUE FAILURE OF RUBBER | 107 |

CHAPTER VI

- | | |
|--|------------|
| SCANNING ELECTRON MICROSCOPIC STUDIES ON ABRASION OF NR/BR BLENDS UNDER DIFFERENT TEST CONDITIONS | 117 |
|--|------------|

CHAPTER VII

- | | |
|--|------------|
| A. NETWORK CHANGES IN NATURAL RUBBER VULCANIZATES UNDER COMPRESSION | 131 |
| B. NETWORK CHANGES IN V-BELT RUBBER BASE DURING SIMULATED SERVICE TESTING | 145 |

| | |
|---------------------------------------|------------|
| <u>SUMMARY AND CONCLUSIONS</u> | 154 |
|---------------------------------------|------------|

| | |
|--------------------------|------------|
| <u>REFERENCES</u> | 161 |
|--------------------------|------------|

| | |
|------------------------------------|------------|
| <u>LIST OF PUBLICATIONS</u> | 177 |
|------------------------------------|------------|

CHAPTER I

INTRODUCTION

The first part of the book is devoted to a general survey of the history of the subject. It begins with a brief account of the early attempts to explain the phenomena of life, and then proceeds to a more detailed consideration of the various theories which have been advanced from time to time. The author then discusses the progress of the science of life, and the various methods which have been employed to study it. He then proceeds to a consideration of the various branches of the science of life, and the various problems which are still to be solved. The book is written in a clear and concise style, and is well illustrated with numerous diagrams and figures. It is a valuable work for all those who are interested in the history and progress of the science of life.

Rubber has been known to the civilized world for the last few centuries and its uses are so widespread that there is hardly any segment of civilization which does not make use of rubber based materials. During the nineteenth century several epoch-making discoveries were made in the processing and applications of natural rubber which resulted in a tremendous increase in the demand for rubber. The then available supplies of natural rubber were highly inadequate to meet the increased demand. This, coupled with the outbreak of the second world war, prompted intensive research on alternative sources for rubber, which culminated in the development of various synthetic rubbers, some of which were equivalent to

NR in properties while the others possessed qualities, which were hitherto unknown to the rubber world. The differences in properties could be achieved by suitable manipulation of the molecular structure of the polymer during its manufacturing process. This has necessitated detailed studies on the relation between structure and properties.

In the manufacture of rubber products, raw rubber has to undergo a process called vulcanization, which involves crosslinking of the polymer chains so as to produce a network with improved properties. The structure of the network greatly influences the properties of the vulcanizate. This has introduced new dimensions in the study of structure-property relations of rubber.

The properties of a rubber vulcanizate depend on the nature of the base polymer, the presence of filler, extending oil and vulcanizing system, which determines the structure of the crosslinks and the extent to which the new polymer chains are modified chemically during vulcanization. The crosslinks may be carbon-carbon, monosulfidic, disulfidic or polysulfidic. Moreover, in accelerated sulfur vulcanization, the main chain may be modified by the formation of cyclic sulfides along the chain or the attachment of accelerator fragments pendant

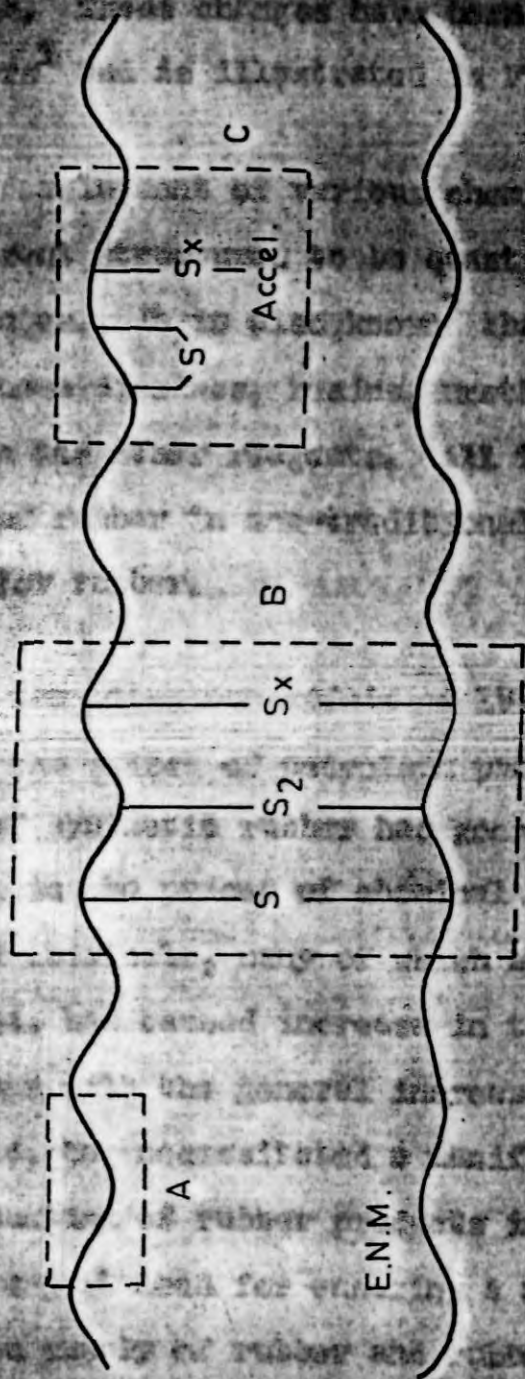


FIG. I.1. STRUCTURE OF AN ACCELERATED SULPHUR VULCANIZATE FROM NATURAL RUBBER

A - MAIN CHAINS OF MODIFIED AND UNMODIFIED POLYISOPRENE ;

B - CROSSLINKS ; C - CYCLIC AND PENDENT GROUPS ;

E.N.M. - EXTRA NET WORK MATERIALS.

to the chain. These changes have been described by Bateman and coworkers¹ and is illustrated in Figure I.1.

The development of various chemical probes² has enabled these different structures to be quantitatively characterized in vulcanizates. It is also known³ that vulcanization can be done by quinone dioximes, resins, urethane reagents, maleimides, metal oxides and other reagents. All these developments led to the use of rubber in non-traditional areas, thus enhancing the demand for rubber.

With the petroleum crisis of 1973 and the consequent increase in the prices of petroleum products, the cost of production of synthetic rubber has gone very high up. Also the increase in the prices of chemical fertilizers and other agricultural chemicals, many of which are derived from petroleum products, has caused increase in the price of NR as well. This, together with the general increase in the prices of other raw materials, has necessitated a manifold increase in the cost of production of rubber products in recent years. Hence there is an urgent need for ensuring a more judicious use of the available supply of rubber and rubber products. This can be achieved by improving the quality of rubber products and by suitably controlling the factors which contribute towards the failure of the products. In either case it is necessary to have a sound knowledge about the various ways in which rubber

products fail during service. Thus studies on the failure properties of rubber has become important in the present context.

Failure of rubber is expected to be accompanied by changes in its structure. Also the failure surface, wherever available, offers a good area of research on the mechanism of failure. The following pages give a brief review of earlier theoretical studies on failure properties of rubber, studies on the structural changes associated with failure and microscopic examinations of failure surfaces.

I. FAILURE PROPERTIES OF RUBBER

Any product can be considered to have failed when it can no longer fulfil the functional requirements expected of it. This is true in the case of rubber products also. Thus failure of a tire can occur by the slow removal of the tread through abrasive wear or by chipping and groove cracking or by flex cracking and the consequent fatigue failure. Permanent set can cause failure in products like gaskets and seals. In rubber products the factors considered to be significant in contributing, either singly or in combination, towards the total failure, are tensile and tear fracture, heat buildup and thermo-oxidative aging, flex cracking, abrasion, ozone cracking and set. The factors like deterioration by light, radiation etc. are also contributing, but only to a lesser

extent. Most of these factors are interrelated and determined by the fundamental characteristics of rubber.

I.1 Tear fracture : The toughness of rubber is conveniently described by its resistance to tearing. In principle, this might be characterized by the magnitude of the stress at which rupture occurs at the tip of a tear, but in practice the measurement of such localized stresses is extremely difficult. Rivlin and Thomas⁴ have shown that the tear quality of rubbers can be expressed by a characteristic energy which is related to the elastic energy stored in the highly strained zone at the tip of the growing tear. The tearing energy T is approximately given by

$$T = d \cdot E_B \quad \dots (I.1)$$

where E_B is the strain energy per unit volume required to break the rubber in simple extension and d is the effective diameter of the small zone of rubber at the tip of the tear. The value of the tearing energy, which is a property of the rubber under the conditions of the test and does not depend upon the type of test used, but varies greatly with the nature of the rubber and of any filler and with the rate and temperature⁵. While giving

more experimental evidence for this tearing energy concept, Thomas^{6,7} has shown that the material exhibited an abrupt change in the mode of tearing as the tearing energy increased through 3×10^6 erg/cm², the rate of tearing suddenly increasing from about 10^{-2} to 10 cm/sec. This correlated with a change in the appearance of the torn surfaces from rough to smooth. Later studies by Veith⁸ and Ahagon and Gent⁹ have also supported these findings.

The enhanced strength resulting from both crystallization and filler reinforcement is also reflected in the mode of tear propagation and in the nature of the torn surface. In unfilled non-crystallizing rubbers the tear proceeds steadily resulting in smooth torn surfaces, but in crystallizing rubbers and in filler-reinforced rubbers, at the rate and temperatures resulting in high strength, the tear proceeds in a stick-slip and sometimes knotty manner and gives rough irregular torn surfaces¹⁰. It is also known that the increased strength in stick-slip and knotty tearing stems largely from an increase in the effective diameter of the tip of the tear. This change in diameter is reflected by a change in the roughness of the torn surface. A broadening of the tip of the tear has been traced to severe mechanical hysteresis in the highly strained region ahead of the growing tear¹¹⁻¹⁵.

1.2 Tensile rupture : Although rubber products are rarely used under high tensile strain, the tensile stress-strain

properties are generally regarded as the best quality index of any rubber vulcanizate. The mode of initiation and propagation of rupture are very closely related to the overall strength of the vulcanizate. Fundamental studies on tensile rupture are thus important.

Borders and Juve¹⁶ have studied the dependence of tensile strength of rubbers on their viscoelastic properties and found good correlation between the tensile strength of both gum and carbon black-filled vulcanizates, and their brittle point in the case of a wide range of rubbers. Rubbers with the highest brittle point have the highest strength. Smith¹⁷, using the WLF transform¹¹, showed the dependence of tensile strength or the breaking elongation of non-crystallizing styrene-butadiene (SBR) gum rubber on rate and temperature. Greensmith¹⁸ studied this aspect in more detail in the case of SBR. With unfilled SBR vulcanizates tensile strength and breaking elongation increase uniformly with the rate of extension. However in the case of HAF black-filled SBR vulcanizate tensile strength appears to pass through a maximum as the rate of extension is increased. It was also found that the rate of extension affects the shape of the load-extension curve. One of the explanations for the observed maximum in the case of filled SBR is that the reinforcing action develops during extension and requires a definite time for development so that it does not occur at high rates of extensions. A possible alternate explanation is that the drop in tensile strength is caused by the heating up of the specimens during extension at high rates.

The effect of temperature on the tensile strength of a number of vulcanizates has been studied by Thomas and Whittle¹⁹. A critical temperature, Q_c , was found for NR at which an abrupt change in strength occurs. This temperature depends on the degree of crosslinking and also on the nature of the vulcanizing system. The presence of carbon black increases the strength above Q_c , but has little influence on the value of Q_c or the strength at temperatures below it. The behavior can be explained qualitatively in terms of a change in the mechanism of rupture from essentially a tear process above Q_c to a crack growth process below it. Bell, Stinson and Thomas²⁰ have studied this aspect further and found out a correlation between the critical temperature and the size of flaws in the case of natural rubber.

1.3 Aging : Aging is the deterioration of the desirable properties during storage or service and is a phenomenon common to a wide range of natural and synthetic materials. It has been known for almost a century that oxygen is the principal agent in the degradation of rubber products. The action of oxygen on rubber is catalyzed by metallic impurities, heat, light, mechanical strain etc. and causes changes in physical properties like tensile strength, elongation and hardness. The exact relation between these physical changes and the chemical reactions brought about by oxygen is still largely obscure and its resolution provides an important area of study. It needs to be stressed that the aging of vulcanized rubber differs from that of raw

rubber and a knowledge of the vulcanizate structure is therefore needed before significant conclusions about the chemical changes and their physical manifestations can be drawn.

A few recent reviews²¹⁻²³ have outlined most of the developments in the studies on aging. Thermo-oxidative aging of rubber is believed to occur in two ways²⁴ : via main chain scission and/or crosslink scission. Veith²⁵, Tobolsky²⁶, Horikx²⁷ and Dunn and Scanlan²⁸ have suggested that only main chain scission occurs during aging. But developments in the structural characterization of natural rubber vulcanizates² have led Colclough and coworkers²⁴ to study the oxidative aging in more detail and to report the occurrence of crosslink scission during aging. Blackman and McCall²⁹ have reported the structural changes in NR vulcanizates during thermal aging and their effect on fatigue life. Bevilacqua and Wenisch³⁰ attributed the changes in properties of vulcanized SBR during aging to reactions involving both the hydrocarbon and the crosslinks. The extent of aging can be assessed by oxygen absorption measurements, changes in stress-strain properties²⁸ and by stress relaxation measurements^{31,32}.

Antioxidants have been successfully used to minimize the oxidative degradation of rubber. They function in two ways : some antioxidants prevent or retard the formation of free radicals in the initiation step, whereas the others interrupt the propagation of the oxidative chain reaction by reacting with the chain carriers. The former type is called preventive antioxidants and the latter chain terminating antioxidants³³. The chain termination

antioxidants like amines and phenols function by donating a hydrogen atom to the peroxy radical. The antioxidant radical so formed can then act as a radical and terminate a second kinetic chain³⁴.

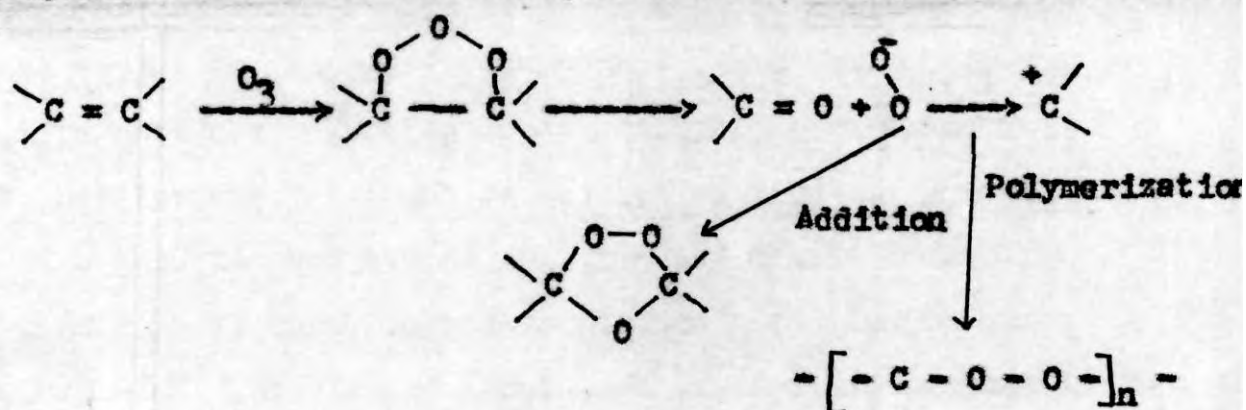


Both the above types of antioxidants have been used in rubber and certain types of chemicals like dithiocarbamates display both modes of action³⁵.

The effect of carbon black on aging has not been studied in detail. In the absence of added antioxidants it acts as a weak antioxidant, but in the presence of a p-phenylene diamine it reduces the efficiency of the antioxidant. Moreover the intensity of these effects varies according to whether the vulcanizate is efficiently vulcanized (EV), accelerated sulfur or peroxide³⁶. Winn and coworkers³⁷ found that carbon black accelerates the oxygen uptake of sulfur-cured rubber and that the reaction is accompanied by a rapid degradation of the polymer. Several mechanisms for the pro-oxidant action of carbon black have been proposed³³⁻⁴⁰. The explanation given by Shelton and Wickham⁴¹ which involves surface catalysis of the reaction between the rubber and oxygen by carbon black seems to be the most probable one. Clearly the action of carbon black is complex and further studies are required to understand its behavior.

As the aging process affects the structure of vulcanizates, the strength properties of rubber products are affected by aging. In fact it is a general practice to assess the extent of aging by following the changes in properties like tensile strength. However the relation between the changes in the structural characteristics of the vulcanizates and the extent of changes in properties has not been widely studied.

I.4 Ozone cracking : Ozone is a well known reagent for cleaving olefinic double bonds and the chemistry of this process is as follows. An unstable ozonide is formed and this breaks up into a carbonyl compound and a Zwitter ionic fragment which may polymerize or add to the aldehyde or ketone to give a true ozonide



The yield of the latter is normally small in most olefins and hence scission of the double bond is an immediate consequence of the attack by ozone⁴². Unsaturated rubbers like NR are attacked by ozone and the chemistry as given above for simple olefins applies to these polymers also. In most regions of the world the concentration of atmospheric ozone near ground level seldom exceeds 5 pphm and is often much less⁴³, but the cracking

it can cause in unsaturated rubbers is the most serious aspect of weathering for products exposed outdoors under tension. The reaction of ozone with rubber is extremely fast and because of the rapidity of this reaction, ozone is unable to penetrate any appreciable distance into the rubber. The effect of this is that the attack on unstretched rubber is negligible for practical purposes since it is restricted to a very thin although highly degraded layer on the surface⁴⁴. The presence of this layer greatly impedes the access of ozone to the inner layers. Under this condition rubber appears inert towards ozone. However in stretched rubber the weak degraded surface layer ruptures and a small crack will open up allowing ozone to penetrate. The reaction takes place repetitively until macroscopic separation (cracking) results and this can be so severe as to ultimately result in failure⁴⁵. Since actual samples of rubber inevitably have microscopic surface imperfections, any stress will not be uniform, but will be greater at these 'stress raisers'. Hence at a given strain the critical energy for cracking will be exceeded only at a certain number of these flawed sites, the number being greater, the higher the strain. This explains the well known phenomenon that a small number of large cracks develop at small strains and a multitude of small cracks at large strains⁴⁴.

Braden and Gent⁴⁵ showed that crack growth by ozone does not take place unless the tearing energy, T , exceeds a characteristic value T_z . Above this, the rate of growth of a single crack (γ_o) is substantially independent of tearing energy.

Understanding the mechanism of ozone cracking has been greatly advanced by studies of the growth of single cracks⁴⁶⁻⁴⁸. These studies have shown that for a number of rubbers including NR and SBR, the single crack growth rate (γ_o) at temperatures well above the glass transition temperature is essentially proportional to the ozone concentration in the test temperature (q_o) so that

$$\gamma_o = a_o q_o \quad \dots (1.2)$$

where a_o is a constant characteristic of the vulcanizate.

McCool⁴⁹ showed that ozone crack growth is not assisted by additional reactions involving oxygen since cracking proceeds at a similar rate in the absence of oxygen and the activation energy is much lower than that required for oxidation processes. Braden and Gent⁴⁶ showed that ozone cracks, once formed, grow at different rates, being smaller in rubbers with higher hysteresis.

Protection of rubbers against ozone attack is achieved by incorporating waxes, flexible coatings⁵⁰ and chemical antioxidants⁵¹. The first two provide a physical barrier against ozone, while chemical antioxidants increase the critical strain. The physical antioxidants are not suitable for dynamic applications and chemical antioxidants are highly staining and are likely to be lost during processing and service^{52,53}. Blending with ozone inert rubbers such as ethylene propylene diene rubber (EPDM) gives protection by providing a physical barrier which hinders the development of macroscopic cracks from microscopic cracks⁵⁴.

1.5 Fatigue failure : Fatigue is yet another important factor causing failure of rubber products. It is defined as the decay caused by cyclic deformations at an amplitude less than that is necessary for fracture in one cycle⁵⁵. The deformation can be caused by tension, compression, flexing or shear. If the stressing is vigorous and the component is large, failure may be due to excessive heat buildup, as may happen in large tyres at high speed. However there are a number of other rubber products like those in engineering applications, where failure occurs as a result of the growth of small cracks across the specimen under repeated stressing⁵⁶. As the failure is essentially a crack growth process from small flaws, the crack growth behavior of the rubber and the size of the initial flaw are the essential factors in determining fatigue life. The crack growth characteristics of vulcanized rubbers have been extensively studied⁵⁷⁻⁵⁹. The form in which they have been expressed has been derived from the work of Rivlin and Thomas⁴. Thomas⁶ and Greensmith⁶⁰ have shown that the tearing energy T governs the magnitude of the stresses around the tip of the crack and also determines the amount or rate of crack growth that occurs in the strained test piece. The relation between the rate of crack propagation and tearing energy is an intrinsic property of the material and independent of the particular type of test piece used.

For NR vulcanizates, provided the value of T for cataphoric tearing T_c is not exceeded, there is only a negligi

of purely time dependent crack growth under a constant load. This behavior appears to be associated with strain induced crystallization which also gives it its characteristic high tensile strength. If the test piece is repeatedly stressed and completely relaxed, however, crack growth occurs during each loading cycle. The amount of crack growth depends on the maximum value of T attained in each cycle.

In any rubber fatigue failure occurs through the development of cracks which are initiated by naturally occurring flaws. Usually the worst flaws are at the surface and are associated with the preparation of the sample by cutting or moulding. However particles of dirt have frequently been observed to initiate failure from the body of the material. It seems probable that poorly dispersed compounding ingredients can also act in a similar way.

The minimum tearing energy required for any crack growth to occur is denoted as T_0 and corresponding to this there is a fatigue limit for tensile stressing below which the life is virtually infinite. For the normal flaw size this fatigue limit is usually between 50 and 100% tensile strain. Its magnitude is of considerable practical significance as most rubber components subjected to repeated stressing will be designed to work below it. The magnitude of T_0 is governed by the molecular structure of the vulcanizate and the strength of the chemical bonds and increases by a factor of about two in vacuum. It can also be increased by incorporating suitable antioxidants, since oxygen facilitates the rupture of the molecules under stress⁶¹.

I.6 Abrasion : Abrasion is an important factor leading to the failure of a number of rubber products including tires. It is, perhaps, the least understood among the various types of fracture of rubber. A number of studies have been made by several authors to understand the abrasion process. Schallamach⁶² was the first to study the abrasion pattern on abraded rubber surfaces, which is believed to play a significant role in the abrasion process. Later studies by the same author⁶³⁻⁶⁵ yielded more information on the phenomenon. But the exact mechanism of formation of the abrasion pattern and the extent of its influence on abrasive wear are not clearly known. Reanikovskii and Brodskii⁶⁶⁻⁶⁸ have described the different types of wear occurring during abrasion of elastic materials and attempted to find out the influence of non-mechanical factors on abrasion as well as the relation between mechanical properties of rubber and its abrasion resistance. Brodskii and coworkers⁶⁹ have demonstrated how the relative role of mechanical and chemical factors in the abrasion of tread rubbers depends on the test conditions. They have shown that on smooth surfaces, with a low thermal conductivity, abrasion is mainly due to thermo-oxidative breakdown, whereas on rough surfaces mainly mechanical abrasion occurs. The wear of a series of rubber compositions under the sliding of a smooth steel indenter has been investigated by Rudakov and Kuvshinskii⁷⁰ and they have reported that atmospheric oxygen influences the wear process.

loading;

Hysteresis influence wear of rubber in three ways⁷¹ the first concerns the magnitude of the frictional force, the second the resistance of rubber to rupture and the third relates to tyre wear and concerns the influence of hysteresis on the amount of relative motion in the contact area of the tyre with the road. Greenwood and Tabor⁷² showed that the friction of rubber on both wet and dry surfaces is dominated by the viscoelastic properties of rubber. By the application of fracture mechanics Southern and Thomas⁷³ showed that the formation of abrasion pattern is followed by crack growth which plays an important role in the abrasion process.

Laboratory tests for abrasion resistance of rubber are used mainly to rank different vulcanizates. Usually these tests are used to control manufacturing uniformity. Over the years a number of tests have been developed to test the abrasion resistance of rubbers⁷⁴. None of these tests can predict precisely the behavior of rubbers under actual service conditions and even the ranking obtained from one test method may not hold good in another.

1.7 Compression set : Set is a very important factor in assessing the useful service life of rubber products like gaskets, seals and engine mounts. Set occurring under compressive strain is called compression set. Jahn and Bortman⁷⁵ have reported the influence of factors like vulcanizing system, filler type and loading, type and quantity of plasticizer etc. on the compression

set of nitrile rubber at different temperatures. Baldwin⁷⁶ studied the influence of the initial vulcanizate structure and the changes therein during heat aging on high temperature compression set of EPDM rubber. He concluded that high temperature compression set is influenced not only by the formation of new crosslinks but also by the interconversion of polysulfidic linkages present initially in the vulcanizates. Bristow, Cunneen and Mullins⁷⁷ have attributed the higher compression set of NR with respect to that of cis-polyisoprene, to the presence of non-rubber constituents in the former. The effect of temperature on the compression set of trans-polyisoprene, cis-polybutadiene and SBR has been studied by Dall' Asta⁷⁸.

Set is always associated with stress relaxation, which may result from either physical or chemical processes. Physical relaxation results from processes such as the flow of chains, the movement of entanglements etc. Examples of chemical processes are chain scission of covalent bonds at the crosslinks or along the main chain. Curro and Salazar⁷⁹ have presented a method whereby these two processes can be distinguished using stress relaxation data of butyl rubber and EPDM at different temperatures. Stanberg and Janson^{80,81} examined this problem further in the case of nitrile rubber vulcanizates and showed that physical mechanism dominates just above room temperature, while chemical mechanism dominates at higher temperatures. Studebaker⁸² studied the changes in crosslink density, polysulfidic linkages and chain scission during compression set test period. He reported that no significant change in crosslink density occurred during the

test. However, there was a marked tendency towards a reduction in polysulfidic crosslinks and in the sulfur rank of the polysulfidic linkages.

II. STRUCTURAL CHANGES DURING FAILURE

Rubber products are subjected to various forms of mechanical and thermal strains during service and it is likely that their network structure undergoes changes during service. Such structural changes contribute considerably towards the deterioration of rubber products. Correlation between network structure and technical properties of rubber vulcanizates has been studied by De and coworkers⁸³⁻⁸⁷. A sound knowledge about the structural changes that are likely to occur in vulcanizates under service conditions will help in understanding their failure phenomena. Nando and De^{88,89} have studied changes in the network structure of NR vulcanizates, subjected to different physical tests, since these tests, either singly or in combination, simulate at least a few service conditions. Stuckey and coworkers⁹⁰ have reported decrease in the proportion of polysulfidic linkages in NR vulcanizates during De Mattia flexing. Cunneen and Russel⁹¹ reported changes in the chemical structure of NR tire tread vulcanizates during simulated and actual service conditions. They found marked reduction in the concentration of polysulfidic linkages and increase in main chain modifications. Increase in the crosslink density of tire treads during service was observed by Howard and Wilder⁹². But the extent of increase depends on the curative

system and the nature of the base polymer. Similar studies on cis-1,4-polyisoprene have been reported by Podkolzina and coworkers⁹³. Wolf⁹⁴ studied the aging behavior of sealing materials under various environmental influences.

III. MICROSCOPIC STUDIES

Microscopy of rubber in its beginning was limited primarily to the study of the size and shape of latex particles, and crystallization and blooming of sulfur. Later it was applied to the study of particle size and shape of filler materials used in rubber. In the last few decades considerable improvement in techniques of microscopical investigations have given a new impetus to rubber microscopy, such that, in addition to the above named applications, new areas of applications have been opened. The developments in rubber microscopy have been reviewed by Kruse⁹⁵

III.1 Microscopes : Most of the different types of microscopes have been used in rubber microscopy. The light microscope, because of its availability, ease of operation and versatility was the most popular. Under ideal conditions its limit of resolution is about a quarter of a micron. Such conditions are seldom realized. The light microscopes working at magnifications up to 500X are used chiefly for identifying compounding ingredients, for assessing dispersion and for particle size measurement of coarser materials. At higher magnifications they are used for studies of latex and the particle size of finer fillers. The

polarising microscopes has made possible the study of crystallization in polymers^{96,97}. The ultra-violet microscope in which visible light is replaced by u.v. illumination to give a slightly higher resolution, has been used for particle size work on lattices and fine fillers. The phase contrast microscope is capable of distinguishing parts of a specimen which differ only in refractive index, and thus indistinguishable in a conventional light microscope. It has been found valuable for studying blends of polymers⁹⁸.

III.2 Electron microscope : The electron microscope is the most revolutionary development in microscopy and has brought an increase in the resolving power that could never be even imagined before. The differences between light and electron microscopes are resulting from the much shorter wave length and charge of the electrons in comparison with the photons of visible light. The shorter wave length permits greater resolution but the charge results in greater interaction with matter. The image in an electron microscope is either observed on a fluorescent screen or recorded photographically. The magnitude of the interaction between the electrons and matter requires that the path of the electrons (the column) be evacuated to a pressure of 10^{-4} mm Hg or less and that the sample be extremely thin. These two factors lead to most of the difficulties in electron microscopy, requiring special sample preparation and handling procedures. A major factor of concern to polymer microscopists is the magnitude of the interaction of the beam and the sample. Polymers rapidly degrade

or undergo chemical changes such as crosslinking when illuminated with electrons of the voltages normally used. This can be minimized by the use of higher accelerating voltage combined with suitable sample preparation. Although every sample is to some extent unique, one generally applies various combinations of shadowing, replication, dispersion and sectioning. These techniques have been described by Kay⁹⁹ and Pease¹⁰⁰. Electron microscopy has been extensively used in various types of studies in rubber. These include studies on the distribution of rubbers in blends¹⁰¹, distribution of carbon black in rubber blends¹⁰²⁻¹⁰⁴, the phenomenon of bound rubber¹⁰⁵, the formation of vacuoles in carbon black-filled vulcanizates during stretching¹⁰⁶ and fractured surfaces of vulcanized rubber specimens^{107,108}.

III.3 Scanning Electron Microscope (SEM) : The limitations of optical microscopes and the electron microscopes have stimulated search for better equipments and this has resulted in the development of scanning electron microscope, the latest addition to the electron microscope family. Since a reasonably high resolution is combined with a great depth of focus, the SEM permits materials to be examined that are unsuitable for replication or whose geometry does not permit optical microscopy. The SEM image gives the scientist an opportunity never before available to see the object in three dimensions. The SEM does not supercede other microscopes, but because of its unique capabilities helps to fill the gap between light and electron optics.

III.3.1 SEM in polymer research : When the SEM first became available commercially, it was used almost exclusively, for biological and medical research, in metallurgy and to study semiconductors and electronic microdevices. More and more publications are beginning to appear, describing SEM studies of polymers, adhesives, dental fillings, filled polymers, short-fiber reinforced plastics, organic coatings, foam plastics, fracture studies etc.

Adhesives and failure thereof can now be analysed more thoroughly. The SEM images indicate readily whether bonds themselves fail under stress or if it is either bulk phase of the adhesive or the adjoining material that breaks away. Adhesive failure may occur under many different conditions and it may even be conducted in the SEM itself while the bond is being observed.

SEM has been used to observe the surface morphology of polymeric materials like chemically treated cotton, fibres¹⁰⁹, polyethylene¹¹⁰, and polymer coatings on metal surfaces¹¹¹. Dennenberg and coworkers¹¹² have prepared a biodegradable plastic material from starch graft poly(methyl methacrylate) copolymer and used SEM to observe their fungus-infected surfaces.

Chang and Slagowski¹¹³ used SEM to show that glass fibers in the glass-reinforced PBT sample nucleate the growth of well defined spherulites along the glass fiber axis. The interphase effects in polymer modified hydraulic cements has been the subject of another SEM study¹¹⁴. Pennings and coworkers^{115,116}

have studied the crystallization of polyamides under elevated pressure.

Fracture in polymers has been the subject of a number of SEM studies. White and Teh¹¹⁷ studied the fatigue fracture surface of polyethylene and poly(vinyl chloride). They observed that the appearance of fracture surfaces reflects to a large extent the microstructure and properties of materials used. They have also shown that in spherulitic low-density polyethylene, the deformation mechanism depends on the temperature of testing as well as the stress field near the crack tip and therefore on the extent of advancement of the crack. Smith and Howard¹¹⁸ studied the post-yield fracture of plasticized cellulose acetate. Parent and Thompson¹¹⁹ studied the fracture surface morphology and phase relationships of polystyrene/poly(methyl methacrylate) systems. The chemical degradative stress cracking of poly(ethylene terephthalate) fibers has been studied by Sweet and Bell¹²⁰. SEM has also been used to study the pull-out failure of glass-fiber-reinforced epoxy composites¹²¹, fracture surfaces of polypropylene containing elastomeric impact modifiers¹²², polycarbonate specimens fractured in tension¹²³, the fibrillar nature of environmental stress-cracked surfaces of polyethylene¹²⁴ and the rupture surface morphology of poly(vinyl chloride)¹²⁵.

III.3.2 SEM of rubber : Use of SEM in rubber research is of comparatively recent origin. As in other fields, in rubber also SEM has been used mainly for morphological studies. Thus Thamm¹²⁶ used SEM to reveal the morphology of the knit lines of an injecti

moulded EPDM-polypropylene blend. Schulz, Calihan and Tate¹²⁷ examined the surface morphology of solution SBR powder. They showed that the slow removal of solvent results in a sponge like surface, while rapid removal of solvent yields an essentially continuous surface. The surface morphology of cured and uncured carbon black-filled NR compounds, exposed to ozone in the unstrained condition, has been studied by Andries and coworkers¹²⁸. On ozone exposure of carbon black loaded NR compounds containing N,N'-dioctyl-p-phenylene diamine anti-ozonant, a continuous film is seen under SEM which has an attenuated total reflectance spectrum essentially identical to that of ozonized antiozonant.

SEM has also been used to study the surface characteristics of fillers used in rubber and also the extent of rubber-filler interaction. The cellular surface characteristics of rice hull ash to be used as filler in rubber, and the effect of grinding on the particle size and shape of this filler have been studied by Haxo and Mehta¹²⁹. Voet, Morawski and Donnet¹³⁰ have demonstrated the presence of improperly dispersed and insufficiently wetted clumps of silica in silica reinforced rubber vulcanizates. These clumps of silica were shown to initiate microtear during rupture.

Perhaps the most important application of SEM in rubber is in fracture studies. O'Conner¹³¹ used SEM to observe the fracture surfaces of short fiber-reinforced rubber composites. with a view to find out the degree of fiber alignment, the

uniformity of fiber dispersion and the extent of fiber-rubber adhesion. De and coworkers¹³²⁻¹³⁵ studied the fracture surfaces of short fiber-rubber composites to show the fiber pull-out failure resulting from poor fiber-rubber adhesion, role of silica in promoting adhesion, the alignment of fibers in the matrix and the nature of the fracture surfaces obtained in different types of failure tests. Murty and De¹³⁶ have also shown that the nature of the fracture surfaces of short jute fiber-reinforced rubber composites is not affected by the presence of particulate fillers.

Bascom¹³⁷ used SEM to study the surface morphology of cyclized nitrile rubber and the tear fracture surface of rubber. It has been shown that cyclization of nitrile rubber produces a brittle surface layer. Microcracks develop when the rubber is flexed and when stretched, severely deform the underlying rubber into an open fibrous network. The study of tear fracture surfaces demonstrated a simple technique which allows observation of the deformation zone at tear tips in rubber specimens. Investigation of various rubbers revealed qualitative information about the type of yielding that occurs in the deformation zone under different conditions. The appearance of fibrous and nodular network in the tear tip material of all the rubbers has been attributed to aging. Boonstra, Heckman and Kabaya¹³⁸ used SEM to study the abraded surfaces of tire tread vulcanizates in a Lambourn abrader at different slip angles. They found that the development of abrasion pattern and significant abrasion occur only at higher slip angles. Bhowmick and De¹³⁹ studied

the abraded surfaces of SBR and polybutadiene rubber (BR) at different levels of abrasion and correlated the difference in the mechanism of abrasion with the difference in technical properties like heat buildup and crack growth rate.

IV. SCOPE OF THE PRESENT WORK

A thorough understanding of the failure properties of rubber will lead to development of new formulations and processes so as to enhance the resistance of rubber vulcanizates to failure. Also a knowledge of the mechanism of initiation and propagation of fracture in rubber will definitely call for improvement in the service conditions. Thus a slight reduction in the temperature of service or in the strain or in the frequency of stress application might bring about remarkable improvement in the service life of rubber products.

The review outlined above indicates that fundamental studies on the failure properties of rubber are quite numerous. However, studies on the chemical and physical changes associated with failure have not kept pace with the fundamental studies. De and coworkers^{88,89} have observed that certain failure properties of rubber are associated with changes in network structure of the vulcanizates. However they have concluded that changes in the network structure alone cannot explain the mechanism of failure. In fact, fracture is highly localized and is a selective process - only a small number of molecules making up a rubber product actually undergo rupture, while the great majority are not affected. Moreover, this will not break simultaneously, but will rupture successively as the fracture propagates across the specimen. Hence it would be interesting to study : (1) how and where and under what circumstances the fracture begins;

(2) how the crack grows once it has been initiated; (3) what role the crosslink structure plays in determining the service life of the specimen; (4) whether the fracture surfaces change under different modes of deformation and also under the same mode of deformation whether different rubbers show different fracture surfaces and (5) upto what extent failure of rubber is associated with changes in the network structure. In the present thesis, which seeks to answer some of these questions, the following studies have been made on the different types of failure of rubber.

- (a) Tensile and tear fracture of rubber have been studied by examining the fracture surfaces under SEM. The effects of crosslink system, filler and type of rubber on these types of failure have been studied.
- (b) Thermo-oxidative aging and its effect on network structure and fracture mode has been studied in the case of unfilled and black-filled natural rubber containing two sulfur vulcanizing systems. The effect of an antioxidant in minimizing aging and the consequent changes in the fracture mode has also been included in this study.
- (c) Flexing and tension fatigue failure of rubber and the consequent changes in network structure and fracture mode have also been studied in the case of natural rubber and natural rubber/polybutadiene rubber blends.

- (d) Abrasive wear of natural rubber/polybutadiene rubber blends, both unfilled and filled, occurring under different test conditions, has been studied using SEM.
- (e) Ozone cracking of NR and NR/EPDM blends has been studied using SEM and chemical analysis of the vulcanizates. The effect of HAF black in these rubbers has also been studied.
- (f) The effect of compressive strain at elevated temperature on the network structure of NR vulcanizates has been studied.
- (g) The failure of V-belt during simulated service testing has been studied by assessing the changes in the network structure of its base rubber vulcanizate.

CHAPTER II

EXPERIMENTAL TECHNIQUES

The materials used and the experimental procedures adopted in the present investigations are given in this chapter.

I. MATERIALS USED

I.1 Natural rubber : The natural rubber used was crumb rubber, ISNR-5, as obtained from the Rubber Research Institute of India, Kottayam. The Indian Standards specifications for this grade of rubber are given below.

| Parameters | Limit |
|---|-------|
| 1. Dirt content, % by mass, Max. | 0.05 |
| 2. Volatile matter, % by mass, Max. | 1.0 |
| 3. Nitrogen, % by mass, Max. | 0.7 |
| 4. Ash, % by mass, Max. | 0.6 |
| 5. Initial plasticity, Po, Min. | 30 |
| 6. Plasticity retention index (PRI), Min. | 60 |

Since it is known that the molecular weight, molecular weight distribution and non-rubber constituents of natural rubber are affected by clonal variation, season, use of yield stimulants and method of preparation^{140,141}, rubber from the same lot has been used in a particular experiment.

I.2 Synthetic rubbers : Styrene-butadiene rubber (SBR-1502) was obtained from Synthetics and Chemicals Ltd., Bareilly. It is a copolymer of styrene and butadiene, manufactured by cold emulsion polymerisation system using fatty acid and rosin soap emulsifier. It is a non-staining and non-discoloring cold SBR grade. The polybutadiene rubber used in the abrasion and fatigue studies was Nipol 1220, while that used in the studies on V-belt was Cisamer 1220, obtained from Indian Petrochemicals Corporation Ltd., Baroda. The EPDM rubber used in the studies on ozone cracking was Nordel 2722, supplied by Indian Cable Company, Jamshedpur.

I.3 Rubber chemicals : Accelerator CBS and antioxidants, phenyl- β -naphthylamine and N-isopropyl, N'-phenyl-p-phenylene diamine were commercial grades obtained from Alkali and Chemical Corporation of India Ltd., Rishra.

I.4 Fillers : HAF (N 330) carbon black was supplied by Phillips Carbon Blacks Ltd., Durgapur and FT (N 880) black was supplied by R.T. Vanderbilt Co. Inc., New York. China clay used in this work was supplied by Dunlop (India) Ltd., Shahaganj. Precipitated Silica (Vulcasil-S) was obtained from Bayer (India) Ltd., Bombay. Ground whiting was obtained from Bata (India) Ltd., Calcutta.

1.5 Other chemicals : Zinc oxide ($\rho = 5.5$), stearic acid ($\rho = 0.92$) and elemental sulfur ($\rho = 1.9$) were chemically pure grade.

1.6 Special chemicals : Propene-2-thiol and piperidine were of analytical grade from Fluka A.G.

1.7 Solvents : Benzene, acetone, n-heptane, petroleum ether (40-60°C) and diethyl ether were of analytical grade.

II. MIXING

Mixes were prepared on a laboratory size two roll mixing mill (33 cm x 15 cm) at a friction ration of 1 : 1.25 in the case of natural rubber and 1 : 1.1 in the case of synthetic rubbers. Natural rubber was first masticated, to attain a Wallace Rapid Plasticity (100°C, 1 cm. platen; BS 1673, Part 3, 1969) around 20 by careful control of temperature, nip gap, time of mastication and by uniform cutting operation. The compounding ingredients were added as per ASTM Designation D15-62T in the following order : activators, fillers, accelerators and sulfur. Before the addition of accelerator and sulfur, the batch was thoroughly cooled.

In the case of blends, natural rubber was masticated to a Mooney Viscosity of 40 (approx.), comparable to that of BR and EPDM. These rubbers were preblended and then the additives were added, unless otherwise stated.

After complete mixing, the stock was sheeted out and passed six times endwise through tight nip and finally sheeted out at a nip gap of 3 mm. Mixing time and temperature were controlled during the studies. When sulfur was incorporated, the temperature of the rolls was maintained at 35°-40°C.

III. VULCANIZATION

Vulcanization was carried out in a David Bridge single daylight electrically heated press having 30 cm x 30 cm platens, at 150°C and at a pressure of 45 kg/cm² on the mould, upto optimum cure times. Mouldings were cooled quickly in water at the end of the curing cycle and stored in a cold and dark place for 24 hr, and were used for subsequent physical tests and chemical analysis. For samples having thickness more than 6 mm (like heat buildup, compression set and abrasion test pieces) additional times based on the sample thickness were used to obtain satisfactory mouldings.

III.1 Time of optimum cure : Optimum cure times at 150°C were determined by using Monsanto Rheometer (R-100). The optimum cure time corresponds to the time to achieve 90 percent (t_{90}) of the cure calculated from the formula,

$$\text{Optimum cure} = 0.9 (L_r - L_1) + L_1 \quad \dots \text{(II.1)}$$

where L_r and L_1 are maximum and minimum torque respectively.

III.2 Cure rate index : Cure rate index was determined from the rheographs of the respective mixes.

$$\text{Cure rate index} = \frac{100}{t_{90} - t_2} \quad \dots \text{(II.2)}$$

where t_{90} and t_2 are the times corresponding to the optimum cure and two units above minimum torque respectively.

IV. PHYSICAL TEST METHODS

At least three specimens per sample were tested for each property and the mean values reported.

IV.1 Modulus, Tensile strength and Elongation at break : In the present work these tests were carried out according to ASTM Designation D412-51T using dumbbell specimens. All the above tests were carried out at $28 \pm 2^\circ\text{C}$. Samples were punched from vulcanized sheets parallel to the grain direction using a dumbbell die (C-type). The thickness of the narrow portion was measured by bench thickness gauge. Two marks were made, 2.5 cm apart, in the middle of the narrow portion. The sample, was held tight by the two grips in a 'Zwick' tensile testing machine (sensitivity 0.1 kg), the upper grip of which being fixed. The rate of separation of the power actuated grip was 50 cms per minute. The load at 300% elongation and at break were read from the dial. The elongation at break was measured using a scale. From the recorded loads, the stress was calculated on the basis of the original cross-sectional area.

The tensile strength and modulus are reported in MPa.
(Conversion factor : $1 \text{ kgf/cm}^2 = 0.098 \text{ MPa}$).

IV.2 Tear resistance : The test was carried out as per ASTM method D624-48; unnicked, 90° angle test pieces were used. The samples were cut from the vulcanized sheets parallel to the grain direction. The test was carried out on a 'Zwick' tensile testing machine. The speed of extension was 50 cms per minute and the temperature $28 \pm 2^\circ\text{C}$.

Tear resistance has been reported in kN/m . (Conversion factor : $1 \text{ kg/cm} = 0.98 \text{ kN/m}$).

IV.3 Hardness : Shore A type Durometer was employed to find out the hardness of the vulcanizates. The instrument uses a calibrated spring to provide the indenting force. Readings were taken after 15 secs. of the indentation when firm contact has been established with the specimens. The method employed is the same as that in ASTM D676-52T.

IV.4 Rebound resilience : Dunlop Tripsometer (BS 903, Pt.22, 1950) was used to measure rebound resilience. The sample was held in position by suction. It was conditioned by striking with the indenter six times. The temperature of the specimen holder and sample was kept constant at 35°C . Rebound resilience was calculated as follows :

$$\text{Rebound Resilience } (\%) = \frac{1 - \cos \theta_2}{1 - \cos \theta_1} \times 100 \quad \dots \text{ (II.3)}$$

where θ_1 and θ_2 are the initial and rebound angles respectively. θ_1 was 45° in all tests.

IV.5 Abrasion resistance : The Croydon-Akron abrasion tester (BS 903, Pt. 49 : 1957 method C) was used to measure this property. The result is commonly represented as the volume in cubic centimeters of the vulcanizate abraded from a specified test piece per 1000 revolutions of the grinding wheel under specified conditions. The angle between the test specimen and the abrasive wheel (slip angle) was kept constant at 20° .

IV.6 Compression set : The samples (1.25 cm thick and 2.8 cm diameter) in duplicate, compressed to constant deflection (25%), were kept for 22 hr in an air oven at 70°C (ASTM D395-61, method B). After the heating period, the samples were taken out, cooled to room temperature for half an hour and the final thickness was measured. The compression set was calculated as follows :

$$\text{Compression set (\%)} = \frac{t_0 - t_1}{t_0 - t_s} \times 100 \quad \dots \text{(II.4)}$$

where t_0 and t_1 are the initial and final thickness of the specimen and t_s is the thickness of the spacer bar used.

IV.7. Flex cracking : Flex cracking was determined by using a De Mattia flexing machine according to ASTM Designation D430-73, method B. Standard specimens 15 cm x 2.5 cm x 0.6 cm, having a semi-circular groove moulded transversely in the centre

of the strip were used. The temperature of the flexing chamber could be controlled with an accuracy of $\pm 1^{\circ}\text{C}$. The machine was run at a frequency of 300 cycles per minute. The number of kilocycles required to produce different levels of flex cracking according to standard photographs (BS 903, Part 26, 1950) showing grade A, grade B and Grade C, and failure was determined.

The length of the eccentric arm and connecting rod were so adjusted that the distance between the stationary and movable grips had a minimum value of 1.9 ± 0.01 cm when grips approached each other and a maximum value of 7.5 ± 0.03 cm when they separated.

IV.8 Crack growth : This property was also determined by using De Mattia flexing machine according to ASTM Designation D430-73. The sample and the conditions of the experiment remain the same as in the case of the flex cracking test. In the case of crack growth test, an initial cut of 0.203 cm wide, parallel to the groove and in the middle of the groove of the sample was made using a standard cut initiator (SATRA piercing tool). The number of kilocycles required to produce a crack of 1.25 cm was taken as the index of crack growth.

IV.9 Heat buildup : The Goodrich flexometer conforming to ASTM Designation D623-67 method A, was used for measuring heat buildup. The test was carried out with the cylindrical sample of 2.5 cm in height and 1.9 cm in diameter. The oven temperature was kept constant at 50°C . The stroke was adjusted to 4.45 mm

and the load to 10.9 kg. The sample was preconditioned to the oven temperature for 20 minutes. The heat development at the base of the sample was sensed by a thermocouple and relayed to a digital temperature indicator. The temperature rise ($\Delta T^{\circ}\text{C}$) at the end of 20 minutes was taken as the heat buildup.

Next the sample was taken out and the thickness was measured after half an hour. The percent permanent set was calculated from the residual height of the sample and expressed as :

$$\text{Permanent set, (\%)} = \frac{t_0 - t_1}{t_0} \times 100 \quad \dots (\text{IL.5})$$

where t_0 and t_1 are the initial height and the final height of the test specimen respectively.

IV.10 Ozone resistance : A quantitative method for determination of ozone resistance, developed by Andrews⁵⁴ and later modified by Wilchinsky and Kresge¹⁷⁴ was used in this study. A tapered specimen was subjected to a tensile force such that the critical stress occurred somewhere within the tapered section. After 16 hr the length L of the sample was measured and the sample, still under stress, was exposed to ozone in a Mast Ozone Test Chamber for 24 hr. The ozone concentration was adjusted at 50 pphm and temperature 37.5°C . Cracks appeared in the high stress region towards the narrow end of the taper

but were absent from the low stress region towards the broad end. The position of the boundary (critical boundary) between the cracked and uncracked regions was recorded. The detailed geometry of the specimen is shown in Figure II.1. The critical stress (σ_c) was determined directly from the experimental data by

$$\sigma_c = F / [at_c (1 + \lambda_c/L_f)] \quad \dots (II.6)$$

where a is the undeformed specimen width at the narrow end ($\lambda = 0$) of the taper, and t_c is the thickness at λ_c , obtained by interpolation between two of three thickness measurements, made at the two ends and at the middle of the specimen. The critical strain ϵ_c was measured using the approximation,

$$\epsilon_c = (1.42 - 1.42/\lambda_{av}) / [(\lambda_c/L_0) - 0.42 + 1.42/\lambda_{av}] \quad \dots (II.7)$$

where λ_{av} is the average elongation. The critical elastic stored energy density was calculated from σ_c and ϵ_c by the following relationship from classical theory of rubber elasticity,

$$W_c = \frac{1}{2} \sigma_c \epsilon_c (\lambda_c^2 + 2) / (\lambda_c^2 + \lambda_c + 1) \quad \dots (II.8)$$

Finally, the elastic modulus E was obtained from σ_c and ϵ_c as

$$E = \lambda_c \sigma_c / \epsilon_c \quad \dots (II.9)$$

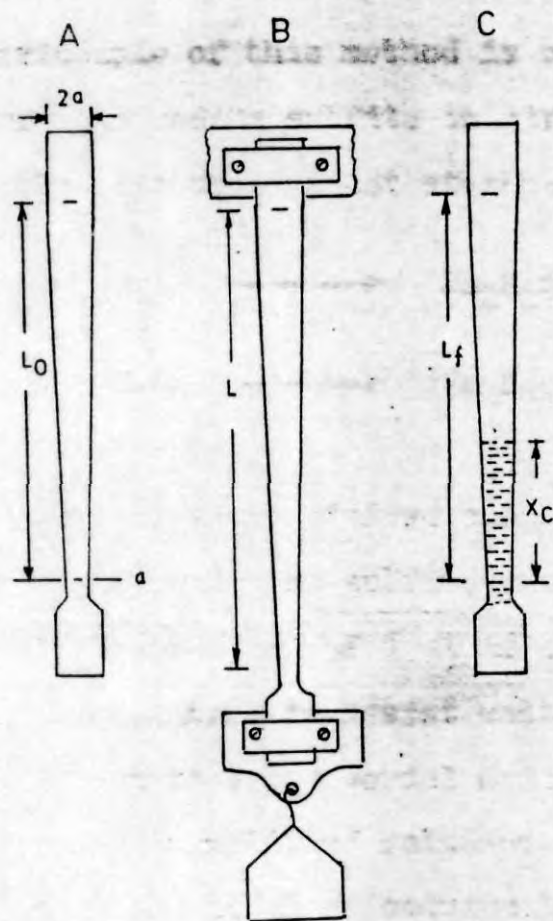


FIG. II.1. GEOMETRY OF THE OZONE TEST SPECIMEN

A- ORIGINAL SPECIMEN WITH FIDUCIAL MARKS,

B- SPECIMEN UNDER STRESS,

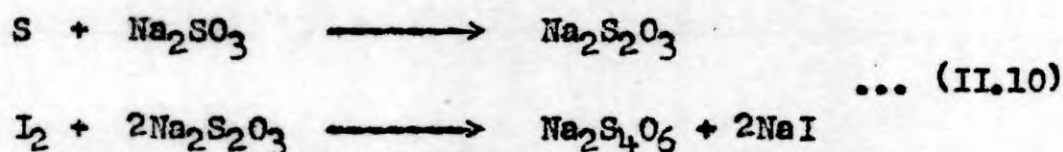
C- SPECIMEN AFTER OZONE EXPOSURE,

$L_0 = 10 \text{ Cm}$, $a = 0.6 \text{ Cm}$.

V. CHEMICAL TEST METHODS

V.1 Free sulfur estimation : Free sulfur was estimated according to ASTM Designation D297 - 72A.

The principle of this method is based on the reaction of free sulfur with sodium sulfite to give sodium thiosulfate which is finally titrated against standard iodine solution.



Two grams of finely divided sample were digested gently with 100 ml of aqueous sodium sulfite solution (50 gm/litre) for 16 hours in the presence of 5 ml of sodium stearate suspension in water (1 gm/litre) to assist wetting and approximately 1 gm of paraffin wax to avoid aerial oxidation. 100 ml of strontium chloride (5 gm/litre) solution was added to precipitate fatty acids and 10 ml of cadmium acetate solution (30 gm/litre) to remove accelerators. For the vulcanizates containing higher proportion of accelerators, additional 10 ml of cadmium acetate solution (30 gm/litre) was added to ensure complete precipitation of the accelerators. Rubber and the precipitate were separated by filtration. It was then washed twice with 75 ml portions of cadmium acetate wash solution (1.2 gm/litre). To the filtrate 10 ml of 40% formaldehyde solution was added with vigorous stirring and subsequently

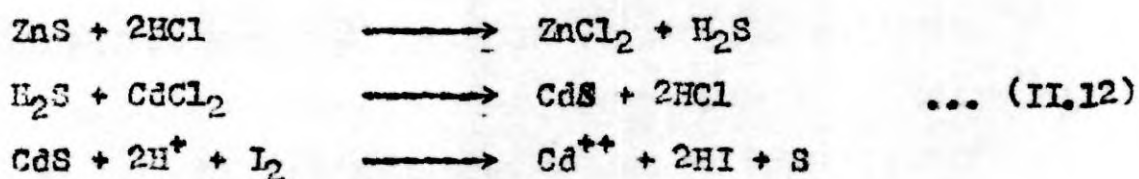
acidified with glacial acetic acid (10 ml). The solution was cooled below 15°C by adding enough crushed ice and titrated with 0.02 N iodine solution using starch as indicator.

A reagent blank was run and this figure was subtracted from the titre value of the sample.

$$\text{Free sulfur, \%} = \frac{(x - y) \times N \times 0.032 \times 100}{W} \quad \dots \text{(II.11)}$$

where x is the volume of iodine solution required for titration of the sample in ml, y is the volume of iodine solution required for titration of the blank in ml, N is the normality of iodine solution and W is the weight of the sample taken.

V.2 Zinc sulfide estimation : The procedure is based on the following reactions :



The finely divided sample (2 gm) along with 25 ml of freshly distilled peroxide-free ether was placed in the digestion flask of the apparatus as adopted by Adam and Johnson¹⁴². The reaction flask was immersed in a constant temperature water bath maintained at 37°C. 100 ml of absorbing solution (5 gms of CdCl₂, 25 gm of sodium acetate and 25 ml of glacial acetic acid per litre of the solution) was used for absorbing the gas

generated during digestion. After the sample had become swollen with ether (1 hour), 25 ml of concentrated HCl was added to the digestion flask and nitrogen gas was bubbled through the reaction mixture for a period of one hour. The amount of H_2S liberated from the sample by the HCl-ether digestion, which is the measure of ZnS-sulfur, was absorbed as cadmium sulfide (CdS) in the absorbing solution. A measured excess of 0.05 (N) iodine solution was added and the excess iodine was back titrated against 0.05 N sodium thiosulfate solution using starch as indicator. A blank titration was also conducted. From the two titre values, the volume of iodine reacted with cadmium sulfide was noted. The amount of zinc sulfide sulfur was calculated as follows :

$$\text{Zinc sulfide sulfur, \%} = \frac{(X - Y) \times N \times 0.016 \times 100}{W} \dots (II.1)$$

where X is the volume of thiosulfate required for the blank in ml and Y that for the sample in ml and N, the normality of thiosulfate solution and 'W' the weight of the sample taken.

V.3 Determination of volume fraction of rubber : The volume fraction of rubber, V_r , was calculated from the equilibrium swelling data as follows :

Samples of approximately 1 cm diameter, 0.25 cm thickness and 0.30 gm weight, were punched out from the central portion of the vulcanizate and allowed to swell in thiophene-free benzene containing 0.5 per cent phenyl- β -naphthylamine

at $35^{\circ}\text{C} \pm 0.1^{\circ}\text{C}$ in a thermostatically controlled water bath. Swollen samples, taken out after 1, 3, 5, 9, 14, 24, 36 and 48 hour intervals were blotted with filter paper and weighed quickly in stoppered weighing bottles. For natural rubber vulcanizates, the 36 hour period was found to be sufficient for attaining the equilibrium swelling whereas for styrene-butadiene rubber and the blends 48 hours were required for the attainment of the swelling equilibrium. Samples were then dried in an oven for 24 hours at $70^{\circ} \pm 1^{\circ}\text{C}$, and then in vacuum and finally weighed after allowing them to cool in a desiccator. Duplicate readings were taken for each sample.

The volume fraction of rubber, V_r , was calculated by the method reported by Ellis and Welding¹⁴³, which takes into account the correction of swelling increment with duration of immersion after the equilibrium is attained.

$$V_r = \frac{(D - FT) \rho_r^{-1}}{(D - FT) \rho_r^{-1} + A_o \rho_s^{-1}} \quad \dots \text{(II.14)}$$

where T is the weight of the test specimen, D , the deswollen weight of the test specimen, F , the weight fraction of insoluble components, A_o , the weight of the absorbed solvent, corrected for the swelling increment and ρ_r and ρ_s are the densities of the rubber and the solvent respectively.

$$\begin{aligned} \rho_r \text{ (NR)} &= 0.92; & \rho_r \text{ (SBR)} &= 0.94 \\ \rho_r \text{ (BR)} &= 0.92; & \rho_r \text{ (EPDM)} &= 0.85 \\ \rho_s \text{ (benzene)} &= 0.875; \end{aligned}$$

From the collected data the value of A_0 can be easily calculated. The crude weight ratio W_t at any time 't' is given by

$$W_t = \frac{S_t - T}{T}$$

where S_t is the swollen weight of the specimen at time 't'.

If the equilibrium time is taken as 'X' hours, the percentage increment d_x after 'X' hours immersion is calculated from

$$d_x = \frac{100 (W_x - W_0)}{W_0} \quad \dots (II.15)$$

where W_0 is the crude weight ratio in the absence of increment and is obtained from the graph of W_t against $t^{1/2}$ by extrapolating the straight line through the data recorded after a long period of swelling, to zero time (Figure II.2). The value of A_0 is then given by

$$A_0 = A_x \left[1 - \frac{d_x}{100} \right] \quad \dots (II.16)$$

where A_x is the weight of the solvent absorbed after 'X' hours' immersion, equal to $(S_x - D)$, where S_x is the swollen weight of the specimen after 'X' hours. The method is simplified by carrying out this method for first fifteen to twenty vulcanizates of varying crosslink density and a graph between W_x and d_x is plotted as shown in Figure II.3. A single reading at equilibrium swelling time, established by the first few samples, can then be used for calculation.

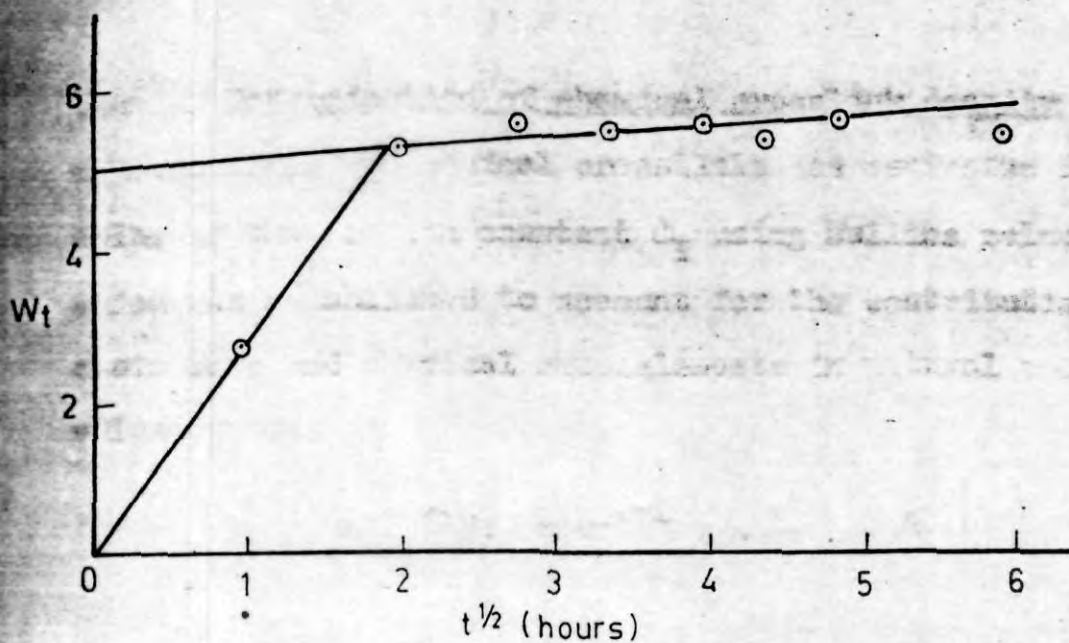


FIG. II-2 DEGREE OF SWELLING (W_t) VERSUS SQUARE ROOT OF TIME ($t^{1/2}$)

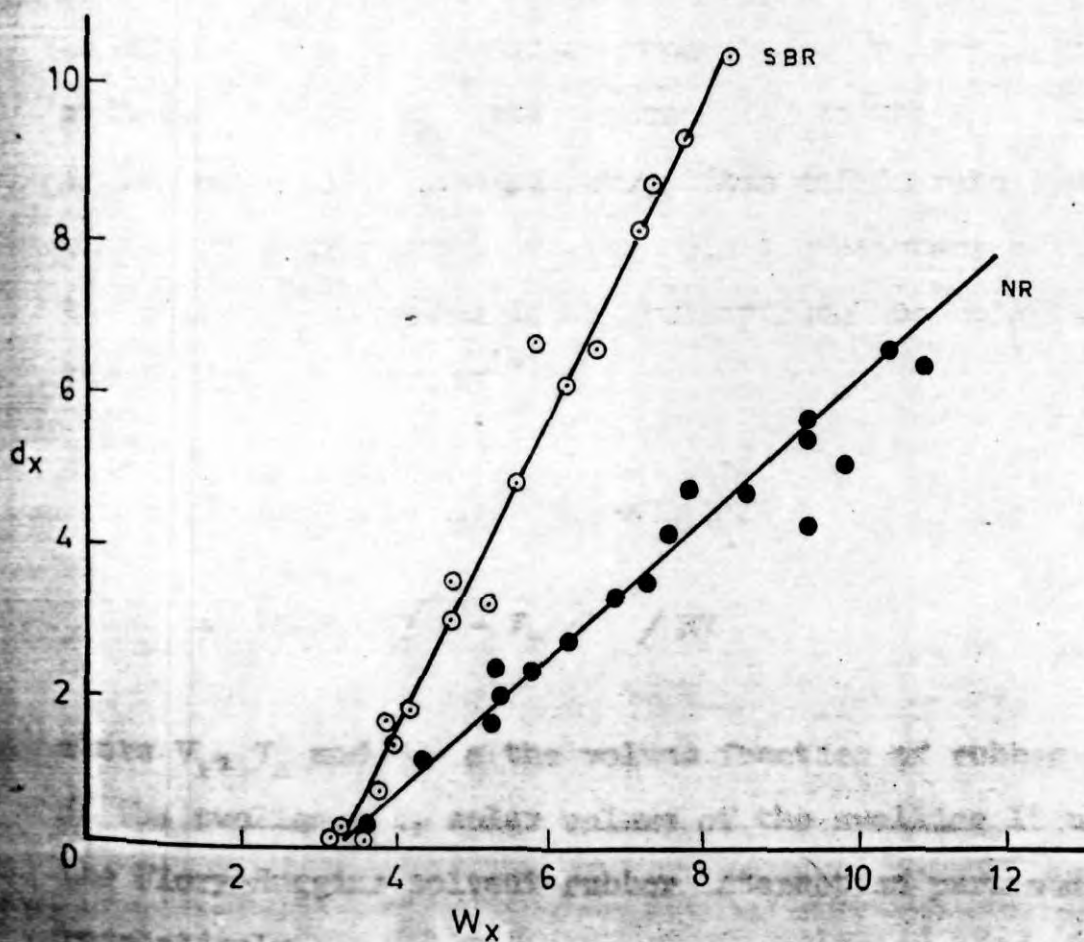


FIG. II-3 INCREMENT (d_x) AGAINST DEGREE OF SWELLING (W_x)

V.4 Determination of chemical crosslink density : The concentration of chemical crosslinks was estimated from the value of the elastic constant C_1 using Mullins relationship¹⁴⁴ which was established to account for the contribution of chain ends and physical entanglements in natural rubber vulcanizates.

$$C_1 = \left[\rho RT (2M_{c, \text{chem}})^{-1} + 0.78 \times 10^6 \right] \left[1 - 2.3 (M_{c, \text{chem}}) \bar{M}_n^{-1} \right] \text{ dynes/cm}^2 \quad \dots \text{ (II.17)}$$

where ρ is the vulcanizate density, R is the molar gas constant, T is the absolute temperature, \bar{M}_n is the initial molecular weight of rubber hydrocarbon in the mix, $2M_{c, \text{chem}}^{-1}$ is the density of chemical crosslinks and is reported as mmol/kg of rubber hydrocarbon. C_1 , the elastic constant pertinent to the rubber hydrocarbon in the vulcanizate was calculated from the following relation¹⁴⁵.

$$\begin{aligned} & - \left[\ln (1 - V_r) + V_r + \chi V_r^2 \right] \\ & = 2C_1 V_s (V_r^{1/3} - V_r / 2) / RT \end{aligned} \quad \dots \text{ (II.18)}$$

where V_r , V_s and χ are the volume fraction of rubber network in the swollen gel, molar volume of the swelling liquid and the Flory-Huggins solvent-rubber interaction parameter, respectively.

The value of χ changes with changes in recipes and V_r according to the following relation¹⁴⁶,

$$\chi = \chi_0 + \beta V_r \quad \dots (II.19)$$

where χ equals to χ_0 (0.44 for NR) when V_r is very small and β is an empirical constant (equal to 0.18 for natural rubber-benzene system).

The initial molecular weight of the rubber hydrocarbon in the mix, \bar{M}_n , was determined from the limiting viscosity number $[\eta]_{\text{toluene}}$ (dl/g) at 25°C by means of the relationship¹⁴⁷,

$$[\eta]_{\text{toluene}} = 1.076 [\eta]_{\text{benzene}} - 0.15$$

$$\text{and } [\eta]_{\text{benzene}} = 2.29 \times 10^{-7} \bar{M}_n^{1.33} \quad \dots (II.20)$$

The \bar{M}_n values of the natural rubber hydrocarbon in the mixes were in the range of 1.4×10^5 to 1.5×10^5 .

V.5 Determination of crosslink density in filled mixes :

Although natural rubber gum vulcanizates have received much attention, less detail is available on network structure of filled vulcanizates, undoubtedly because of the uncertainties introduced by filler-rubber interaction.

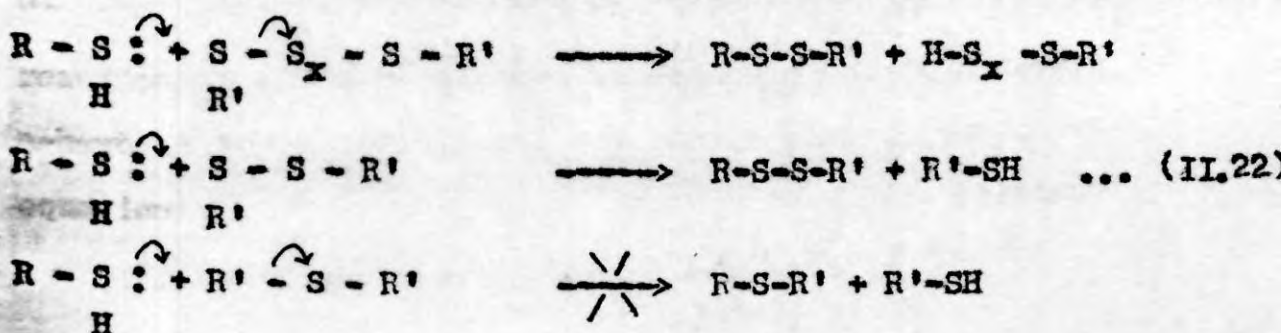
In the case of vulcanizates containing HAF black, the values of V_r , obtained as above, were converted into V_{ro}

(the value V_r would have had in the absence of the black) by means of the following equation which was derived by Porter¹⁴⁸.

$$V_{ro}/V_r = 0.56 e^{-Z} + 0.44 \quad \dots (II.21)$$

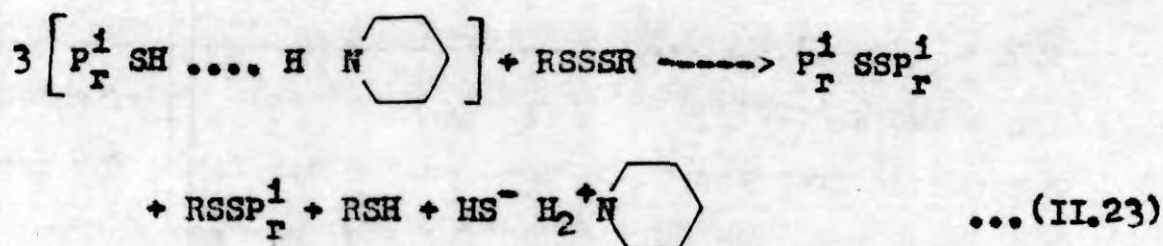
V.6 Determination of concentration of different types

of crosslinks : The concentrations of polysulfidic crosslinks ($-S_x-$) were estimated from the determination of chemical crosslink densities of vulcanizates before and after treatment with thiolamine chemical probe. Treatment of vulcanizates with propane 2-thiol (0.4M) and piperidine (0.4M) in n-heptane solution at room temperature for 2 hours cleaves the polysulfidic crosslinks in the network. The experimental methods used were described in detail by Campbell¹⁴⁹ and Campbell and Saville¹⁵⁰. Action of propane 2-thiol is based on nucleophilic displacement reactions by alkane thiols on sulfur atoms of polysulfides to cleave the sulfur bonds as shown below. They depend on their relative rates of the two displacement reactions and high resistance of the carbon-sulfur linkage in monosulfides to such nucleophilic displacement.



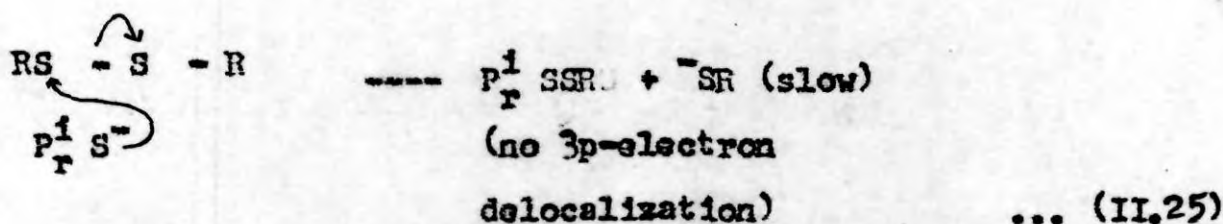
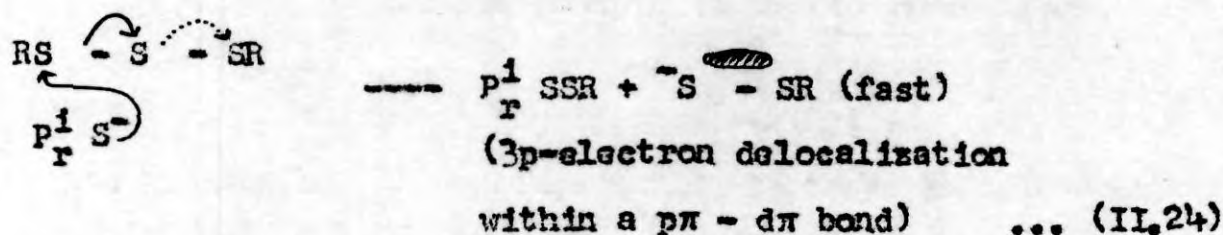
V.6.1 Treatment with propane-2-thiol : The samples (1 mm thick) were placed in a cylindrical tube 30 cm long and 3 cm in diameter, clamped horizontally and purged with nitrogen. The specimens were well covered with 100 ml thiol-amine (prepared by dissolving 37.6 ml propane-2-thiol and 39.5 ml redistilled piperidine in n-heptane and making up to one litre with further pure heptane). The gas tap was closed to maintain the nitrogen blanket in the tube. The apparatus was agitated occasionally during the two hour period.

After renewing the stream of nitrogen through the apparatus, the reagent was run off and replaced by 100 ml of petroleum ether (b.p. $40^{\circ} - 60^{\circ}\text{C}$) and the apparatus was agitated occasionally during one hour. This cold extraction was repeated with fresh petroleum ether every hour until four such extractions were made under nitrogen. The specimens were then removed and dried overnight in vacuum to constant weight. Then the chemical crosslink density was measured by equilibrium swelling method as described earlier. When the sample thickness was more than 1 mm, the specimens were swollen in n-heptane overnight at room temperature under nitrogen and sufficient propane 2-thiol and piperidine were added to give concentrations of 0.4M for each reagent in the final solution. The cleavage reaction in the presence of propane-2-thiol, piperidine, and n-heptane is exemplified for trisulfide in the following equation :



where $\text{P}_R^1 = \text{Isopropyl}$.

The thiol-amine combination gives as associate, possibly piperidinium propane-2-thiolate ion pair, in which the sulfur atom has enhanced nucleophilic properties¹⁵¹, which is capable of cleaving organic trisulfides (equation II.24) and higher polysulfides within 30 minutes at 20°C, while reacting with corresponding disulfides (equation II.25) at about one thousandth of this rate. The favored polysulfidic cleavage is due to $p\pi - d\pi$ delocalization of the displaced 6-electron pair of RSS^- as shown in the equation (II.24).



$\text{P}_R^1 \text{S}^-$ is used to represent the nucleophilic thiol-amine associate.

V.7 Combined sulfur and crosslink inefficiency parameter :

The network combined sulfur, $[S_c]$, of the vulcanizates was determined from the compounded sulfur available for crosslinking minus the zinc sulfide sulfur and the free sulfur.

For example, if the compounded sulfur is 2.5 gm per hundred gram of rubber and if sulfur donated by sulfur donor is 0.5 gm per hundred gram of rubber, then the total sulfur available for crosslinking is $(2.5 + 0.5)$ gm. If the zinc sulfide sulfur as determined earlier of the same vulcanizate is 0.25 gram per hundred gram of rubber and free sulfur as determined by the standard method is 0.35 gm phr, then the sulfur available for crosslinking is $(2.5 + 0.5) - (0.25 + 0.35)$ gm i.e., 2.4 gram per hundred gm of rubber hydrocarbon. The network combined sulfur is expressed in mmol per kg of rubber hydrocarbon.

The sulfur inefficiency parameter² E is defined as the number of atoms of sulfur combined in the network per chemical crosslink. It gives a measure of overall structural complexity of a sulfur vulcanized network. Higher the value of E, the higher is the sulfur inefficiency in the vulcanizate. Hence,

$$E = \frac{[S_c]}{[2Mc, \text{ chem}]^{-1}} \quad \dots (II.26)$$

Details of calculations of crosslink type and sulfur modification index, E have appeared elsewhere, but some essential arguments and algebraic analysis have been reproduced here. The assumptions used are :

- (a) Polysulfidic crosslinks include not only the types RSS_xSR ($x \geq 1$) but also vicinal polysulfidic crosslinks which act physically as a single crosslink.
- (b) all crosslinks are tetrafunctional.

V.8 Determination of Sol content :

The extent of chain scission in a vulcanizate is assessed by estimating its sol content. The estimation was done by the method described by Bristow¹⁵² in which the samples were extracted with cold acetone in the dark for 8 to 10 days, the acetone being replenished four times during this period. The samples were then dried to constant weight in vacuo at room temperature. Weighed samples of the extracted vulcanizates (about 2 g) were extracted with cold benzene in the dark, for 8 to 10 days, the benzene being replenished four times during this period. After benzene extraction, samples were dried to constant weight in vacuo. The sol content was then calculated from the weight loss during benzene extraction.

VI. SCANNING ELECTRON MICROSCOPY

The single most useful tool available to the rubber technologist interested to study the fracture surfaces is the

Scanning Electron Microscope (SEM). This is because it requires the least amount of technical expertise for the interpretation of the results and it presents a physical picture of the fracture surfaces. The sample preparation is very simple compared to other microscopic studies. Only care should be taken that the sample be kept in a dust-free condition after failure. Due to the non-conducting nature of the rubber specimen the fracture surface shall be coated with a conducting material.

The principle of the SEM is given in Figure II.4¹⁵³. Electrons from an emission source or filament are accelerated by a voltage usually in the range of 1-30 kV and directed down the center of an electron-optical column consisting of two to three magnetic lenses. These lenses cause a fine electron beam to be focussed on to the specimen surface. Scanning coils placed before the final lens cause the electron spot to be scanned across the specimen surface in the form of a square raster, similar to that of a television screen. The currents passing through the scanning coils are made to pass through the corresponding deflection coils of a cathode ray tube, so as to produce a similar but larger raster on the viewing screen in a synchronous fashion.

The electron beam incident on the specimen surface causes various phenomena, of which the emission of secondary electrons is used in SEM. The emitted electrons strike the

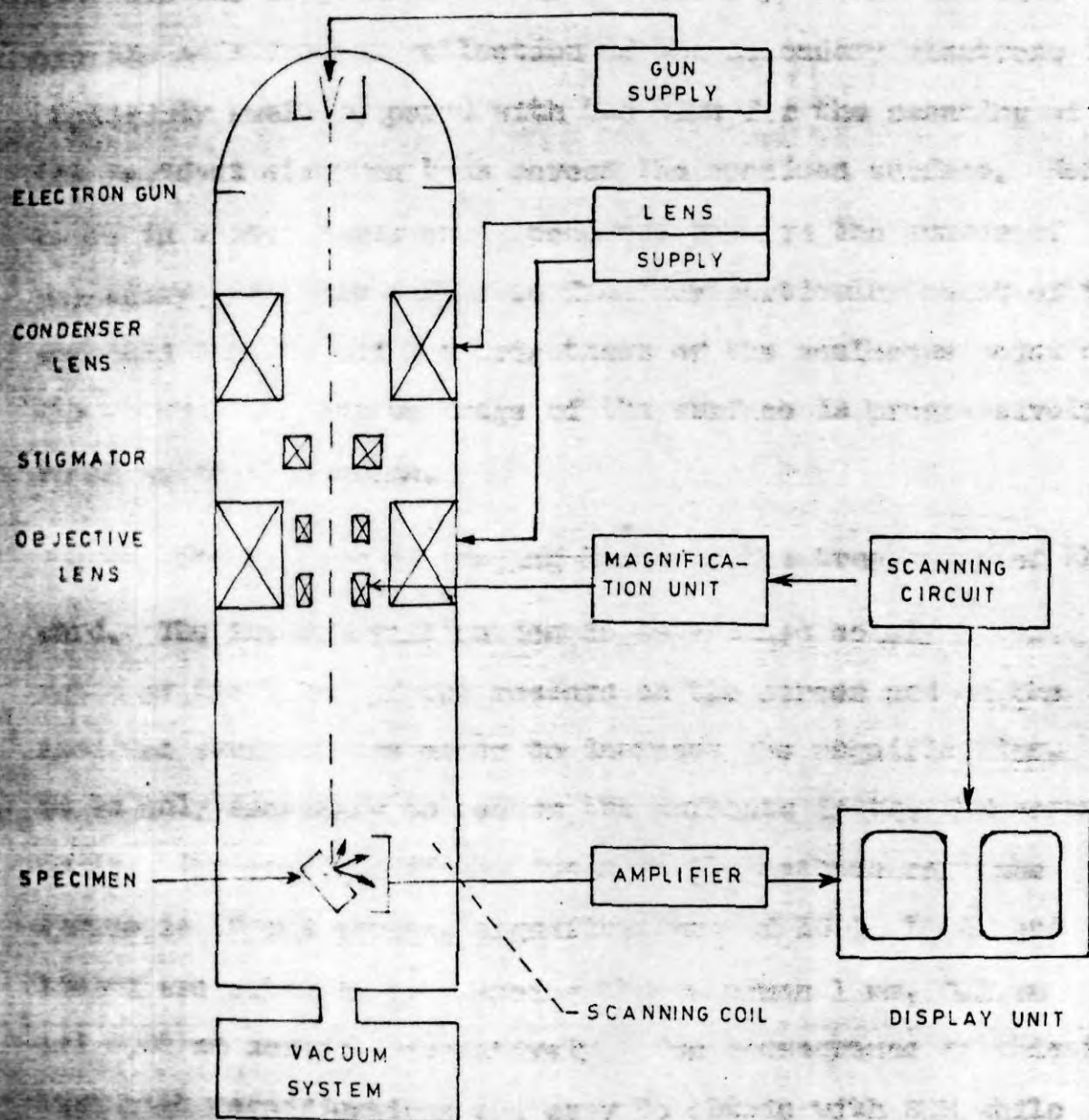


FIG. II.4. SIMPLIFIED BLOCK DIAGRAM OF AN SEM

collector and the resulting current is amplified and used to modulate the brightness of the cathode ray tube. The time for the emission and collection of the secondary electrons is negligibly small compared with the time for the scanning of the incident electron beam across the specimen surface. Hence there is a one-to-one correspondence between the number of secondary electrons collected from any particular point of the specimen surface and the brightness of the analogous point on the screen and thus an image of the surface is progressively built up on the screen.

The SEM has no imaging lense in the true sense of the word. The image magnification is determined solely by the ratio of the sizes of the rasters on the screen and on the specimen surface. In order to increase the magnification, it is only necessary to reduce the currents in the SEM scanning coils. For example, if the image on the cathode ray tube screen is 10 cms across, magnifications of 100X, 1000X and 10000X are obtained by scanning the specimen 1 mm, 0.1 mm and 0.01 mm across, respectively. One consequence of this is that high magnifications are easy to obtain with SEM while for very low magnifications of 10X, it would be necessary to scan a specimen approximately 10 mm across and this presents difficulties because of the large deflection angles required. For instance, the electron beam may strike the lens pole pieces or aperture and at the extremes, the scan linearity may not be maintained.

The completely different operation of the SEM compared with most other microscopes is possible because there is no imaging lens, and any signal that arises from the action of the incident electron beam (reflected electrons, transmitted electrons, emitted light etc.) can be used to form an image on the screen.

The SEM observations reported in the present investigations were made using ISI-60 and Philips 500 model scanning electron microscopes. The fracture surfaces were carefully cut from the failed test pieces without disturbing the surface. The shape of the test specimens and the portion from where the fracture surface has been removed for SEM observations are illustrated in the respective chapters. The fracture surfaces were sputter-coated with gold within 24 hours of testing. The SEM observations were made within one week after gold coating. The tilt was adjusted at 0° and the orientation of the photographs was the same in all cases. The fracture specimens were stored in a desiccator before and after gold coating till the SEM observations were made. From preliminary studies it was found that storage of fracture specimens upto a period of one week before gold coating and upto a period of one month after gold coating does not alter the fracture surface topography as observed in SEM. The operating conditions of the SEM are summarised below.

| | | |
|----|-------------------------|-----|
| 1. | Specimen positions tilt | 0° |
| 2. | Spot size, Å | 640 |
| 3. | H.T., kV | 25 |
| 4. | Emission current, Amp. | 26 |
| 5. | Aperture, microns | 200 |

CHAPTER III

SCANNING ELECTRON MICROSCOPIC STUDIES ON :

PART A. TEAR FRACTURE OF RUBBER

PART B. TENSILE RUPTURE OF RUBBER

**PART A. SCANNING ELECTRON MICROSCOPIC STUDIES
ON TEAR FRACTURE OF RUBBER**

This part has been published in Polymer, 23, 632 (1982)

The service life of rubber products depends on their resistance to various types of fracture, among which an important one is tear. Theories have been proposed in the past to describe tear fracture of rubber vulcanizates^{4,5,7-9}, but little is known about the damaged zone, where deformation and fracture take place. Recently scanning electron microscopy (SEM) has been used as a tool to study the characteristics of the fracture surfaces of rubber vulcanizates^{137-139, 162-164}. These studies are expected to throw more light on the mechanism of rubber fracture. In this part SEM studies on tear fracture of natural rubber vulcanizates are reported. The parameters studied are, (a) effect of crosslinking system and (b) effect

of filler. The formulations of the mixes are given in Table III.1. The optimum cure times, physical properties and V_r values are given in Table III.3. The rheographs of the mixes are shown in Figures III.1, III.2 and III.3. Figure III.4A gives the direction of force in the tear test and that of tear propagation. The tear testing was done at a rate of pulling of 50 cm per minute at room temperature (30°C).

From Table III.3 it is seen that the tear resistance of natural rubber vulcanizates are very much dependent on the cross-linking system. As expected, the peroxide-cured vulcanizates (Mixes A and B) show low tear resistance both in unfilled and in filled systems. The sulfur vulcanizing system gives appreciable tear resistance even in the unfilled vulcanizate (Mix C). Addition of HAF black to this system (Mix D) enhances its tear resistance remarkably. FT black and china clay are only mildly reinforcing fillers as shown by their effect on tear resistance (Mixes E and F). Stress dissipation near the tip of a growing crack by viscoelastic processes is essential for the development of high strength. In the case of sulfur-cured vulcanizates, stress dissipation is possible through the slippage of sulfur crosslinks. In peroxide-cured vulcanizates on the other hand, crosslink slippage is prevented as the crosslinks are carbon-carbon type and, therefore, stress dissipation is minimized. Addition of reinforcing black causes additional mechanisms by which strain energy is dissipated. Mechanical energy dissipation through

increased hysteresis resulting from the inclusion of particles in a viscoelastic medium has been studied by Radok and Tai¹⁵⁴. Any loss of segmental mobility in the polymer matrix resulting from interaction with the filler, further increases hysteresis. Motion of filler particles, chain slippage or breakage and de-wetting at high strains also accentuate hysteretic behavior. In addition to causing increased energy dissipation, dispersed particles finally serve to deflect or arrest growing cracks, thereby further delaying failure¹⁵⁵.

The low level of interaction between clay and rubber as reported by Mukhopadhyay and De¹⁵⁶, causes the formation of loose agglomerates in the matrix, which act as stress raisers, thereby causing premature failure. This accounts for the low tear resistance of the clay-filled mix. The SEM observations discussed later in this part support some of these explanations. Failure to enhance the tear resistance of peroxide-cured NR vulcanizate by HAF black might be due to the dominant effect of the crosslink type, as discussed earlier, which is not influenced even by the reinforcing filler.

Figure III.5, which is the SEM photograph of the tear fracture surface of the peroxide-cured unfilled vulcanizate, shows a typical tear path on the surface. From the figure it is apparent that the tear propagates in a stick-slip manner. A similar mode of fracture was described by Glucklich and Landel¹⁰. De and coworkers¹⁵⁷

also made similar observations in their SEM studies on failure of carboxylated nitrile rubber. One end of the fracture surface is shown in Figure III.6, which shows microfolds on the surface. Addition of HAF black to the same system changes the fracture pattern (Figure III.7), although it does not enhance the tear resistance. The surface is rough and has a layered structure. Separation of the matrix near the filler agglomerates is also seen in this photomicrograph.

The SEM fractograph of the sulfur-cured unfilled NR vulcanizate (Mix C) is shown in Figure III.8. The surface shows a large number of broad tear lines which propagate by the stick-slip process. There is appreciable branching of the tear lines, which indicates tear deviation. This accounts for the higher tear resistance of the sulfur-cured vulcanizate as compared to the peroxide-cured one. Formation of parabolic tear lines on the fracture surface has been attributed to the interaction of the main fracture front with subsidiary fracture fronts initiated from flaws just ahead of the crack¹⁵⁸. A model showing the formation of parabolic tear lines on the fracture surface is given in Figure III.4B. The addition of HAF black to the same system changes the fracture mode remarkably as seen from Figure III.9, which is the SEM fractograph of vulcanizate from Mix D. The high tear resistance of this vulcanizate can be correlated to the roughness of the surface and to the appearance of a large number of short but rounded tear lines which are distributed at random. Reinforcing HAF black provides

improved wetting and adhesion characteristics and prevents tear from proceeding straight.

Addition of FT black improves tear resistance only slightly. The fracture pattern as given in Figure III.10 is also different from that obtained with HAF black. The surface is smoother with a few long but straight tear lines. Figure III.11 is the SEM fractograph of the clay-filled vulcanizate. The surface does not show any tear line. The poor bonding between clay agglomerates and rubber causes the former to come out of the matrix. This results in the formation of a large number of pits on the surface and thus makes the surface appear rough. Figure III.12 is a magnified image of the same surface, where the formation of pits on the surface as a result of clay agglomerates coming out of the matrix is clearly seen. As pointed out earlier, such loose agglomerates in the matrix act as stress raisers, thereby reducing the overall strength of the vulcanizate. The low level of polymer-filler interaction in the case of FT black- and clay-filled vulcanizates is also evident from their V_r values, which are lower than that of the HAF black-filled sulfur-cured vulcanizate. Since the actual crosslink density of vulcanizates is not much influenced by the presence of fillers, changes in V_r may be taken as a measure of polymer-filler interaction^{148,159}. The increase in V_r on the addition of HAF black is much less with the DCP curing system. If this indicates less interaction between rubber and filler, this could account for the lack of reinforcement as discussed earlier.

TABLE III.1

FORMULATIONS OF THE MIXES A-F

| MIX | A | B | C | D | E | F |
|-------------------|-----|-----|-----|-----|-----|-----|
| Natural rubber | 100 | 100 | 100 | 100 | 100 | 100 |
| Zinc oxide | - | - | 5 | 5 | 5 | 5 |
| Stearic acid | - | - | 2 | 2 | 2 | 2 |
| HAF black (N 330) | - | 50 | - | 50 | - | - |
| FT black (N 880) | - | - | - | - | 50 | - |
| China clay | - | - | - | - | - | 50 |
| Naphthenic oil | - | 5 | - | 5 | 5 | 5 |
| CBS | - | - | 0.8 | 0.8 | 0.8 | 0.8 |
| Sulfur | - | - | 2 | 2 | 2 | 2 |
| Dicumyl peroxide | 2 | 2 | - | - | - | - |

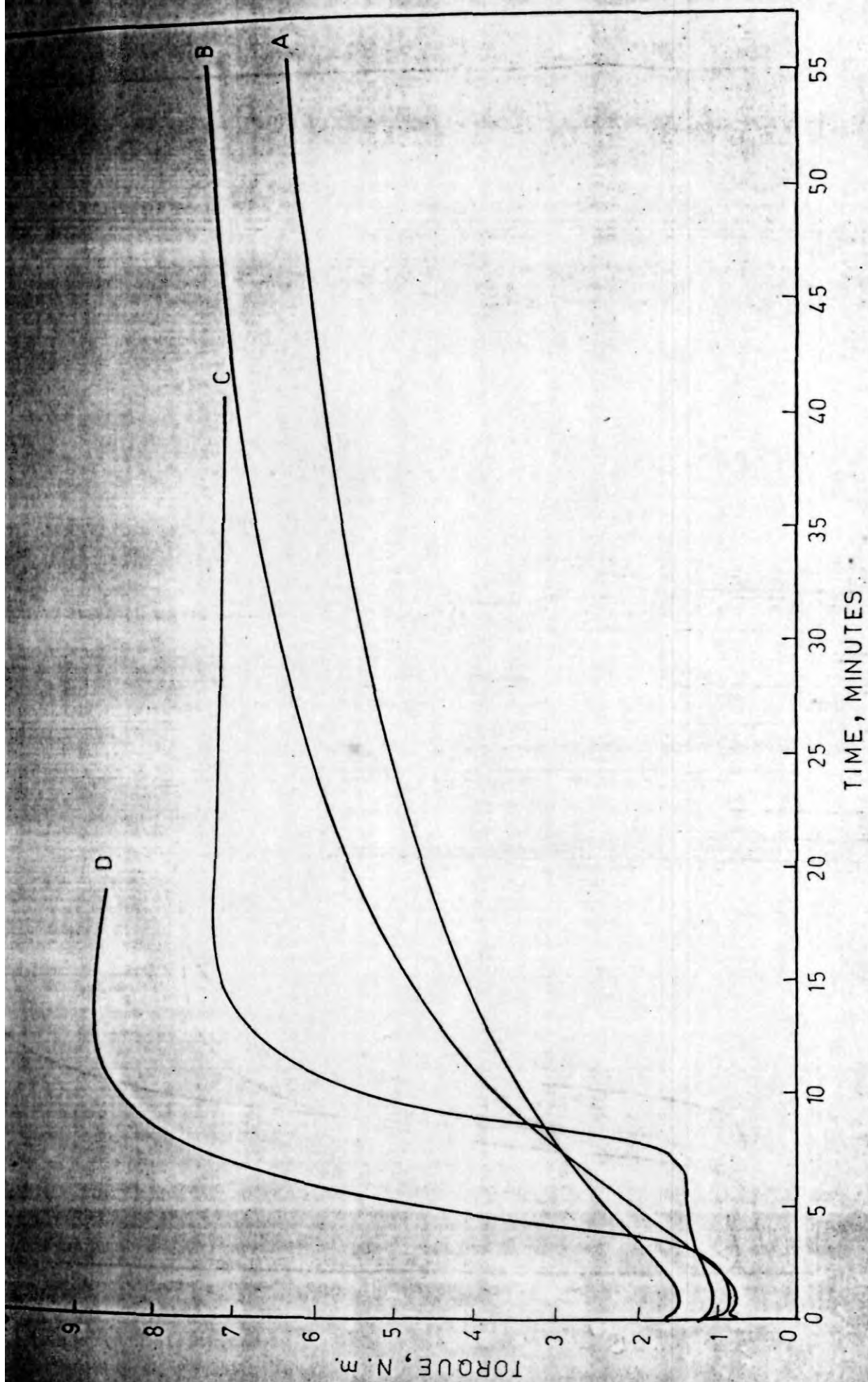


FIG. III.1. RHEOGRAPHS OF MIXES A, B, C AND D

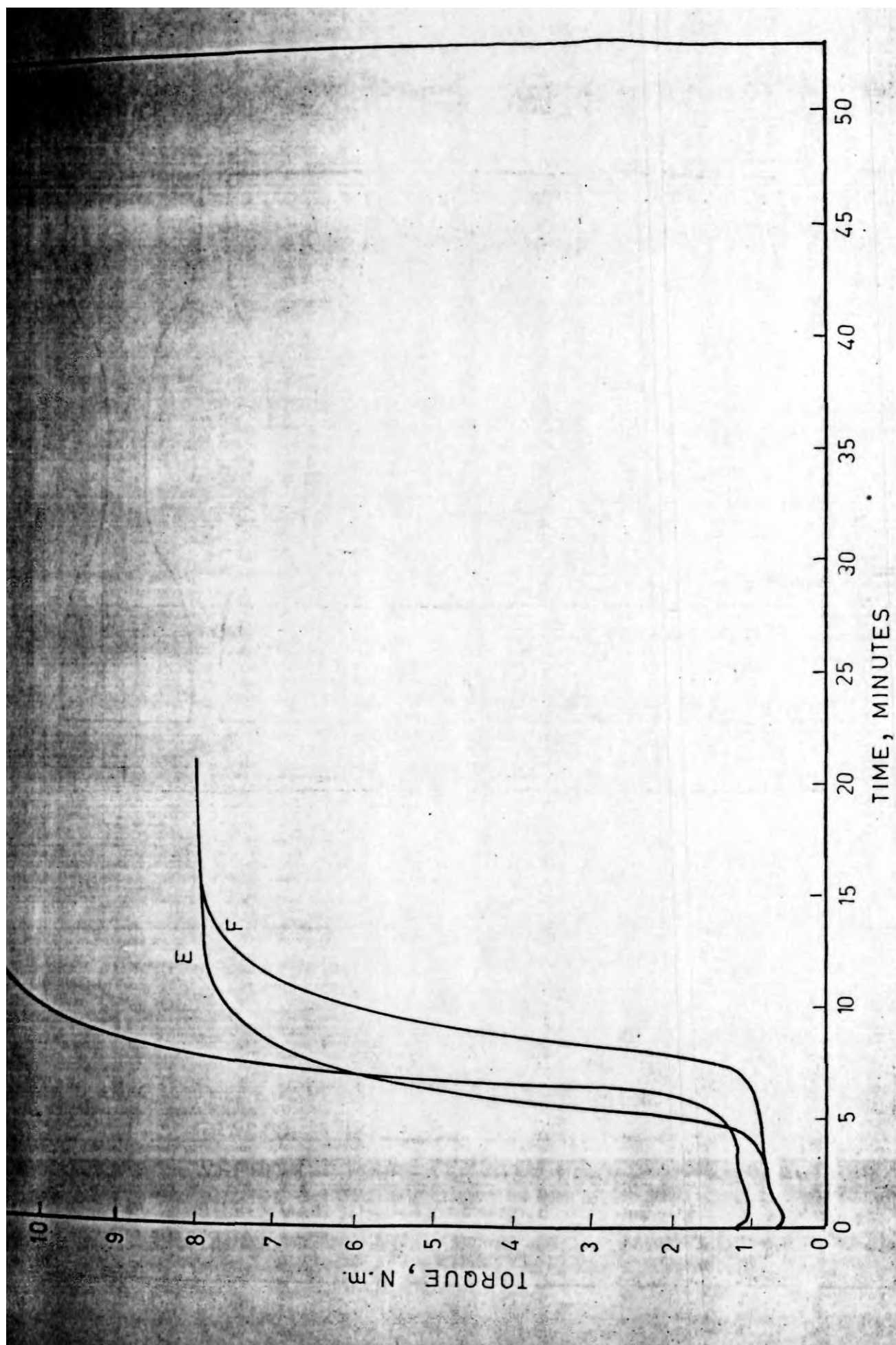


FIG.III 2. RHEOGRAPHS OF MIXES E, F AND G

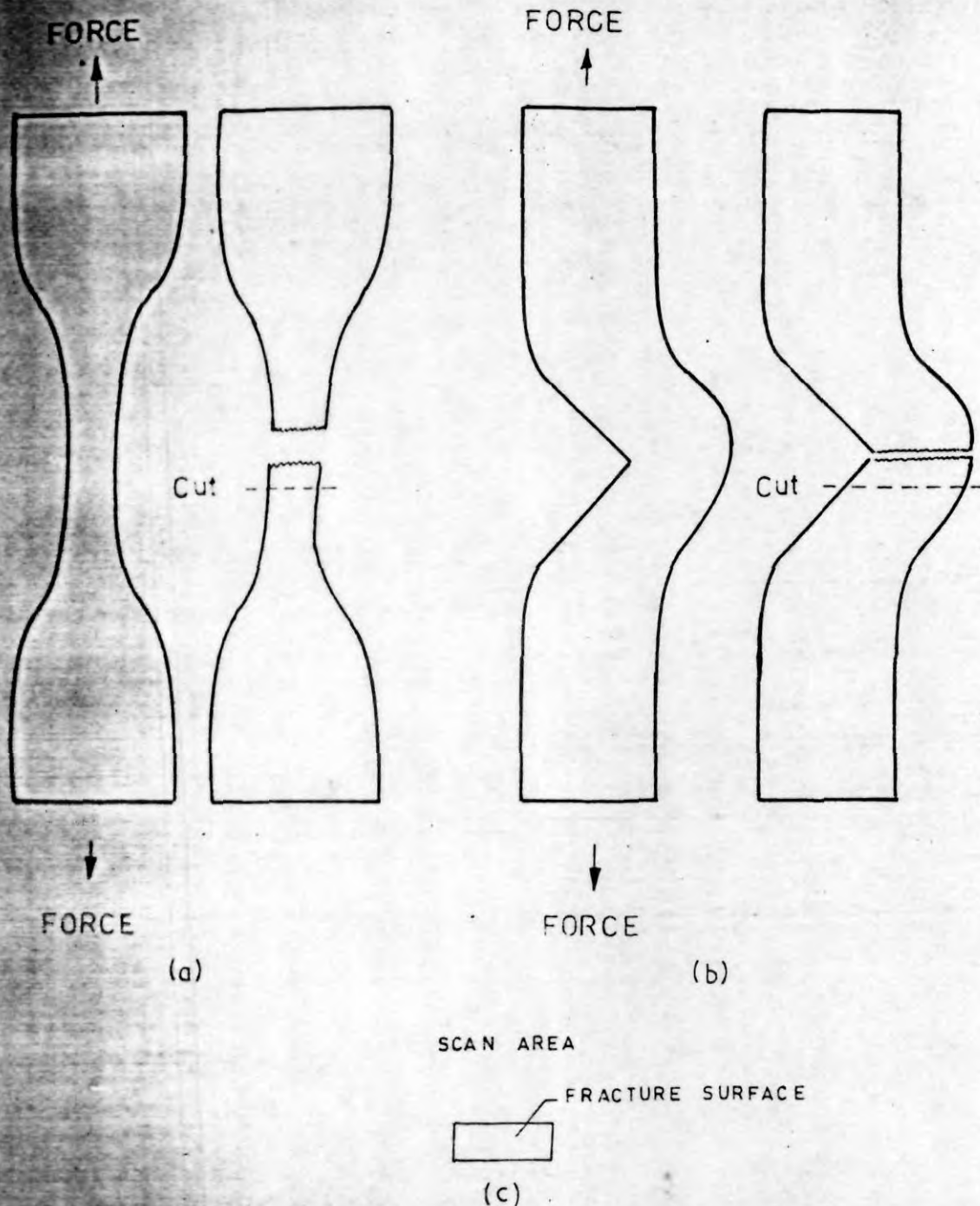


FIG. III-4.A. THE SHAPE OF THE TEST SPECIMENS, DIRECTION OF FRACTURE PROPAGATION AND THE PORTION FROM WHERE THE SURFACE HAS BEEN CUT FOR SEM OBSERVATIONS. (a) TENSILE (b) TEAR

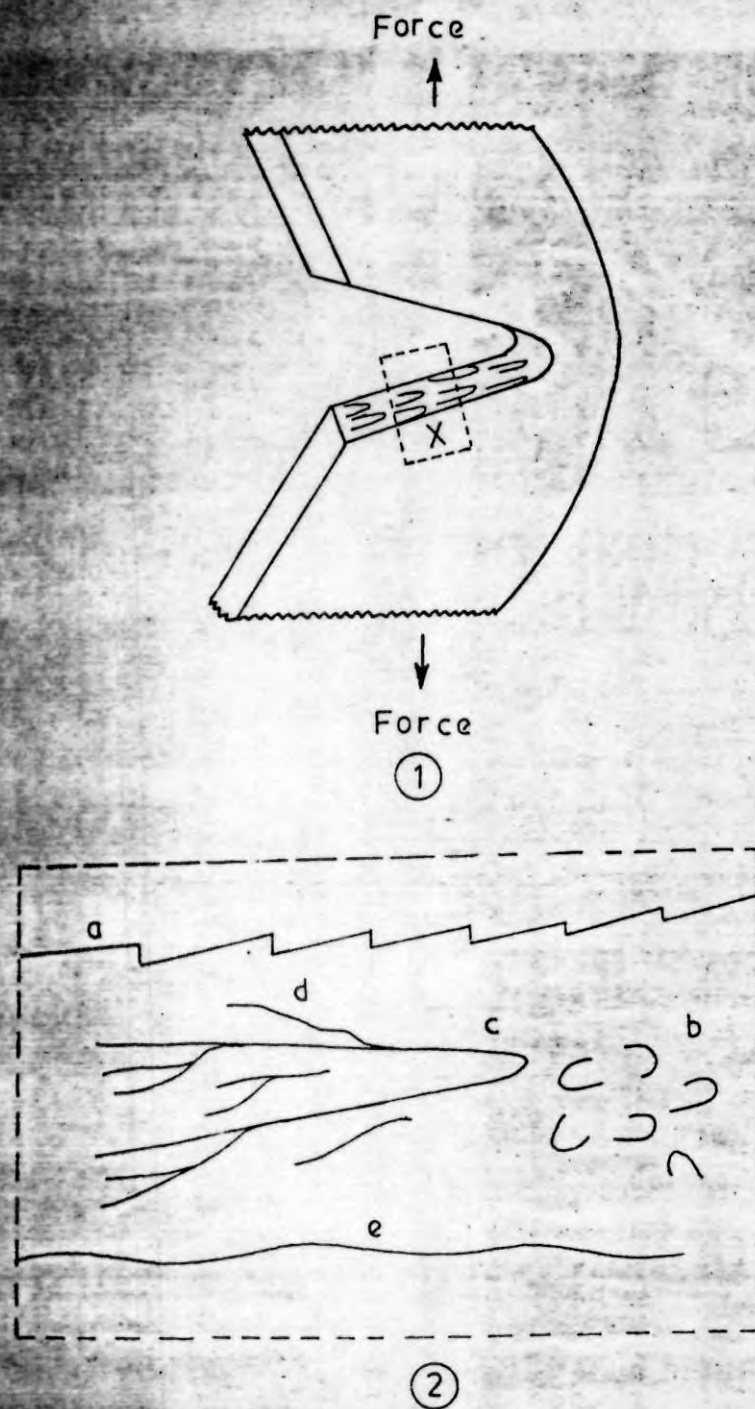


FIG. III-4 B. 1. TEST SPECIMEN BEING TORN

2. PORTION X IN 1 ENLARGED

a. STICK SLIP TEAR, b. ROUNDED TEAR LINES,

c. MAIN PARABOLIC TEAR PATH,

d. SECONDARY TEAR LINES, e. STEADY TEAR.

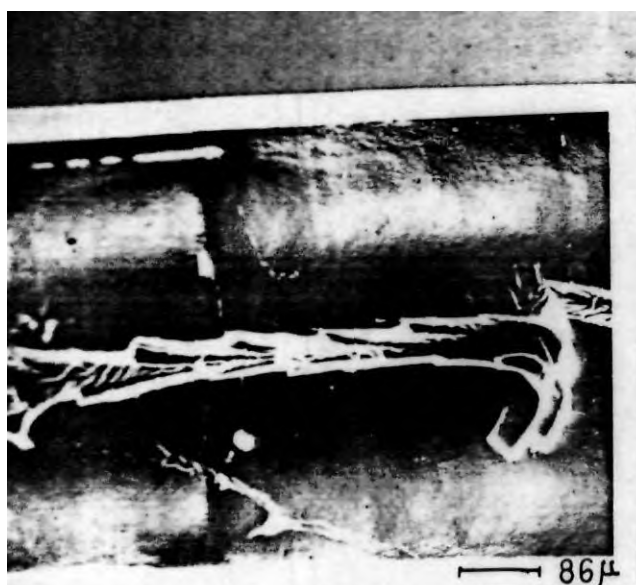


FIG. III.5 : Tear fracture of DCP-cured unfilled NR; stick-slip process.

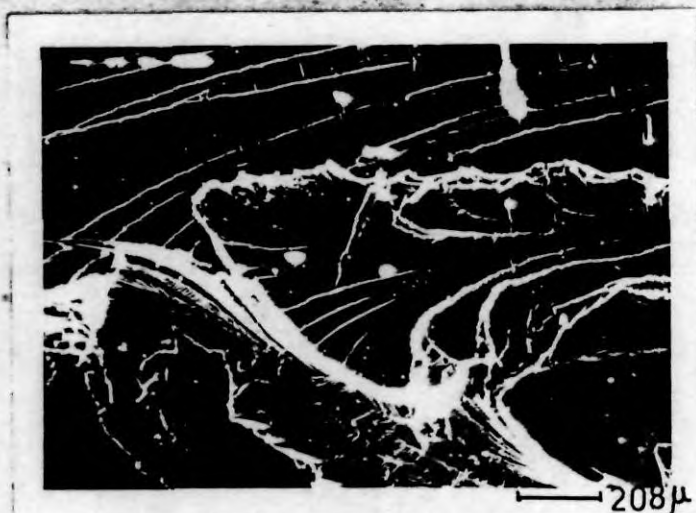


FIG. III.6 : Tear fracture of DCP-cured unfilled NR; microfolds on the surface.



FIG. III.7 : Tear fracture of DCP-cured HAF black-filled NR; layered fracture.



FIG. III.8 : Tear fracture of sulfur-cured unfilled NR; branching of tear lines.



FIG. III.9 : Tear fracture of sulfur-cured HAF black-filled NR; rough surface with rounded features.

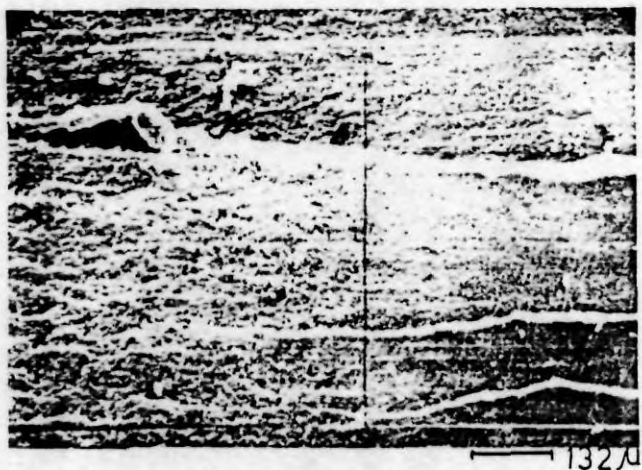


FIG. III.10 : Tear fracture of sulfur-cured FT black-filled NR; smooth tear lines.



FIG. III.11 : Tear fracture of sulfur-cured clay-filled NR; smooth surface.

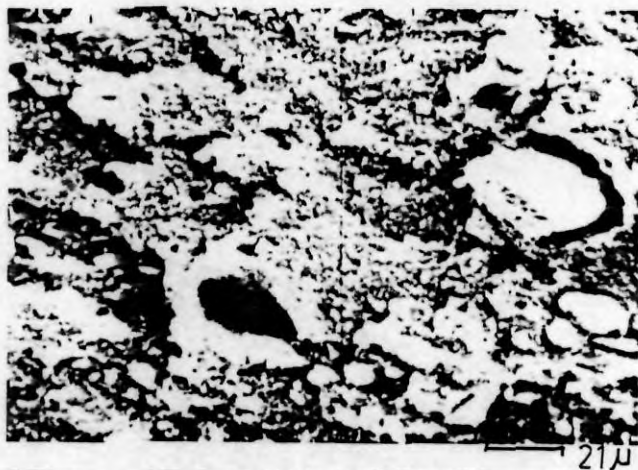


FIG. III.12 : Tear fracture of sulfur-cured clay-filled NR; formation of pits on the surface.

**PART B. SCANNING ELECTRON MICROSCOPIC STUDIES
ON TENSILE RUPTURE OF RUBBER**

This part has been published in Journal of Materials
Science, 17, 2594 (1982)

In continuation of the studies on tear fracture, reported in Part A, the tensile rupture characteristics of rubbers studied by SEM are reported in this part. The parameters studied are : (a) two different rubbers, namely NR and SBR, (b) the effect of type and extent of crosslinking and (c) effect of filler.

Theories of tensile rupture have been described previously by Greensmith¹⁸, Thomas and Whittle¹⁹, Smith¹⁷ and Gent¹⁶⁰. These authors correlated strength with tearing energy or work to break per unit volume. But the nature of the fracture surface under tensile rupture was not fully explored in those studies. The present study attempts to reveal the nature of the fracture surface formed in different types of vulcanizates.

The formulations of the mixes (A-D and F-J) are given in Tables III.1 and III.2. The properties of these mixes are given in Tables III.3 and III.4. The rheographs of the mixes are shown in Figures III.1, III.2 and III.3. Figure III.4A shows the shape of the test specimen, the direction of application of force and the portion from where the fracture surface has been removed for the SEM observations. The test was done at a rate of pulling of 50 cm per minute, at room temperature (30°C).

The tensile strengths of the different vulcanizates are furnished in Tables III.3 and III.4. Figure III.13 is the SEM fractograph of the peroxide-cured unfilled NR vulcanizate. Long but thin tear lines are observed on the surface. A large number of bright spots are also seen on the surface, which act as nuclei for microfolds emanating radially as seen in Figure III.14. We believe that these spots are characteristic of a strain-crystallized matrix undergoing rupture at high strain. The fracture surface of the sulfur-cured unfilled NR vulcanizate (Mix C) shows a rough zone near one end of the surface (Figure III.15). The surface also shows a number of bright spots, which act as nuclei for microfolds (Figure III.16). The crosslink density of the vulcanizate G is high, as indicated by its V_r in Table III.4, and the fracture mode changes appreciably. Figure III.17 is the SEM fractograph of the tensile fracture surface in the case of the vulcanizate G. The figure shows folding on the surface and random distribution of tear lines. The sample breaks at a much lower elongation, even before the occurrence of strain-induced

unfilled ones. This shows that the mechanism of fracture is different in unfilled and filled NR vulcanizates and in filled vulcanizates nature of filler (reinforcing/non-reinforcing) changes the fracture mode.

In the case of SBR, the peroxide curing system makes the vulcanizate brittle with very low tensile strength and elongation at break. The fracture surface shows 'slip lines' as seen from the fractograph (Figure III.22). This type of slip lines has been described as a characteristic of brittle fracture in the case of polymethylmethacrylate¹⁶¹. These slip lines are 'hyperbolae' formed on the fracture surface at the junction of two advancing cracks, which start from two different centres at the same speed, but at different timings. Figure III.23 is a magnified image of the surface which shows microfolding on a portion of one of the tear paths. The sulfur-cured unfilled SBR vulcanizate shows a different type of fracture. The surface is smooth with a few tear lines (Figure III.24). Unlike in the case of NR, small bright spots which are believed to be due to crystallites, are much less in SBR. This again confirms the idea that these spots result from strain-induced crystallization, which cannot be realized in non-crystallizing copolymer rubbers like SBR. With the addition of HAF black the strength of SBR increases remarkably. This improvement in strength is reflected in the nature of the fracture surface also. The surface is rough with curved tear lines (Figure III.25). Compared with the corresponding NR fracture surface, here the number of tear lines

is less, but their size larger. Figure III.26 is a magnified fractograph of the HAF black-filled SBR vulcanizate which shows a crack along one of the tear lines. The high level of polymer-filler interaction in the case of HAF black-filled vulcanizates causes formation of regions of high strength in the composite and hence smooth propagation of fracture is hindered. This results in the occurrence of a rough fracture surface and curved tear lines and enhanced tensile strength of the vulcanizate.

TABLE III.2

FORMULATIONS OF THE MIXES G-J

| MIX | G | H | I | J |
|--------------------------|-----|-----|-----|-----|
| Natural rubber | 100 | - | - | - |
| Styrene-butadiene rubber | - | 100 | 100 | 100 |
| Zinc oxide | 5 | - | 5 | 5 |
| Stearic acid | 2 | - | 2 | 2 |
| HAF black (N 330) | - | - | - | 50 |
| Naphthenic oil | - | - | - | 5 |
| CBS | 1.5 | - | 0.8 | 0.8 |
| Sulfur | 4.0 | - | 2.0 | 2.0 |
| Dicumyl peroxide | - | 2.0 | - | - |

TABLE III.4
PROPERTIES OF THE MIXES G-J

| MDX | G | H | I | J |
|-----------------------------------|-------|-------|-------|-------|
| Optimum cure time, min. | 9.5 | 25.0 | 33.0 | 19.5 |
| V_r , volume fraction of rubber | 0.275 | 0.223 | 0.176 | 0.225 |
| 300% modulus, MPa | 1.9 | - | 1.7 | 10.9 |
| Tensile strength, MPa | 3.6 | 0.3 | 2.3 | 20.6 |
| Elongation at break, % | 360 | 40 | 330 | 460 |
| Tear resistance, kN/m | 31 | 2 | 7 | 63 |

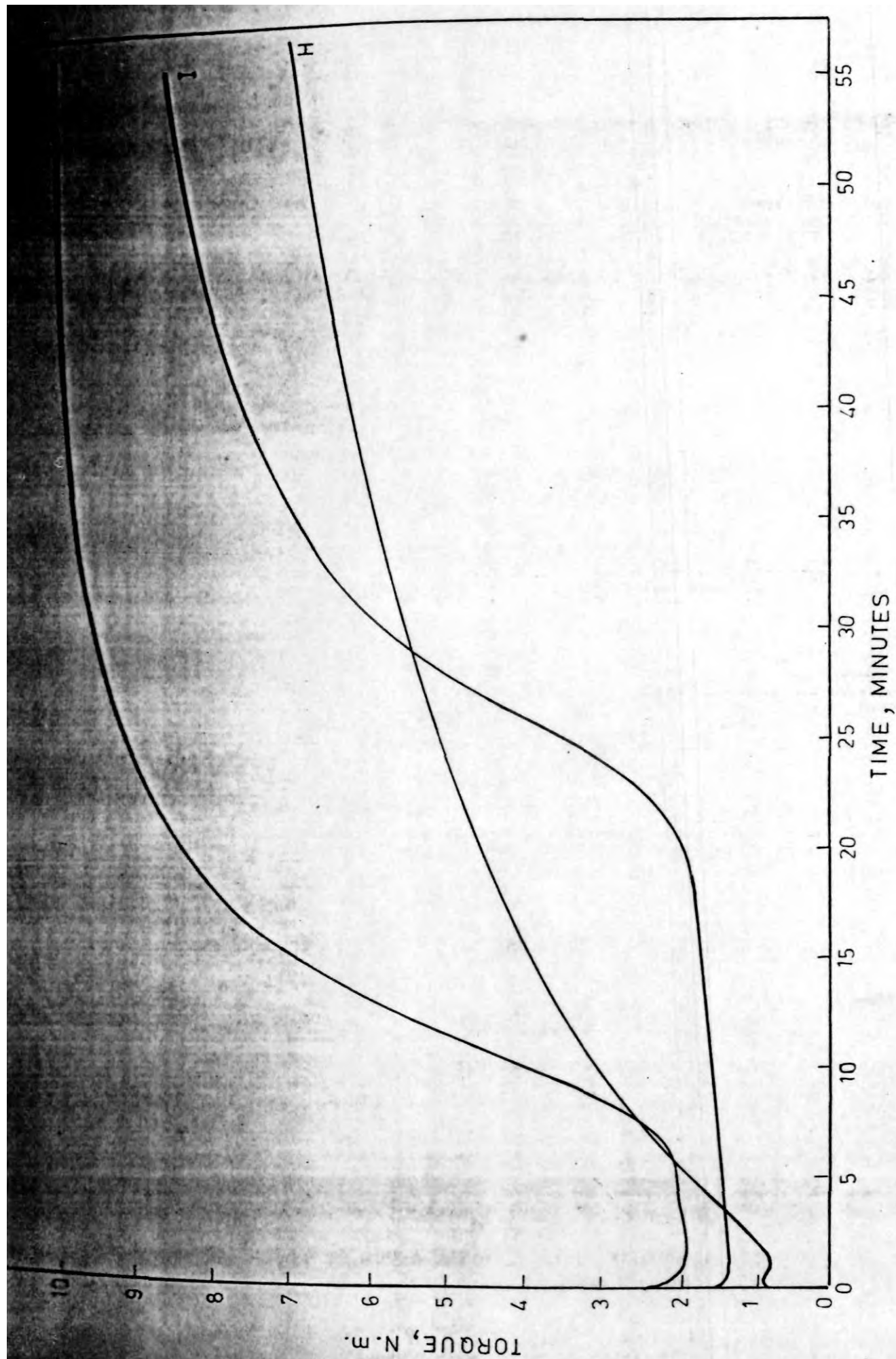


FIG. III.3. RHEOGRAPHS OF MIXES H, I AND J



FIG. III.13 : Tensile fracture of DCP-cured unfilled NR; general surface.



FIG. III.14 : Tensile fracture of DCP-cured unfilled NR; nucleation of microfolds.



FIG. III.15 : Tensile fracture of sulfur-cured unfilled NR; rough surface.

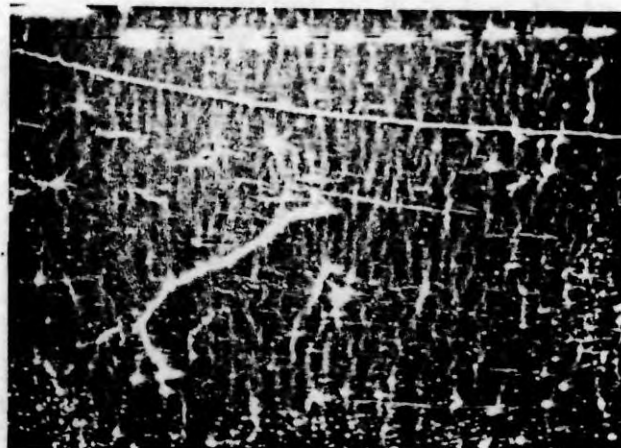


FIG. III.16 : Tensile fracture of sulfur-cured unfilled NR; general surface.

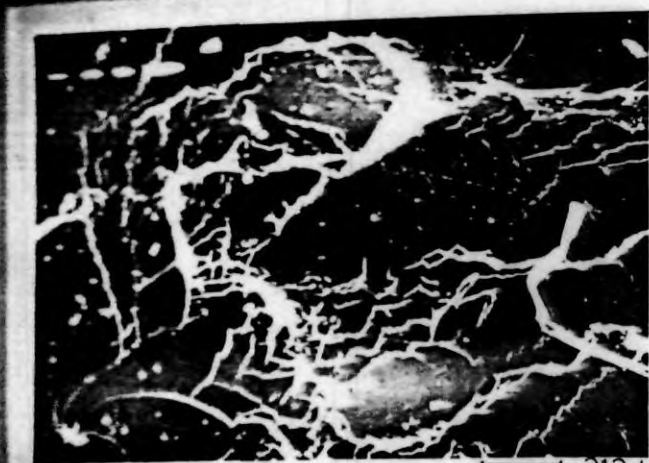


FIG. III.17 : Tensile fracture of highly crosslinked sulfur-cured unfilled NR; general surface.



FIG. III.18 : Tensile fracture of DCP-cured black-filled NR; straight and curved tear lines.



FIG. III.19 : Tensile fracture of sulfur-cured black-filled NR; rough surface with curved tear lines.

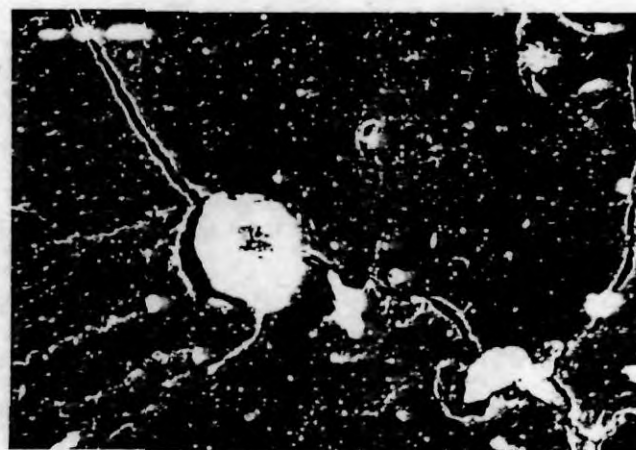


FIG. III.20 : Tensile fracture of sulfur-cured black-filled NR; filler agglomerates nucleating fracture.



FIG. III.21 : Tensile fracture of sulfur-cured clay-filled NR; pitted surface with fissures.

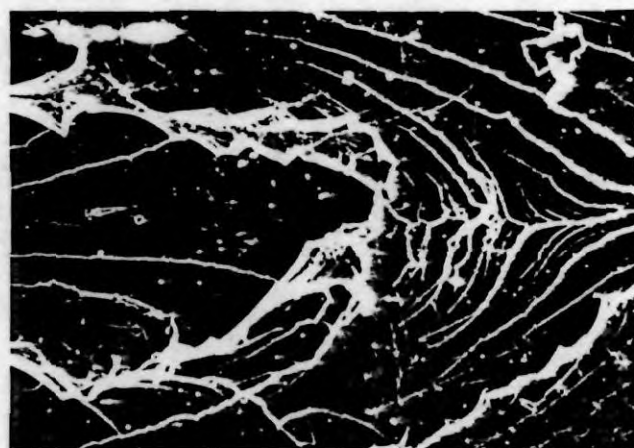


FIG. III.22 : Tensile fracture of DCP-cured unfilled SBR; slip lines.

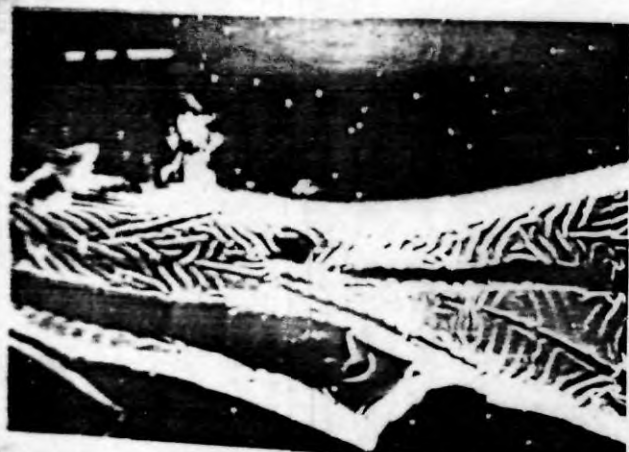


FIG. III.23 : Tensile fracture of DCP-cured unfilled SBR; details of the tear path.



FIG. III.24 : Tensile fracture of sulfur-cured unfilled SBR; smooth surface with tear lines.



FIG. III.25 : Tensile fracture of sulfur-cured black-filled SBR; curved tear lines.



FIG. III.26 : Tensile fracture of sulfur-cured black-filled SBR; crack along a tear line.

CHAPTER IV

CHEMICAL AND SCANNING ELECTRON MICROSCOPIC STUDIES ON :

PART A. THERMO-OXIDATIVE AGING OF RUBBER

PART B. OZONE CRACKING OF RUBBER

**PART A. THERMO-OXIDATIVE AGING AND ITS EFFECT ON
NETWORK STRUCTURE AND FRACTURE MODES OF
NATURAL RUBBER VULCANIZATES**

This part has been accepted for publication in Polymer.

The presence of a high level of unsaturation in natural rubber molecule makes it highly susceptible to attack by oxygen. Several factors like heat, light, presence of pro-oxidants and mechanical strain, accelerate the oxidation process. Among these the effect of heat is the most significant. During service a number of rubber products are subjected to varying levels of heat, either generated as a result of cyclic mechanical strain as in the case of a running tire or in the form of a high ambient temperature. Prolonged exposure to heat causes thermo-oxidative degradation of rubber and results in the deterioration of its desirable properties, eventually leading to premature failure. A few recent reviews²¹⁻²³ have outlined most of the developments in the studies on aging of rubber. Thermo-oxidative aging of

rubber is believed to occur in two ways²⁴ : via main chain scission or crosslink scission. Veith²⁵, Tobolsky²⁶ and Horikx²⁷ have suggested that only main chain scission occurs during aging and a later study by Dunn and Scanlan²⁸ has confirmed this idea. But developments in the structural characterization of natural rubber vulcanizates² have led Calclough and coworkers²⁴ to study the oxidative aging of rubber in more detail and they have reported the occurrence of crosslink scission during aging. Blackman and McCall²⁹ have reported the structural changes in NR vulcanizates during thermal aging and their effect on fatigue life. One of the objectives of the present study is to correlate the changes in tensile properties and tear resistance of NR vulcanizates during aging with the changes in their network structure including the extent of main chain scission.

In recent years fracture of rubber has been gaining attention and various studies on fracture have been reported¹⁰⁻¹⁹. These theoretical studies are now being supplemented by microscopic observations of the fracture surfaces^{137, 162-164} using scanning electron microscope as the tool. It is well known that the weakening of the rubber matrix during aging affects its failure properties. Hence the second objective of the present work is to study the effect of thermo-oxidative aging on the fracture mode of rubber using SEM.

The parameters included in this study are : (1) effect of vulcanizing system, (2) effect of reinforcing carbon black and (3) effect of antioxidant. The formulations of the mixes are given in Table IV.1. The rheographs of the mixes are shown in Figures IV.1 and IV.2. Aging of the tensile and tear test specimens was done at 100°C upto a period of 48 hr in a Blue M F.C 712 model air oven. Samples were withdrawn from the oven at different intervals and their tensile strength, tear resistance and chemical characteristics determined. The shape of the test specimens were already given in Chapter III (Figure III.4A). The fracture surfaces were carefully cut from the failed test specimens as shown in Figure III.4A.

The changes in tensile strength of the unfilled and filled vulcanizates with respect to the period of aging are given in Figures IV.3 and IV.4 respectively. In the case of the unfilled conventional (Conv.) vulcanizate, there is a progressive drop in tensile strength after 6 hr of aging, whereas the addition of 1 phr of phenyl- β -naphthylamine (PBNA) to the same mix causes the tensile strength to increase upto a period of 12 hr and then to drop. The rate of fall in tensile strength is almost the same in both cases, although the absolute values are always higher for the vulcanizate containing the antioxidant. In the case of the efficiently vulcanizing (EV) mix, the tensile strength increases to a maximum and then drops, although the extent and rate of decrease are much less pronounced than in the Conv. vulcanizates. The effect of antioxidant is more or

less similar to that in the Conv. vulcanizate, although the actual difference between the absolute values, caused by the presence of the antioxidant is different in the two cases. From Figure IV.3 it appears that the antioxidant is almost twice as effective in the Conv. system as in the EV system. The incorporation of carbon black affects the aging behavior appreciably, as is clearly shown in Figure IV.4. In all the cases there occurs a drop in tensile strength right from the beginning of aging. The decrease is abrupt in the early stages of aging for the Conv. vulcanizates, which slows down as the aging progresses. The antioxidant protects the vulcanizate initially, but the level of protection decreases as the aging progresses. The EV system also shows the same type of behavior. The vulcanizate without antioxidant shows a fairly rapid reduction in tensile strength, which levels off as the aging is continued. As expected, the retention of tensile strength during aging is much higher in the EV than in the Conv. vulcanizates. Here also the level of protection obtained from the antioxidant is more pronounced during the initial periods of aging.

Figure IV.5 gives the chemical crosslink density of the unfilled vulcanizates, plotted against the period of aging. As expected, the Conv. system has a higher crosslink density and aging causes an initial increase in its crosslink density, which decreases as the aging is continued. The increase is much

more pronounced, when antioxidant is present in the system. It is also noted from Figure IV.5 that the drop in crosslink density takes place only after a longer period of aging, when antioxidant is present. Although the initial crosslink density of the EV vulcanizate is lower than that of the Conv. vulcanizate, it increases steadily during aging and at the end of the aging period its crosslink density exceeds that of the Conv. vulcanizate. The presence of antioxidant in the EV vulcanizate causes a higher level of crosslink density throughout the aging period, although the difference is not as marked as in the case of the Conv. vulcanizates. The changes in the crosslink density of the carbon black-filled vulcanizates during aging are given in Figure IV.6. The drop in crosslink density during aging starts at a period earlier than that observed in the case of the unfilled vulcanizates. Here also the antioxidant helps in retaining the crosslink density at a higher level throughout the aging period. In the filled EV vulcanizate the crosslink density remains almost constant, although the presence of antioxidant causes an increase.

A comparative study of Figures IV.3 and IV.4 with Figures IV.5 and IV.6, shows that changes in crosslink density alone cannot explain the fall in tensile strength of vulcanizates. Except in the Conv. vulcanizate containing no antioxidant, in all the cases the crosslink density at the end of the aging period of 48 hr is either the same as or higher than the original value. But there is a definite decrease in tensile strength.

This is especially true in the case of the black-filled vulcanizates. The sol content of a vulcanizate, as determined in these studies, is a direct measure of the extent of main chain scission. Figures IV.7 and IV.8 are the plots of sol content as a function of aging period in the case of the unfilled and filled vulcanizates respectively. The Conv. vulcanizates undergo a higher level of chain scission. The rate of chain scission is slow initially, but increases rapidly as the aging proceeds, thereby indicating the autocatalytic nature of the scission reaction. The presence of the antioxidant helps in minimizing chain scission during the early periods of aging, but its activity is reduced as the aging is continued. The EV vulcanizates show almost a linear increase in chain scission, but the absolute values of sol content are lower than the Conv. vulcanizates. The effect of antioxidant is not significant in this system. With the addition of HAF carbon black there is almost a five-fold increase in main chain scission. The Conv. vulcanizate shows a linear increase in sol content right from the beginning. It may be noted here that the initial sol content of these vulcanizates are much higher than those in the unfilled ones. Hence it can be assumed that the radicals capable of catalyzing the scission reaction are already present in the vulcanizate in sufficient quantity so that there is a steady increase in the sol content right from the beginning of aging. But here again antioxidant is found to reduce the rate of chain scission during the initial periods of aging. The

filled EV vulcanizates show a much lower rate of chain scission throughout the aging period. It is also found from Figure IV.8 that the effect of antioxidant is not significant in the EV vulcanizates.

From the above results it is clear that the fall in tensile strength of the rubber vulcanizates during aging is mainly due to main chain scission. The effect of changes in crosslink density is only marginal.

Modulus at 300% elongation can be considered an index of crosslink density of vulcanizates. Therefore, changes in crosslink density of vulcanizates during aging is reflected more in their modulus values than in any other property. Figures IV.9 and IV.10 are the plots of modulus against aging period in the case of the unfilled and filled vulcanizates respectively. The Conv. vulcanizates show broad maxima and their crosslink density values also show a similar trend. The EV vulcanizates show a continuous increase in modulus, which is supported by the changes in their crosslink density. The increase in modulus on aging is observed in the black-filled vulcanizates also. In the Conv. vulcanizates 300% modulus values could not be obtained as its elongation at break was below 300% beyond the 6 hr aging period. But with the addition of antioxidant modulus curve shows a maximum and then drops. A comparison of Figures IV.9 and IV.10 shows that the percentage increase in modulus during aging is more in the unfilled vulcani-

zates. From Figures IV.5 and IV.6 it is also seen that the increase in crosslink density is more pronounced in the unfilled vulcanizates, thereby confirming the idea that the increase in modulus during the early periods of aging is due to the increase in the crosslink density. The increase in crosslink density during aging is contributed by both oxidative crosslinking^{28,165} and by the postcuring reactions. The large increase in crosslink density in the case of the Conv. vulcanizates can be ascribed to : (1) the presence of a larger amount of free sulfur, which results in postcuring and which is evident from the increase in the value of combined sulfur, $[Sc]$, as shown in Table IV.2 and (2) the maturation of polysulfidic linkages which causes the formation of more number of crosslinks with a lower sulfur rank, which is evident from the changes in the percentage of the polysulfidic crosslinks and sulfide sulfur during aging, as shown in Table IV.2. The decrease in modulus during the latter part of the aging period is due to the general weakening of the matrix resulting from extensive chain scission.

Elongation at break (EB) is a more sensitive measure of the extent of aging as seen from Figures IV.11 and IV.12. Figure IV.11, where elongation at break of the unfilled vulcanizates are plotted as a function of the aging period, shows a steady decrease in EB with aging. Only the EV vulcanizate containing the antioxidant shows a certain level of retention of EB, but here also the EB drops as the aging is continued.

The superior aging resistance of the EV vulcanizates and the more pronounced effect of antioxidant in the Conv. vulcanizates are also evident from Figure IV.11. The drop in elongation on aging is caused mainly by the weakening of the matrix as a result of the chain scission. The crosslink maturation reactions, which result in the conversion of the flexible polysulfidic linkages into the less flexible di- and monosulfidic linkages also might be contributing towards the decrease in elongation. The black-filled vulcanizates show a more drastic reduction in EB during the early periods of aging (Figure IV.12), which levels off as the aging is continued. The better aging resistance of the more stable network of the EV vulcanizates and the effect of antioxidant on aging are evident from this figure also.

The changes in tear resistance during aging, are more or less similar to those in tensile strength. Figure IV.13 is a plot of the tear resistance of the unfilled vulcanizates against aging period. The Conv. vulcanizate shows a steady decrease in tear resistance, although the rate of decrease is not as high as in the case of tensile strength. The antioxidant helps in retarding the fall in tear resistance during aging. The EV vulcanizates do not show any change in tear resistance throughout the aging period. Here the effect of antioxidant is not significant. In the case of the black-filled vulcanizates there is a drastic decrease in tear resistance during the early periods of aging (Figure IV.14), the change being more pronounced in the Conv.

vulcanizate. The rate of fall in tear resistance is found to decrease as the aging is continued. The vulcanizate containing antioxidant shows a higher retention of tear resistance throughout the aging period. It appears that, during aging, tear resistance is affected mostly by chain scission than by changes in crosslink density.

From the above discussion it is clear that, during aging, degradation of rubber results from two types of reactions; chain scission and crosslink scission. The initial increase in tensile strength modulus and tear resistance is caused by an increase in crosslink density whereas as the aging proceeds, the effect of chain scission overshadows the effect of an increased crosslink density. Moreover, the crosslink density also falls when the aging is continued for a longer period. Antioxidant helps in retarding both crosslink scission and chain scission. Carbon black causes an increase in the rate of chain scission and crosslink scission. This is in agreement with the observations of Winn and coworkers³⁷ who found that carbon black accelerates the oxygen uptake of sulfur-cured rubber and that the reaction is accompanied by a rapid degradation of the polymer. These investigators have shown that the rate of oxidation of carbon black-loaded vulcanizates is directly proportional to the amount of carbon surface. Several possible mechanisms for the pro-oxidant behavior of carbon black in rubber have been proposed³⁸⁻⁴⁰. The explanation by Shelton and Wickham⁴¹ which

involves surface catalysis of the reaction between the rubber and oxygen by carbon black seems to be the most probable one. In the present study it is also observed that the effect of carbon black is more pronounced in the Conv. vulcanizates. Hence it is believed that the catalysis of oxidation of rubber by carbon black involves the polysulfidic linkages and cyclic sulfides in the network, whose concentration is much higher in the Conv. vulcanizates than in the EV. The decrease in the rate of fall of tensile strength, elongation and tear resistance and crosslink density of the black-filled vulcanizates as the aging is continued, is probably due to the decrease in the rate of penetration of oxygen into the inner layers of the vulcanizates. Because of the higher rate of oxygen uptake of black-filled vulcanizates, penetration of oxygen to the inner layers will be slower in them. This causes the presence of a fairly undegraded inner layer of rubber in the vulcanizate. During the tensile and tear tests most of the applied load is carried by this undegraded layer. As the size of this layer of rubber is reduced only slowly, there occurs a decrease in the rate of fall of these properties during the latter part of the aging period. The SEM studies reported later in this part support this idea. In the case of the unfilled vulcanizates, the rate of oxygen uptake is much slower and hence the rate of penetration of oxygen to the inner layers is not hindered as in the case of the black-filled vulcanizates. Hence chances for the

presence of an undegraded inner layer are less and therefore during aging no decrease in the rate of fall in properties was observed.

SEM STUDIES

In the present study the main objective is to find out the effect of the weakening of the matrix resulting from oxidative degradation, on the fracture surface topography. Both tensile and tear fracture surfaces of the various vulcanizates both before and after aging for 36 hr have been examined, because the inherent differences in the aging resistance of the various vulcanizates are reflected more after the 36 hr period as seen from Figures IV.3 to IV.14. The various photomicrographs are shown in Figures IV.15 to IV.40.

Tensile fracture : Figures IV.15 and IV.16 are the photomicrographs of the fracture surfaces of the unfilled Conv. vulcanizate. The surface shows a rough zone (Figure IV.15) followed by a comparatively smooth region (Figure IV.16). The other unfilled vulcanizates used in this study also show more or less the same surface characteristics. The presence of antioxidant or the change in the vulcanizing system do not cause any notable change in the mode of fracture as seen in SEM. Although the application of tensile force is considered to be uniform throughout the test specimen the occurrence of natural

flaws and edge nicks in the tensile test specimen, which are quite unavoidable, causes stress concentration in certain localized areas. Failure starts at these points, where the actual stress experienced is much higher than that in the bulk of the specimen. Because of the high stress-rupture and the complex stress distribution around the natural flaws, the fracture surface become rough at the point of initiation. Gent and Lindley¹⁶⁶ suggested that the high stress realized near the flaws would be adequate enough to produce cavitation in a rubber of conventional modulus and that this may be the cause of the roughness developed around the tip. Once the failure starts, it proceeds as a catastrophic tear giving rise to a comparatively smooth surface with a number of tear lines. The SEM tensile fractographs of the unfilled vulcanizates after aging are shown in Figures IV.17 to IV.20. The low tensile strength of the Conv. unfilled vulcanizate after aging is reflected in its fracture surface (Figure IV.17). There is no rough zone. But the Conv. vulcanizate containing antioxidant, as is evident from its fractograph (Figure IV.18), shows a rough zone although the size of this zone appears to be less than that of the original vulcanizate. The fracture surface of the unfilled EV vulcanizate (Figure IV.19) shows a few tear lines, but no rough zone, although its tensile strength after aging is almost the same as that of the original sample. This behavior appears unexpected. However the unfilled EV vulcanizate containing PBNA, after aging, shows on its fracture surface a rough zone followed

by a number of tear lines (Figure IV.20) and its tensile strength also is high.

The addition of carbon black makes the matrix stiffer. In natural rubber, though the tensile strength is not improved significantly by carbon black, the mode of stress distribution during tensile testing is different from that in the unfilled vulcanizates. Hence the fracture surface shows a much different pattern. Figure IV.21 is the SEM photograph of the tensile fracture surface of the black-filled Conv. vulcanizate. The whole surface appears rough with a large number of curved tear lines. The regions of high strength, resulting from strong polymer-filler interaction, prevent the fracture from proceeding straight. The addition of antioxidant does not cause any notable change in the fracture surface. However, the fracture surface of the black-filled EV vulcanizate (Figure IV.22) is slightly different from that of the Conv. vulcanizate. The surface is generally rough as in the case of the Conv. vulcanizate, but it shows a prominent tear path. Here also addition of antioxidant does not cause any appreciable difference in the surface characteristics. Figures IV.23 to IV.26 are the SEM photographs of the tensile fracture surfaces of the black-filled vulcanizates, which underwent aging for 36 hr. The Conv. black-filled vulcanizate shows a much smoother surface giving a tear path with secondary tear lines near the centre of the specimen. It may be noted that in this specimen, only the innermost layer is not affected much by aging and hence this region, which is

comparatively stronger, gives rise to a slightly rough surface. The major portion of the specimen, however, is weak and hence gives rise to a smooth surface. The presence of antioxidant helps in retarding oxidative degradation and hence the Conv. vulcanizate containing PBNA shows a slightly more rough surface. (Figure IV.24). The EV vulcanizate containing carbon black shows a higher level of retention of tensile strength during aging, though the absolute value is lower. The fracture surface is rough (Figure IV.25), although not as rough as that of the same vulcanizate before aging. Here the effect of antioxidant is not notable as is evident from the SEM fractograph of the black-filled EV vulcanizate containing PBNA (Figure IV.26).

Tear fracture : The dependence of tear fracture topography on the degree of aging and hence on the strength of the matrix is not very clear. It is difficult to correlate the tear strength of the vulcanizate with its fracture surface topography. However, it is believed that the mechanism of fracture propagation is affected by the strength of the matrix and hence the extent of aging will be reflected more in the mode of propagation of tear than in the other surface characteristics. Figures IV.27, to IV.40 are the SEM photographs of the tear fracture surfaces of the various vulcanizates before and after aging. The fractograph of the original unfilled Conv. vulcanizate (Figure IV.27) shows a main tear path with secondary tear lines. The main tear

path is the region of the highest stress concentration.

Figure IV.28 shows a magnified image of the tear path. The addition of antioxidant does not cause any appreciable change in tear fracture topography. However, when the vulcanizing system is changed to EV, the fracture surface also shows some difference. The SEM photograph of the tear fracture surface of the unfilled EV vulcanizate (Figure IV.29) does not show any large tear path. Instead, it shows a large number of thinner tear lines, showing thereby the different nature of stress distribution in this vulcanizate. Here also the presence of antioxidant does not have any significant effect on the fracture surface characteristics. The tear fractograph of the unfilled Conv. vulcanizate after aging is shown in Figure IV.30. The size of the main tear path is less, but the number of secondary tear lines is more. A magnified image of a portion of the tear path (Figure IV.31) shows that the tear proceeds in a stick-slip manner. The Conv. vulcanizate with antioxidant, shows a better retention of tear strength and its fracture surface shows more number of tear paths (Figure IV.32). The unfilled EV vulcanizate shows a slight improvement in tear resistance during aging and its tear fracture surface, as shown in Figure IV. 33, has become more or less similar to that of the original Conv. vulcanizate. However, the secondary tear lines are less in number. The EV vulcanizate containing PBNA, after aging, gives rise to a stick-slip type tear as shown in Figure IV.34. The secondary tear lines which join the main tear path are very feeble.

The addition of reinforcing carbon black causes the formation of a large number of small curved tear lines as shown in Figure IV.35, which is the SEM tear fractograph of the black-filled Conv. vulcanizate. On a closer examination, the surface was found to have a layered structure (Figure IV.36) with the layers aligned in the direction of tear. Addition of antioxidant or changing the vulcanization system to EV do not cause any change in these surface characteristics. But upon aging, the strength of the black-filled Conv. vulcanizate decreases appreciably and this decrease is reflected in their fracture surface topography. The Conv. vulcanizate containing no antioxidant gives rise to a smooth fracture surface as shown in Figure IV.37, whereas the one containing PBNA shows a few tear lines (Figure IV.38) and a slightly higher tear resistance. The black-filled EV vulcanizates show better retention of tear resistance during aging and their fracture surfaces (Figures IV.39 and IV.40) are also more or less similar to the original tear fracture surface.

TABLE IV.1

FORMULATIONS OF THE MIXES

| MIX | A | B | C | D | E | F | G | H |
|----------------------------------|------|------|------|------|------|------|-----|-----|
| Natural rubber | 100 | 100 | 100 | 100 | 100 | 100 | 100 | 100 |
| Zinc oxide | 5 | 5 | 5 | 5 | 5 | 5 | 5 | 5 |
| Stearic acid | 2 | 2 | 2 | 2 | 2 | 2 | 2 | 2 |
| PEBA | - | 1 | - | 1 | - | 1 | - | 1 |
| HAF black (N 330) | - | - | - | - | 50 | 50 | 50 | 50 |
| Naphthenic oil | - | - | - | - | 5 | 5 | 5 | 5 |
| CBS | 0.6 | 0.6 | 3.5 | 3.5 | 0.6 | 0.6 | 3.5 | 3.5 |
| Sulfur | 2.5 | 2.5 | 0.5 | 0.5 | 2.5 | 2.5 | 0.5 | 0.5 |
| Optimum cure time at 150°C, min. | 11.0 | 12.0 | 18.0 | 17.0 | 10.5 | 12.0 | 9.0 | 8.0 |

TABLE IV.2

CHEMICAL CHARACTERIZATION OF THE VULCANIZATES BEFORE AND AFTER AGING AT 100°C

| AGING PERIOD (HR) | CHARACTERISTICS | A | B | C | D | E | F | G | H |
|-------------------|--|------|------|------|------|------|------|------|------|
| 0 | $[2M_c, \text{chem}]^{-1}$ (mmol/kg RH) | 36.3 | 34.5 | 23.7 | 26.0 | 28.8 | 30.8 | 21.5 | 21.8 |
| | Polysulfidic linkages, (%) | 73 | 70 | 15 | 21 | 58 | 62 | 25 | 27 |
| | Combined sulfur (mmol/kg RH) | 655 | 633 | 150 | 151 | 559 | 561 | 139 | 141 |
| | Sulfide sulfur (mmol/kg RH) | 46 | 55 | 1 | 1 | 46 | 48 | 5 | 6 |
| 6 | $[2M_c, \text{chem}]^{-1}$ (mmol/kg RH) | 43.8 | 50.1 | 26.9 | 28.6 | 35.2 | 43.8 | 21.2 | 22.0 |
| | Polysulfidic linkages, (%) | 73 | 64 | 19 | 31 | 60 | 67 | 24 | 21 |
| | Combined sulfur (mmol/kg RH) | 718 | 714 | 150 | 150 | 690 | 683 | 138 | 142 |
| | Sulfide sulfur (mmol/kg RH) | 53 | 53 | 3 | 3 | 52 | 53 | 7 | 5 |

TABLE IV.2 (CONT'D.)

| AGING PERIOD (HR) | CHARACTERISTICS | A | B | C | D | E | F | G | H |
|-------------------|---|------|------|------|------|------|------|------|------|
| 12 | $[2\text{MC}_2\text{ chem}]^{-1}$ (mmol/kg RH) | 43.7 | 52.7 | 27.5 | 30.1 | 31.4 | 40.7 | 20.8 | 25.0 |
| | Polysulfidic linkages, (%) | 65 | 62 | 15 | 18 | 49 | 57 | 22 | 30 |
| | Combined sulfur (mmol/kg RH) | 718 | 717 | 152 | 150 | 705 | 696 | 143 | 148 |
| | Sulfide sulfur (mmol/kg RH) | 51 | 54 | 1 | 1 | 54 | 54 | 7 | 5 |
| 24 | $[2\text{MC}_2\text{ chem}]^{-1}$ (mmol/kg RH) | 39.5 | 53.0 | 29.0 | 32.4 | 27.4 | 38.0 | 21.3 | 22.4 |
| | Polysulfidic linkages, (%) | 64 | 61 | 18 | 21 | 27 | 52 | 19 | 21 |
| | Combined sulfur (mmol/kg RH) | 710 | 718 | 149 | 149 | 707 | 709 | 142 | 140 |
| | Sulfide sulfur (mmol/kg RH) | 65 | 53 | 3 | 3 | 62 | 58 | 5 | 5 |

TABLE IV.2 (CONTD.)

| AGING PERIOD (HR) | CHARACTERISTICS | A | B | C | D | E | F | G | H |
|-------------------|------------------------------------|------|------|------|------|------|------|------|------|
| 36 | $[2Mc, chem]^{-1}$ (mmol/kg RH) | 30.7 | 43.0 | 28.5 | 30.7 | 22.8 | 31.2 | 21.6 | 23.2 |
| | Polysulfidic linkages, (%) | 36 | 55 | 14 | 15 | a | 38 | 18 | 22 |
| | Combined sulfur (mmol/kg RH) | 731 | 730 | 151 | 152 | 737 | 735 | 143 | 140 |
| | Sulfide sulfur (mmol/kg RH) | 64 | 64 | 4 | 2 | 56 | 60 | 5 | 5 |
| 48 | $[2Mc, chem]^{-1}$ (mmol/kg RH) | 24.8 | 36.1 | 29.3 | 31.5 | 23.3 | 30.2 | 20.3 | 21.7 |
| | Polysulfidic linkages, (%) | 51 | 51 | 15 | 15 | a | 30 | 14 | 12 |
| | Combined sulfur (mmol/kg RH) | 718 | 740 | 150 | 139 | 737 | 746 | 142 | 143 |
| | Sulfide sulfur (mmol/kg RH) | 85 | 73 | 4 | 2 | 56 | 75 | 6 | 5 |

a negligible

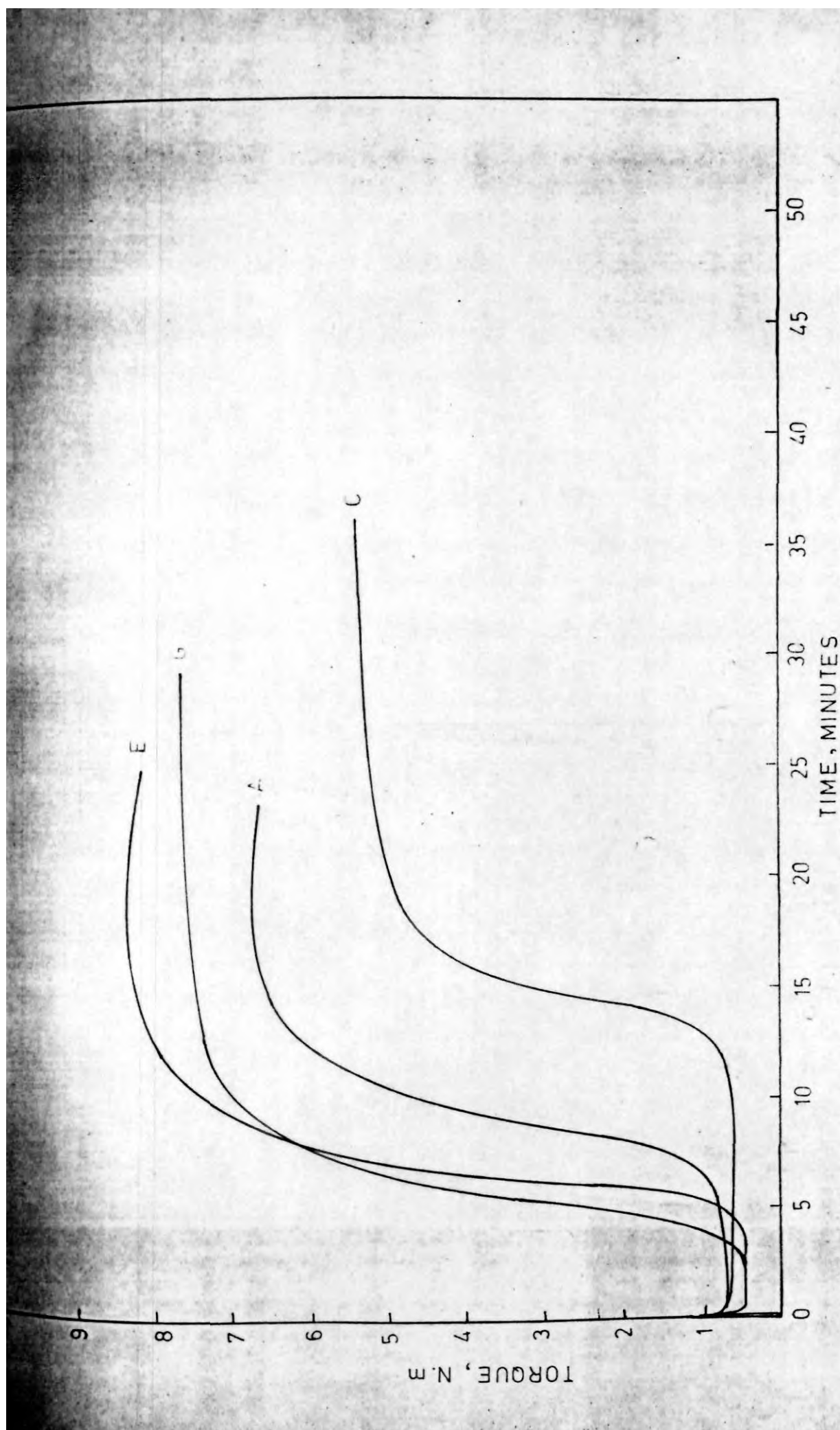


FIG IV.1. RHEOGRAPHS OF MIXES A,C,E AND G

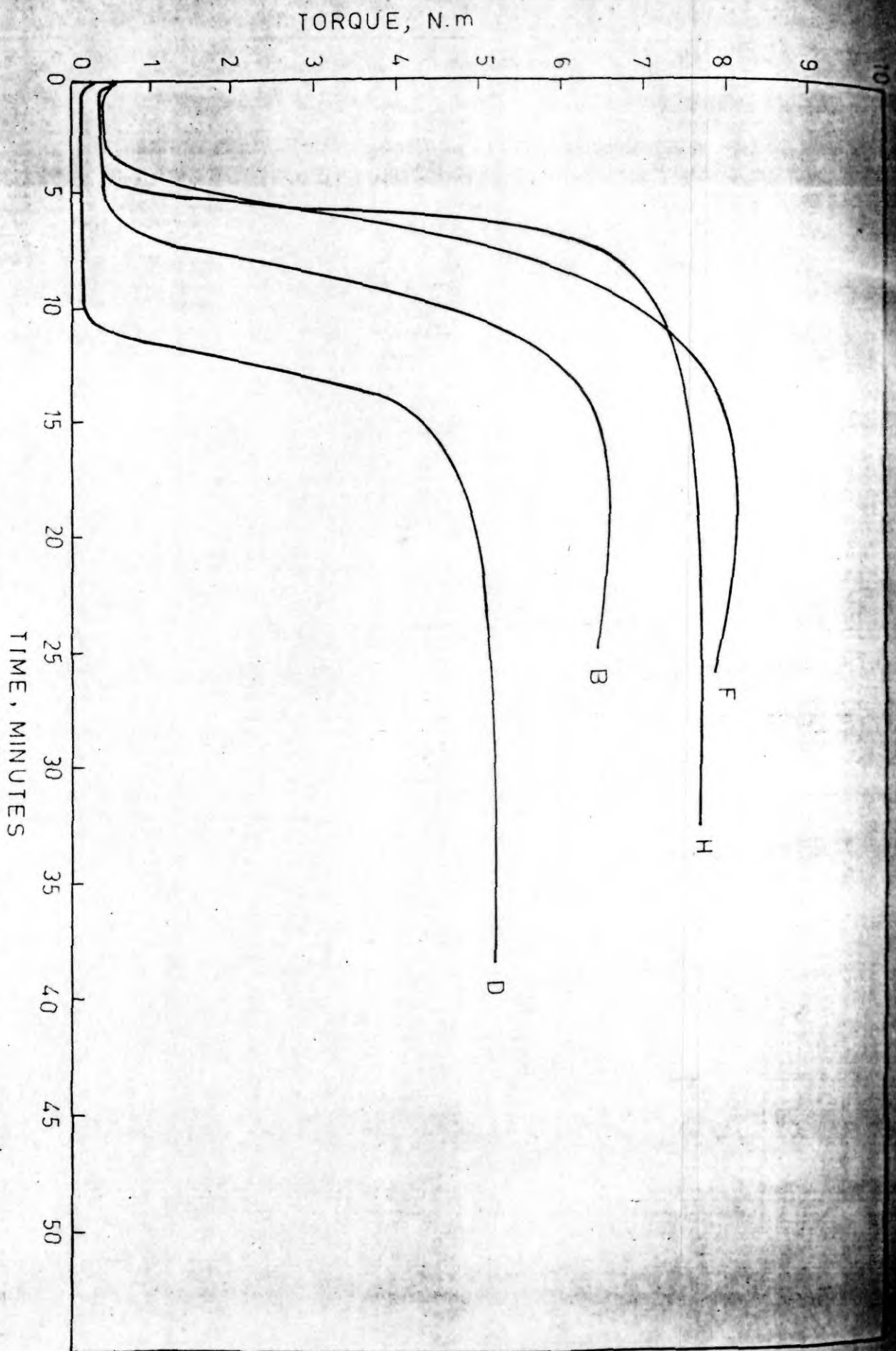


FIG. IV-2. RHEOGRAPHS OF MIXES B,D,F AND H

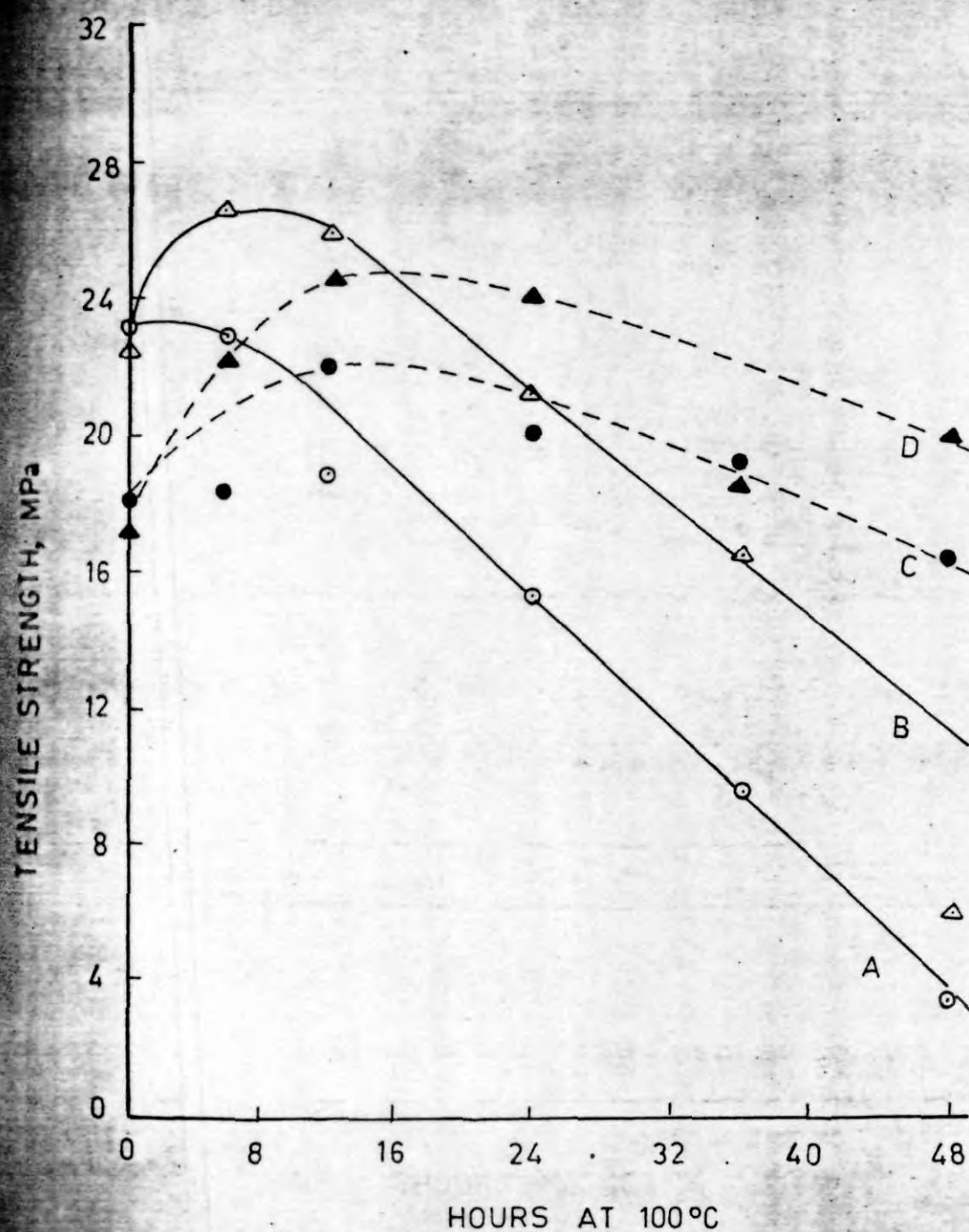


FIG. IV-3. CHANGES IN TENSILE STRENGTH OF THE UNFILLED VULCANIZATES DURING AGING.

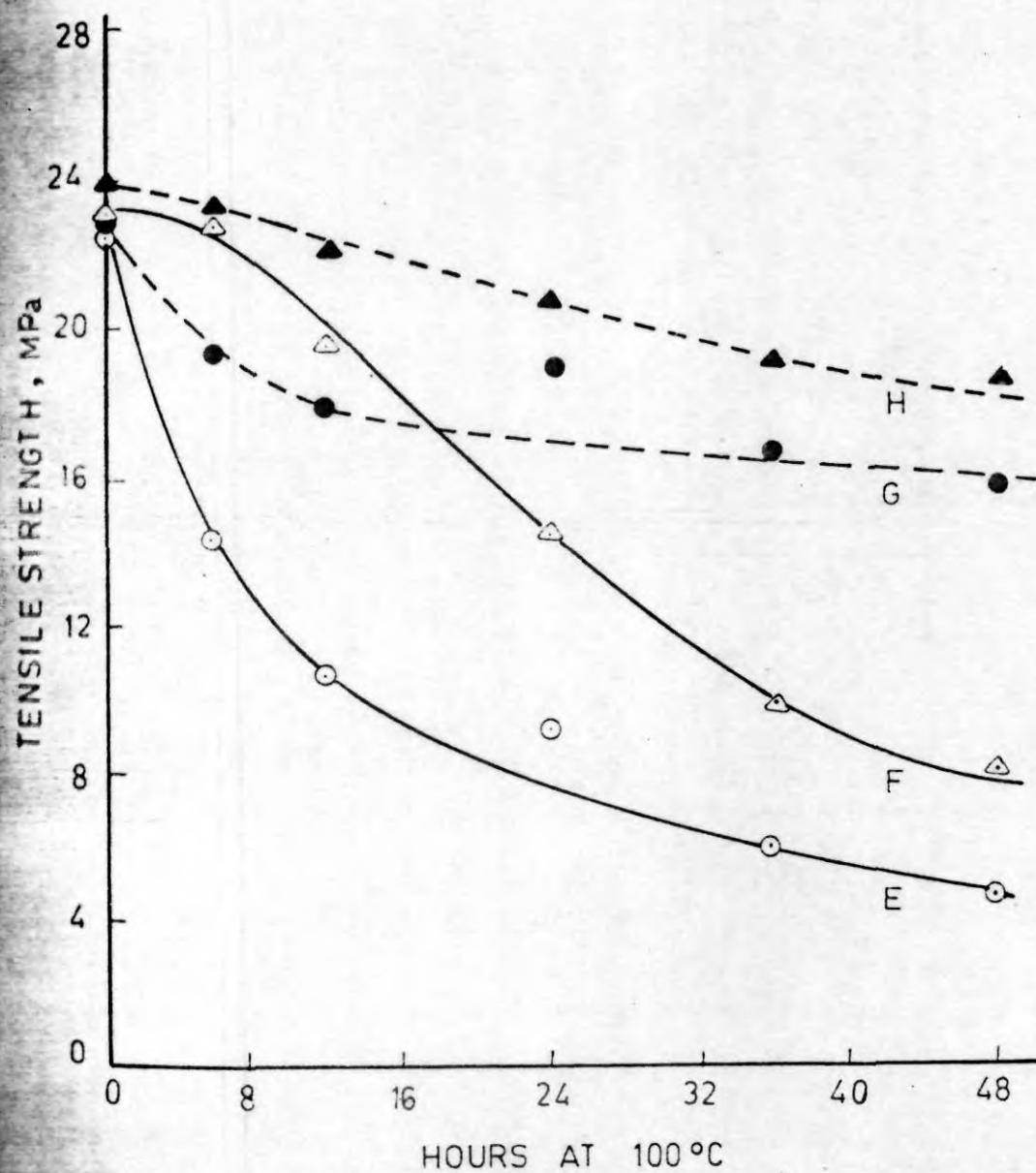


FIG. IV-4. CHANGES IN TENSILE STRENGTH OF THE FILLED VULCANIZATES DURING AGING

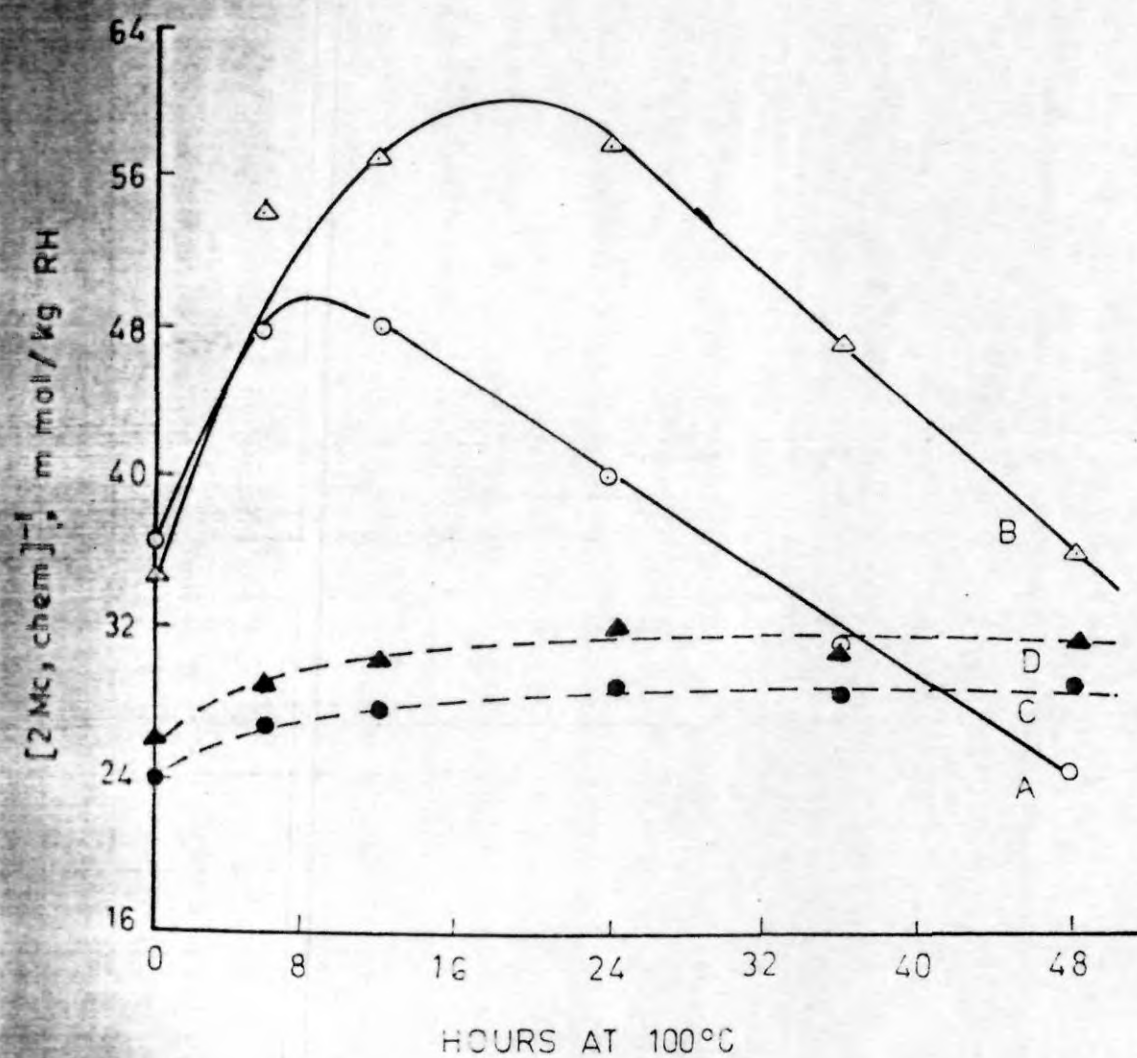


FIG.IV-5. CHANGES IN CROSSLINK DENSITY OF THE UNFILLED VULCANIZATES DURING AGING.

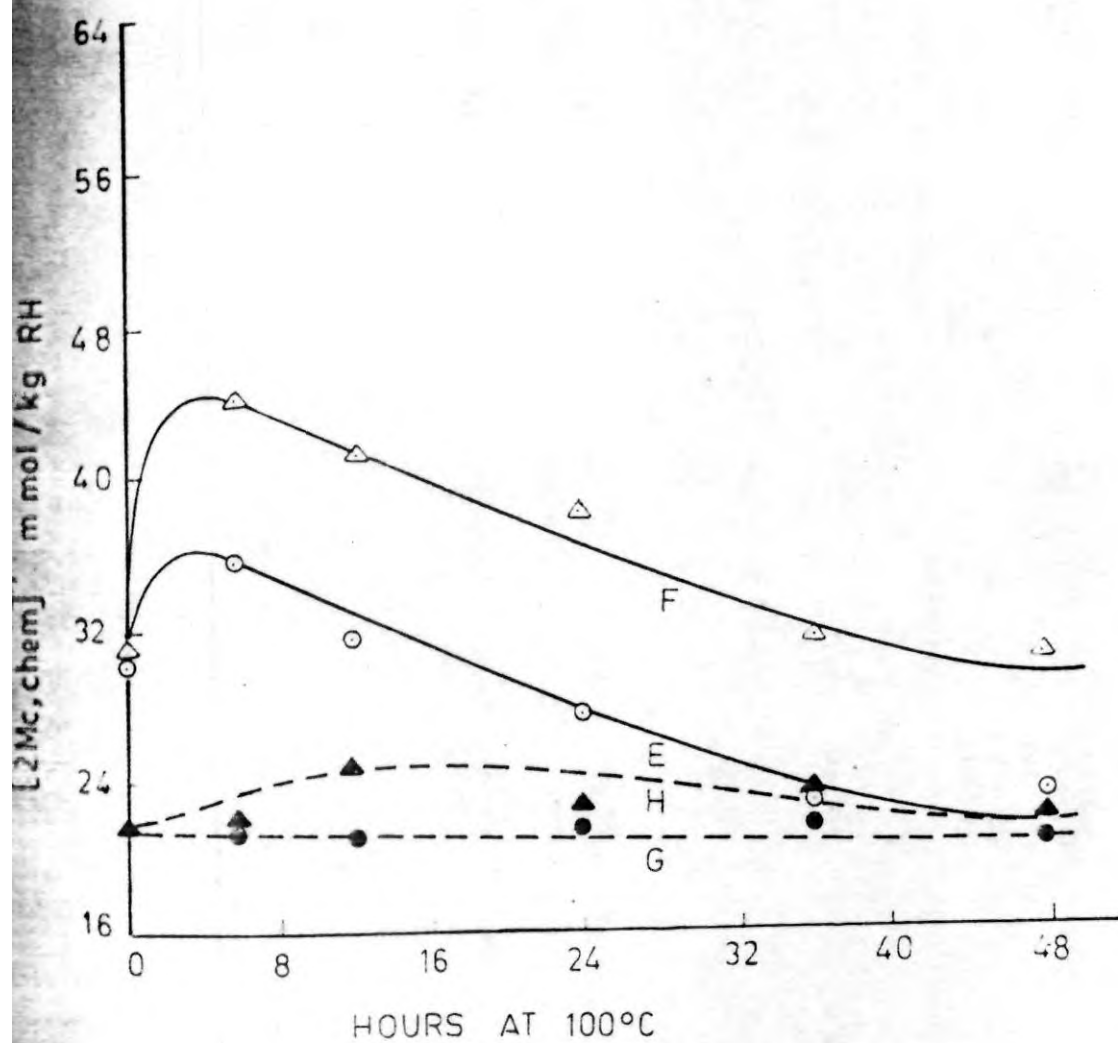


FIG. IV.6. CHANGES IN CROSS LINK DENSITY OF THE FILLED VULCANIZATES DURING AGING.

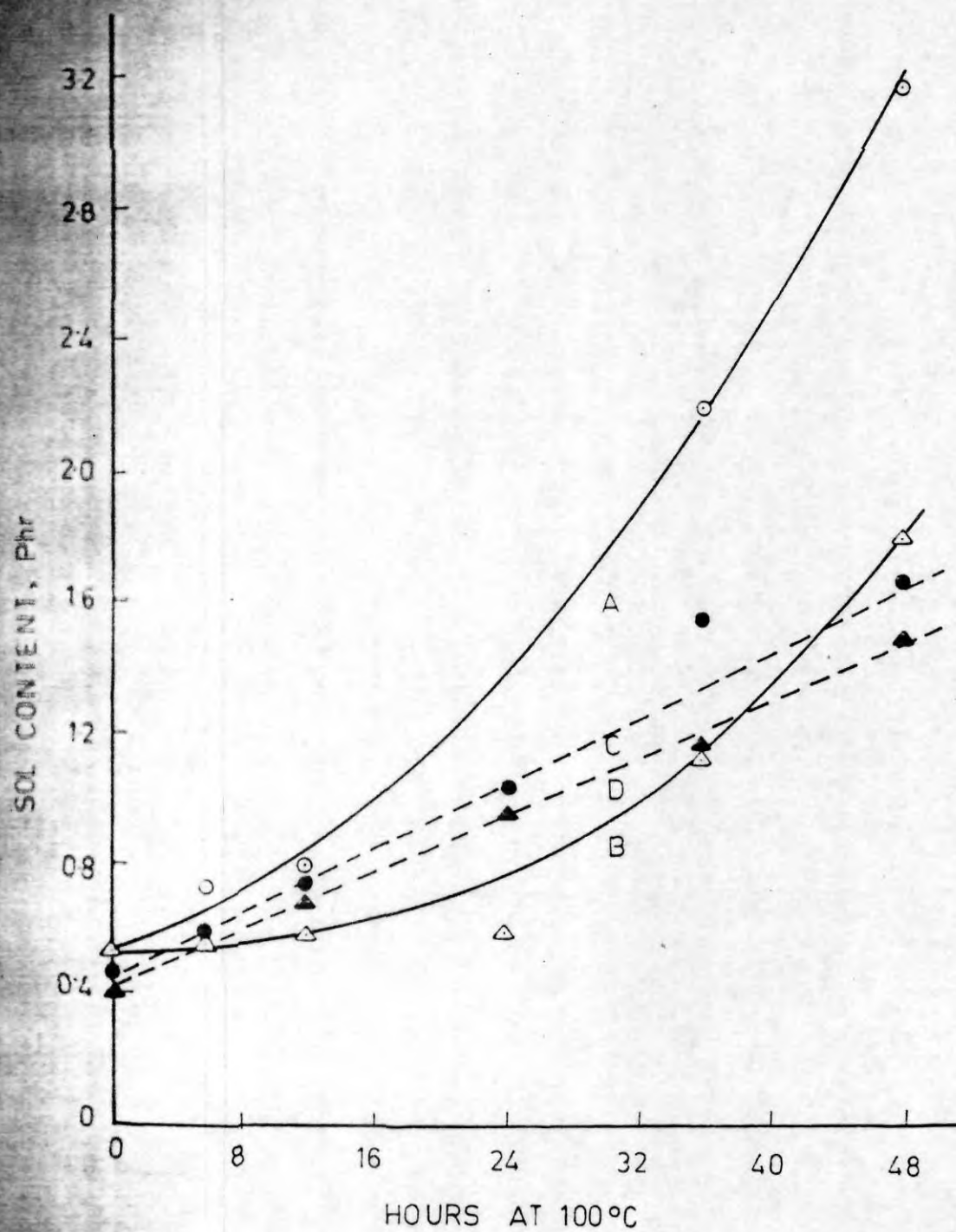


FIG. IV 7. SOL CONTENT OF THE UNFILLED VULCANIZATES PLOTTED AGAINST PERIOD OF AGING.

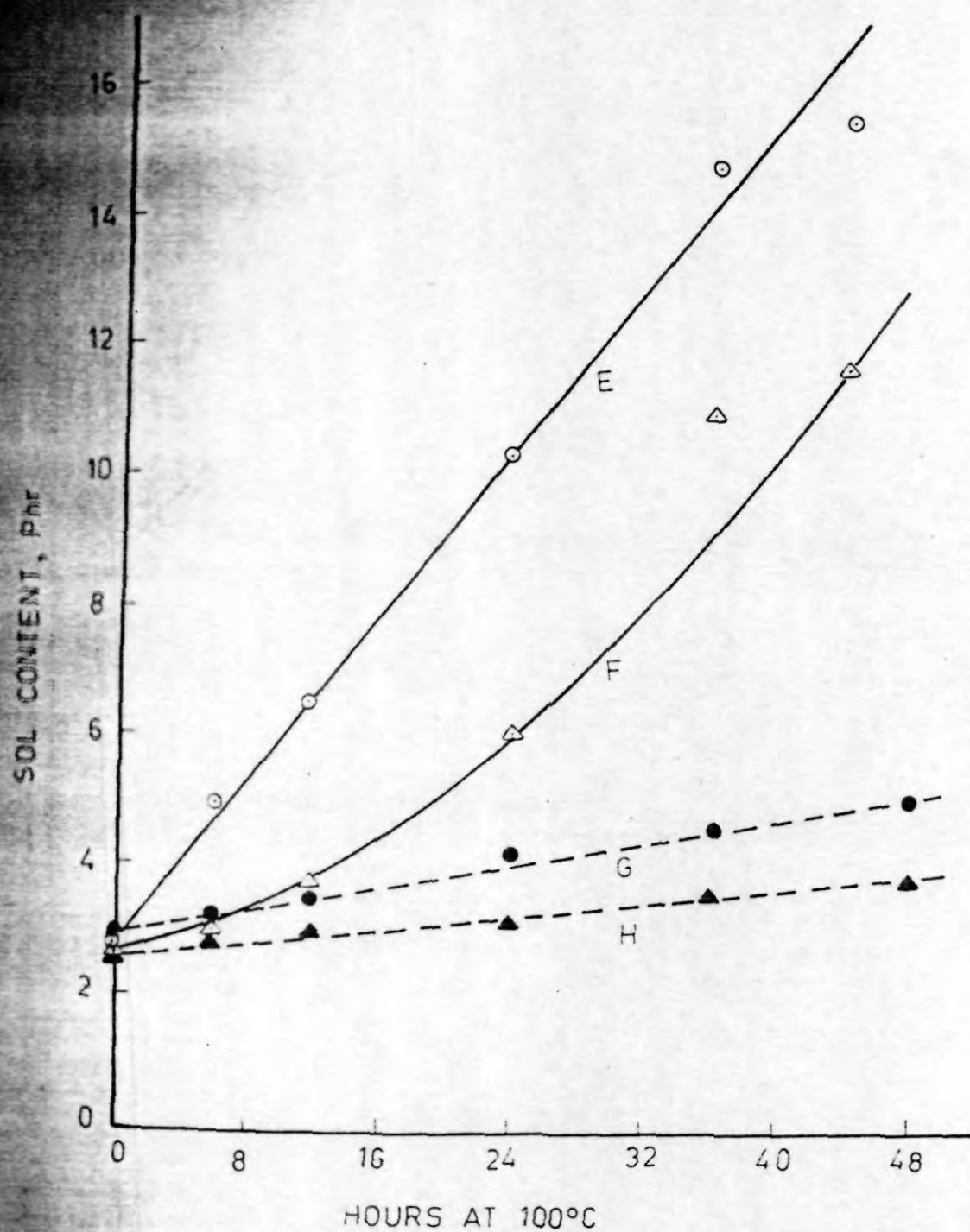


FIG. IV-8. SOL CONTENT OF THE FILLED VULCANIZATES
PLOTTED AGAINST PERIOD OF AGING.

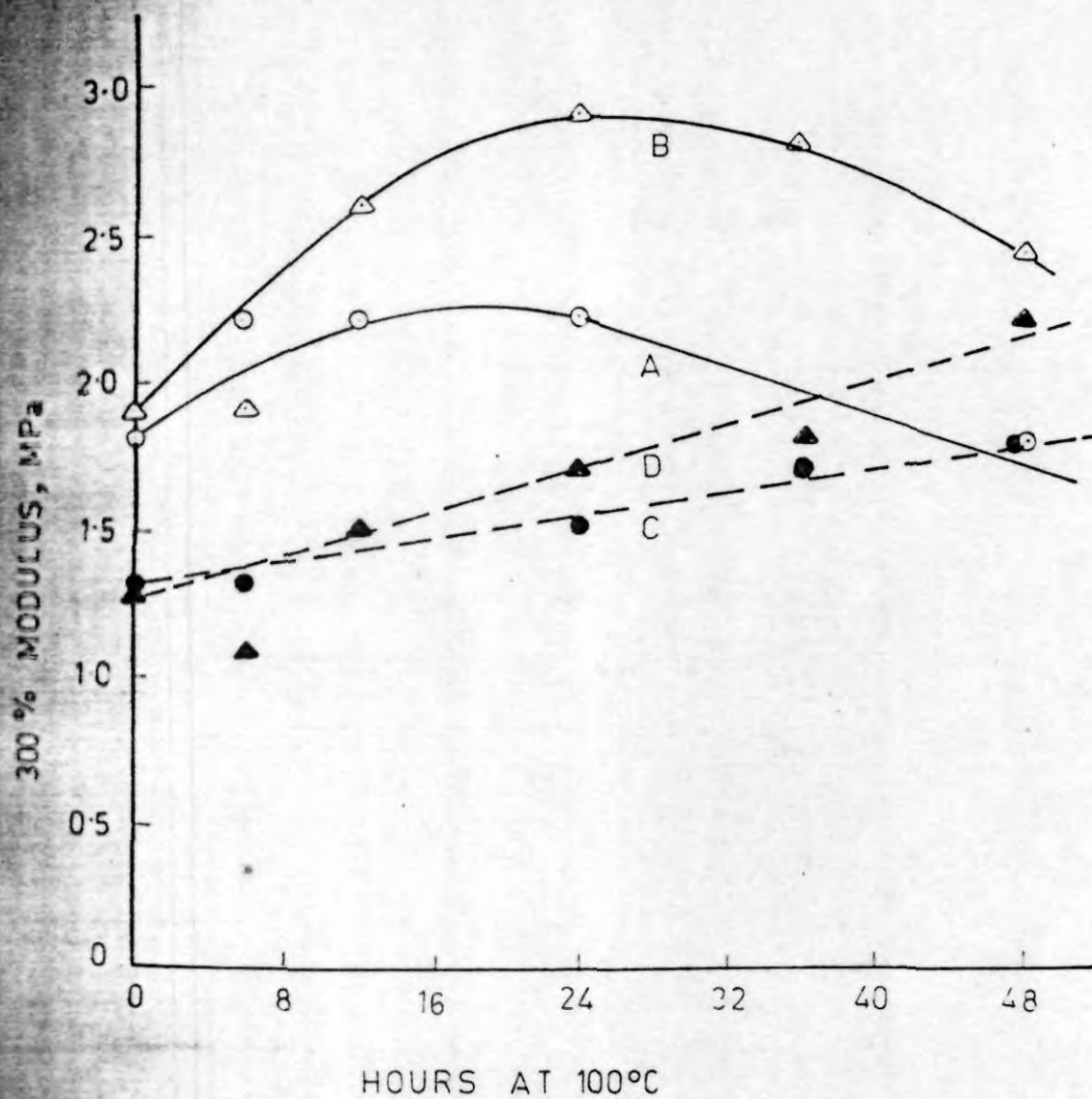


FIG. IV-9. VARIATION IN 300 % MODULUS OF THE UNFILLED VULCANIZATES DURING AGING

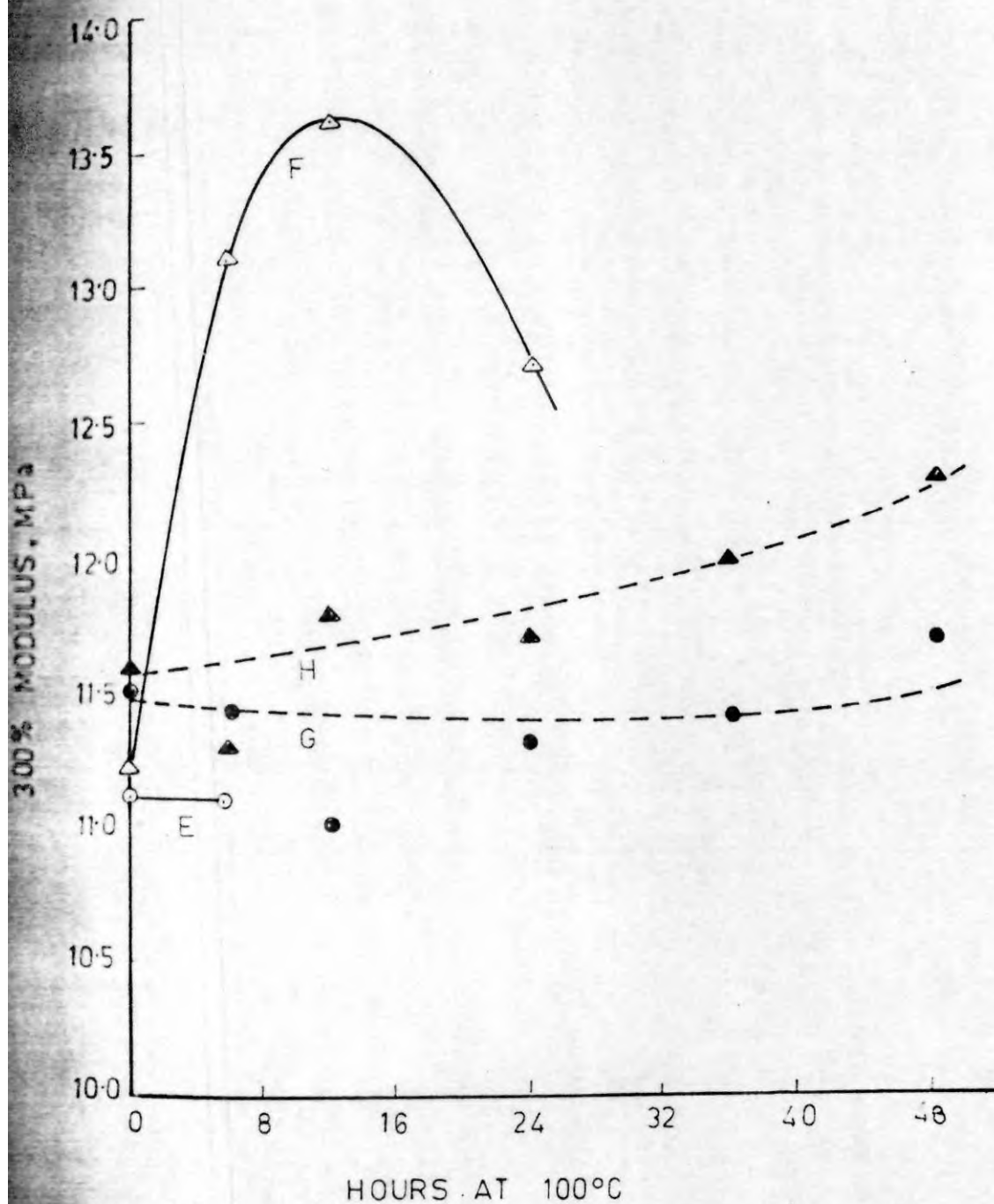


FIG. IV-10. VARIATION IN 300 % MODULUS OF THE FILLED VULCANIZATES DURING AGING.

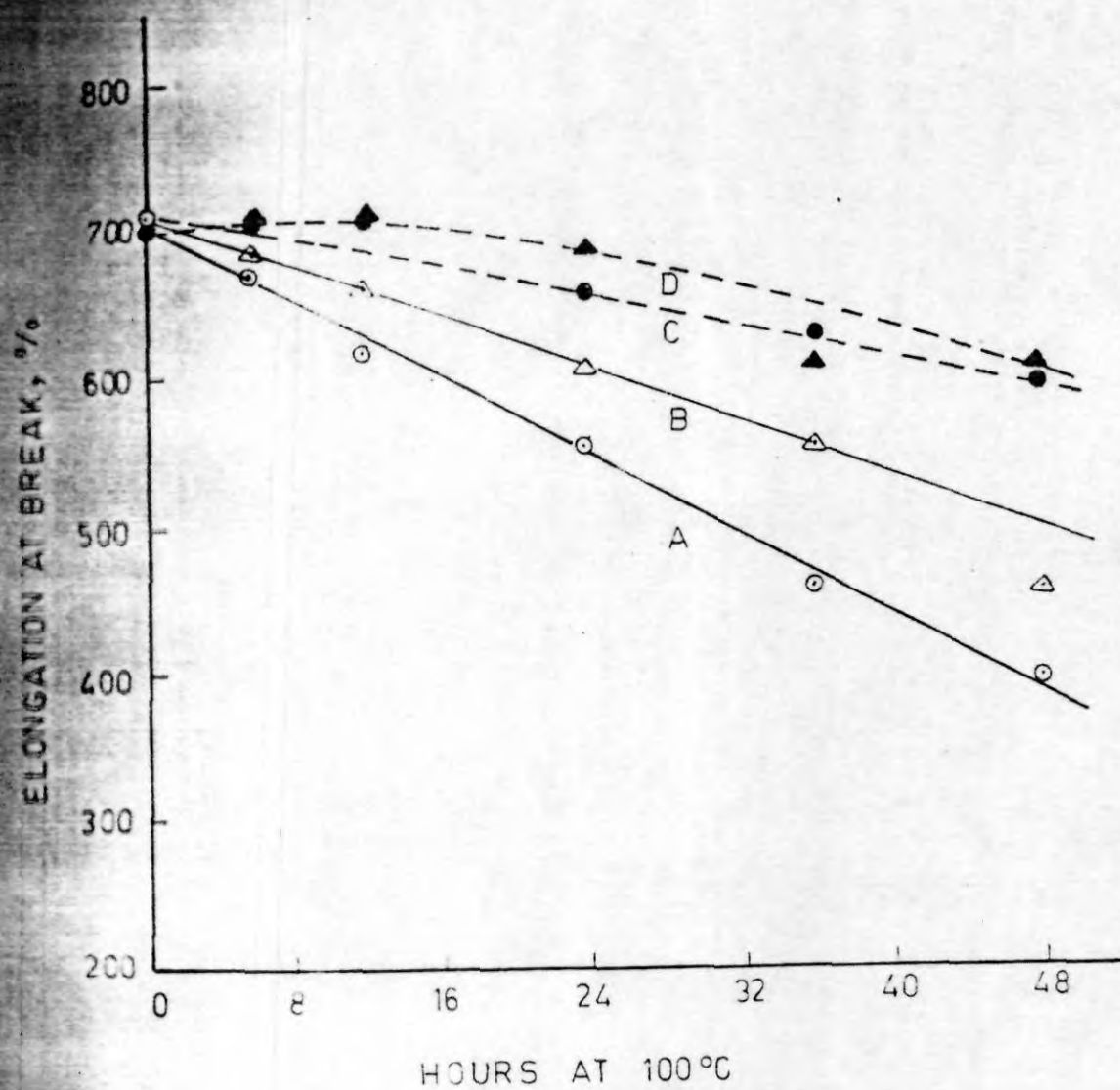


FIG. IV-11. CHANGES IN ELONGATION AT BREAK OF
THE UNFILLED VULCANIZATES DURING AGING

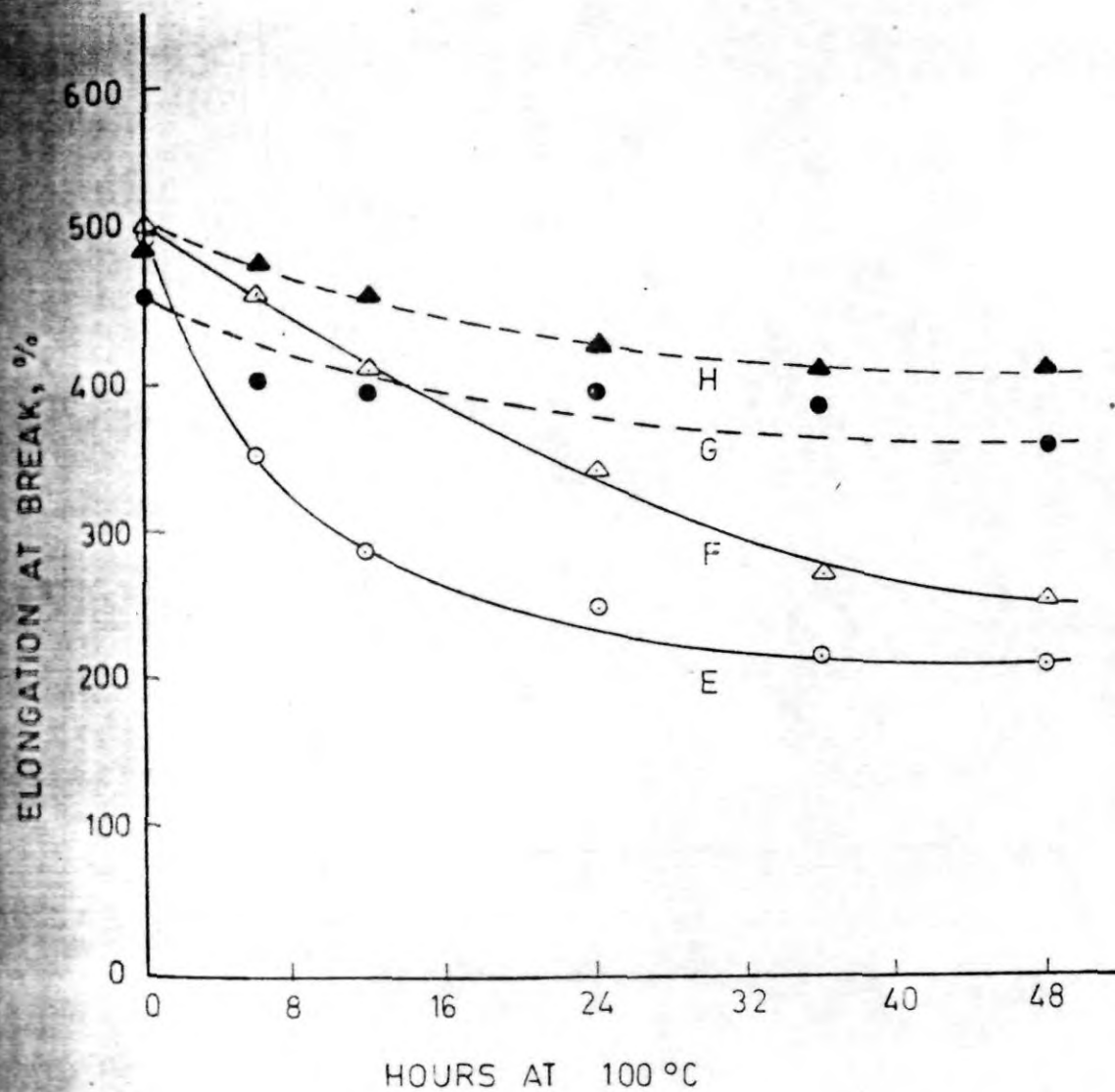


FIG. IV-12. CHANGES IN ELONGATION AT BREAK OF THE FILLED VULCANIZATES DURING AGING.

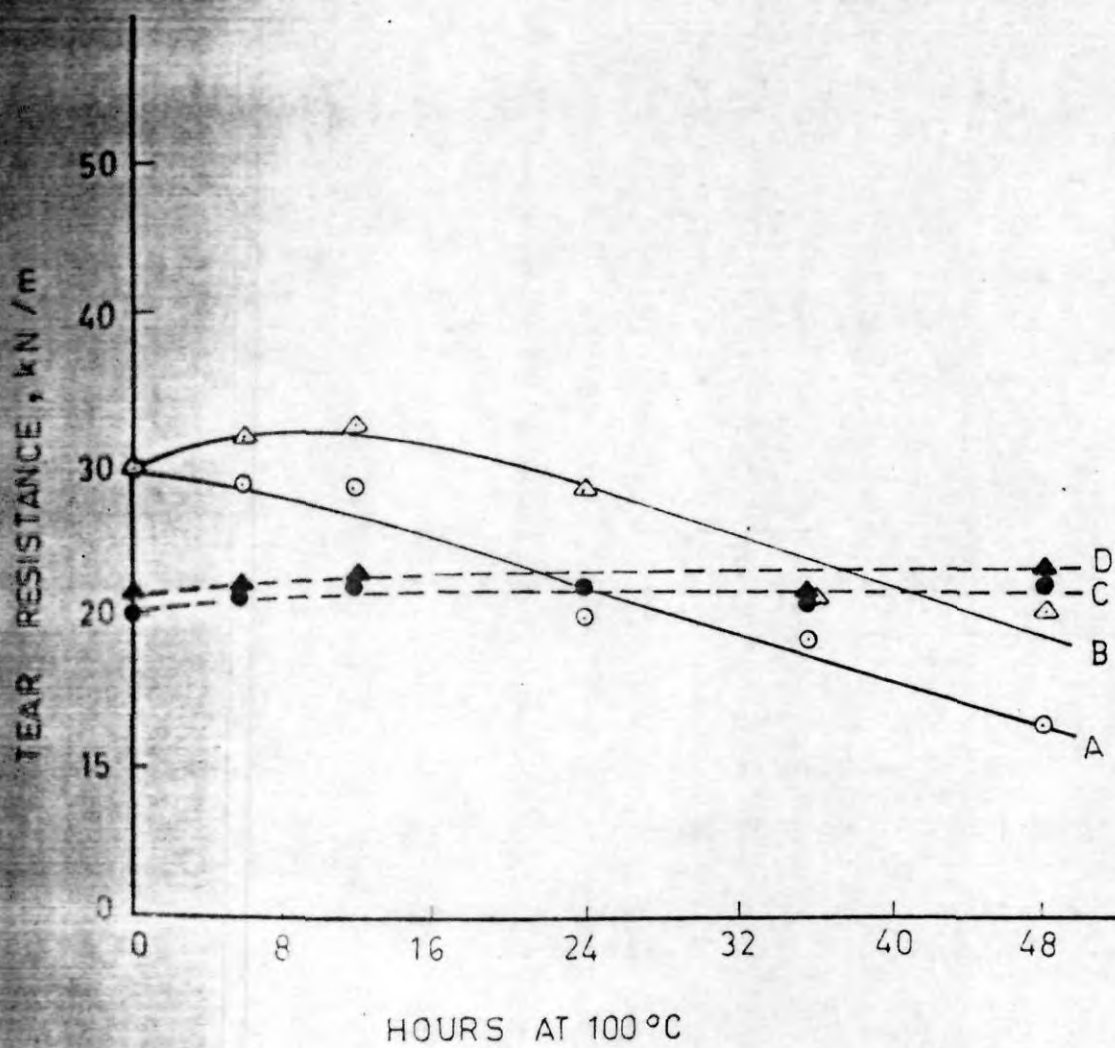


FIG. IV-13. CHANGES IN TEAR RESISTANCE OF THE UNFILLED VULCANIZATES DURING AGING

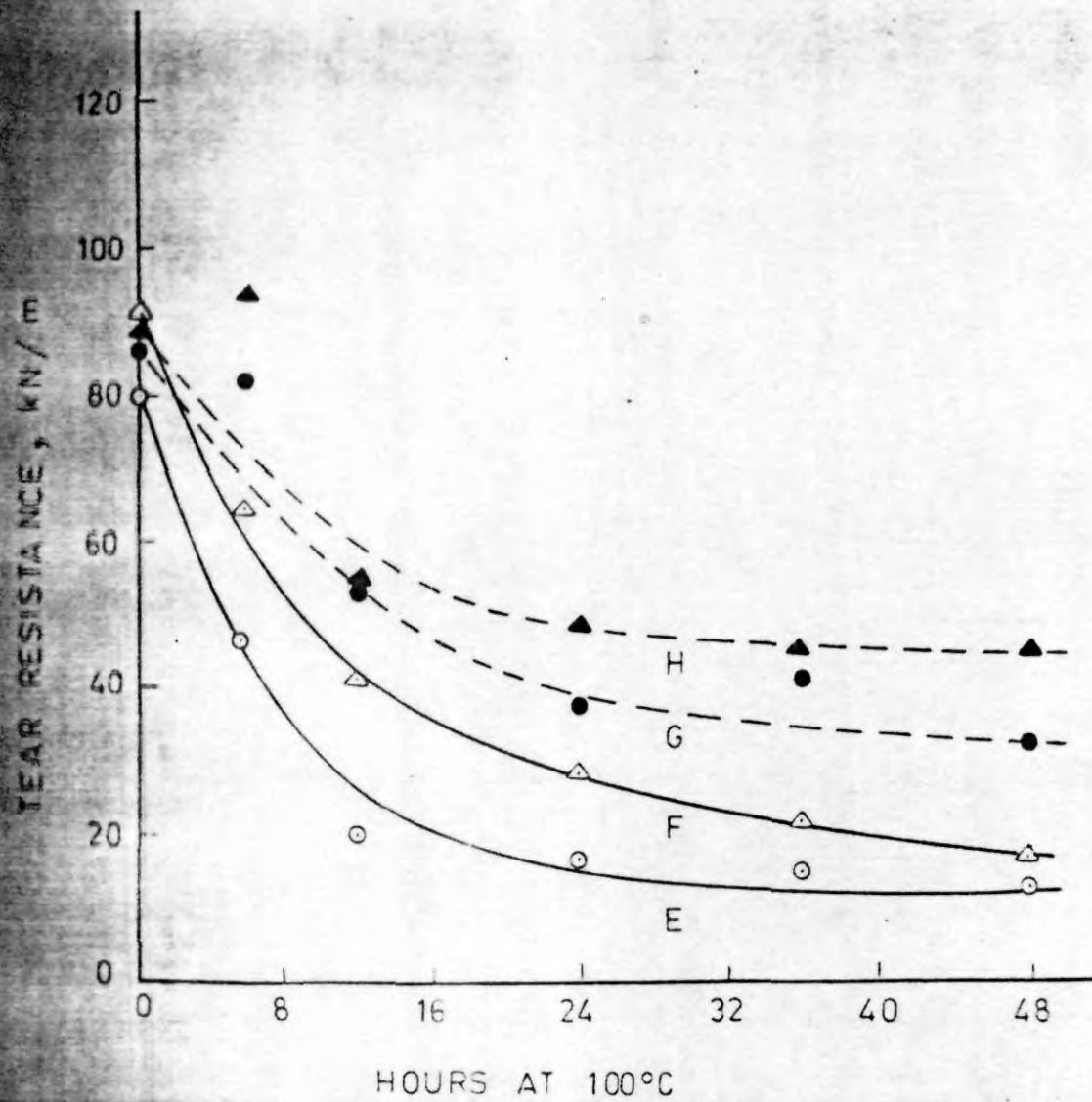


FIG. IV-14. CHANGES IN TEAR RESISTANCE OF THE FILLED VULCANIZATES DURING AGING

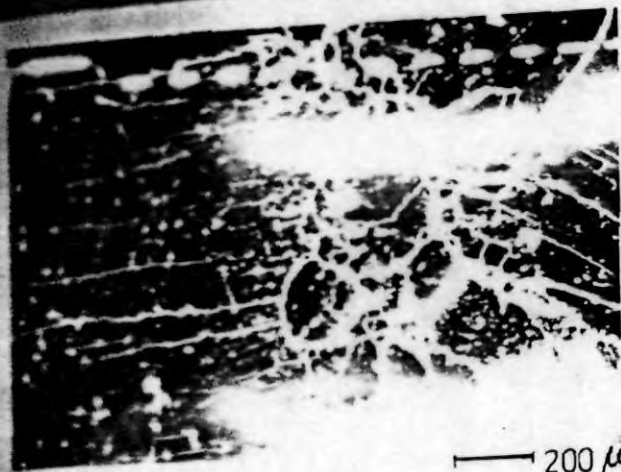


FIG. IV. 15 : Tensile fracture before aging, unfilled Conv. mix; rough zone.

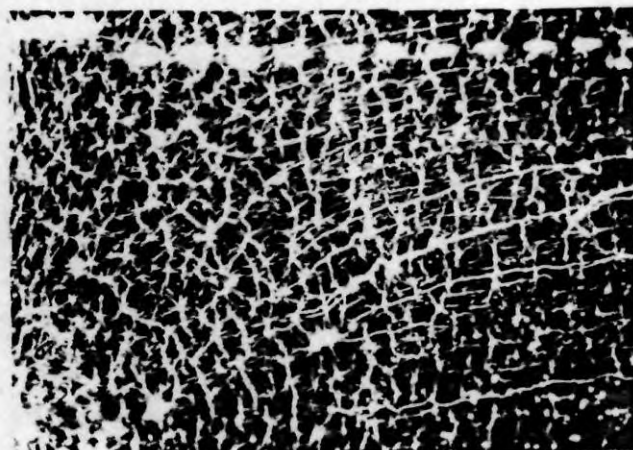


FIG. IV. 16 : Tensile fracture before aging, unfilled Conv. mix; general surface.

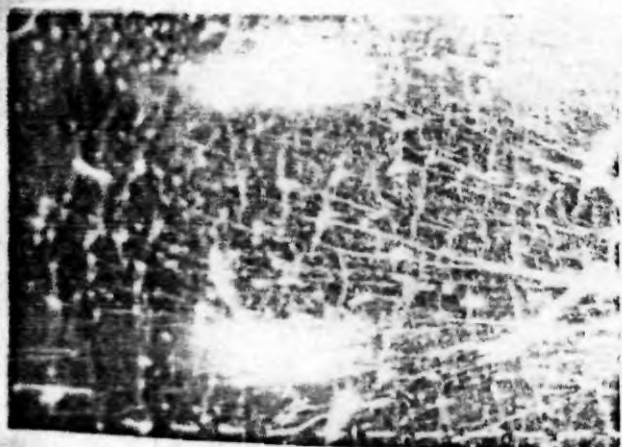


FIG. IV.17 : Tensile fracture after aging, unfilled Conv. mix; smooth surface.



FIG. IV.18 : Tensile fracture after aging, unfilled Conv. mix with PBNA; rough zone.

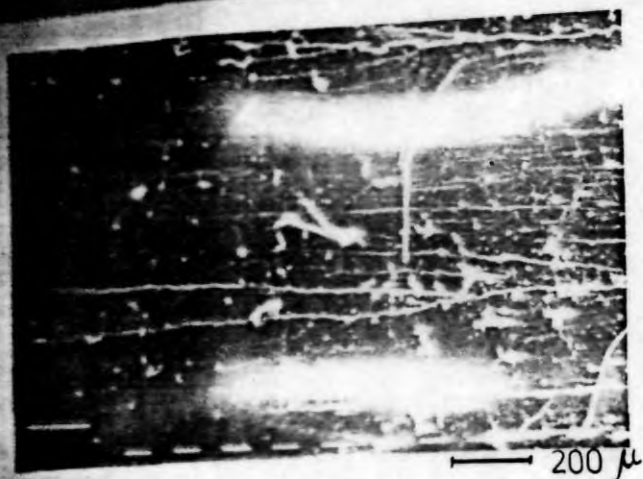


FIG. IV. 19 : Tensile fracture after aging, unfilled EV mix; tear lines on the surface.

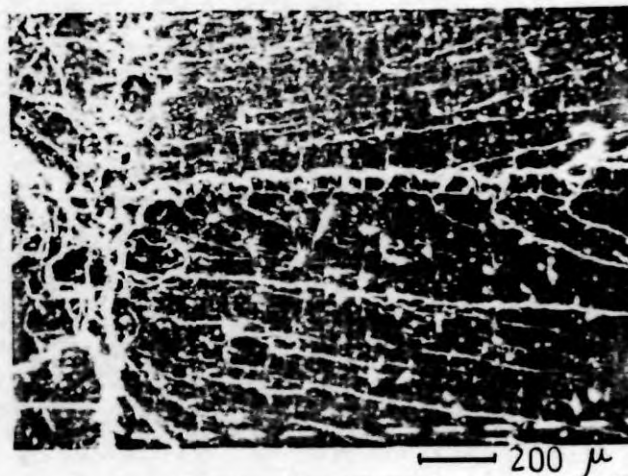


FIG. IV. 20 : Tensile fracture after aging, unfilled EV mix with PBNA; rough surface.

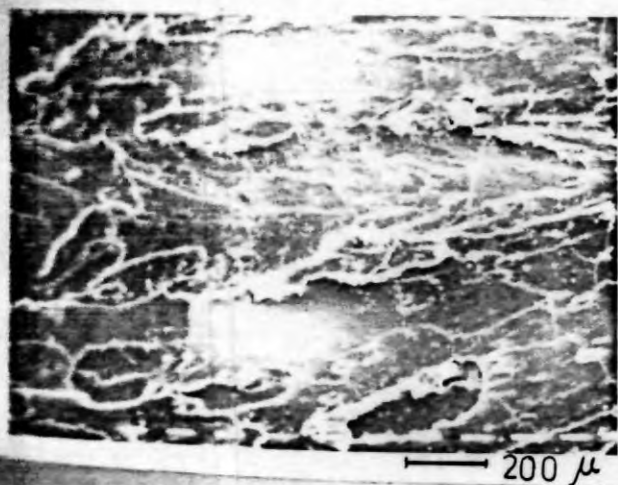


FIG. IV. 21 : Tensile fracture before aging, black-filled Conv. mix; rough surface with curved tear lines.

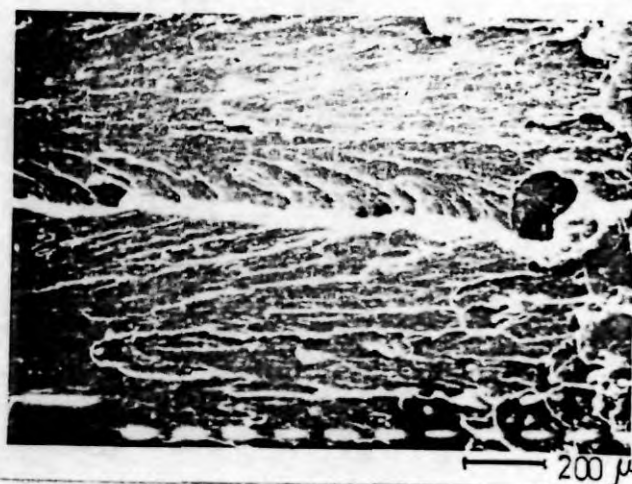


FIG. IV. 22 : Tensile fracture before aging, black-filled EV mix; rough surface.

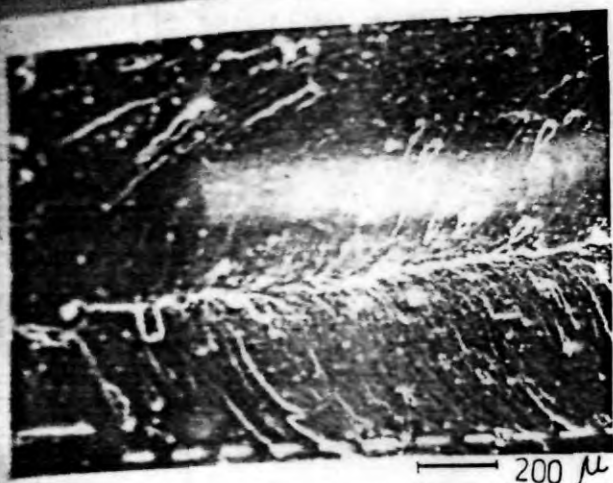


FIG. IV.23 : Tensile fracture after aging, black-filled Conv. mix; tear path at the centre.

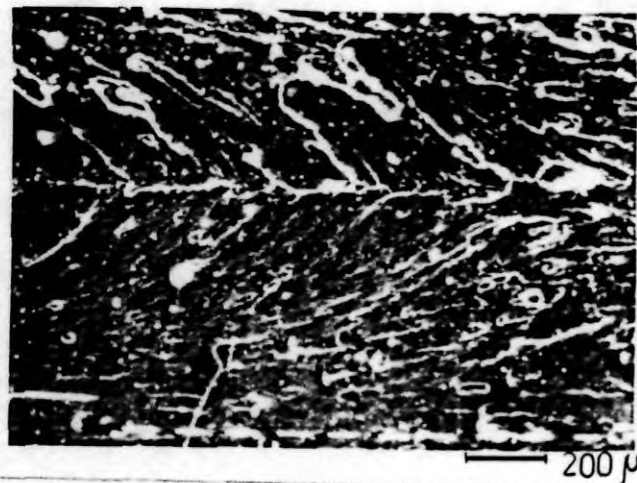


FIG. IV.24 : Tensile fracture after aging, black-filled Conv. mix with PBNA; general surface.

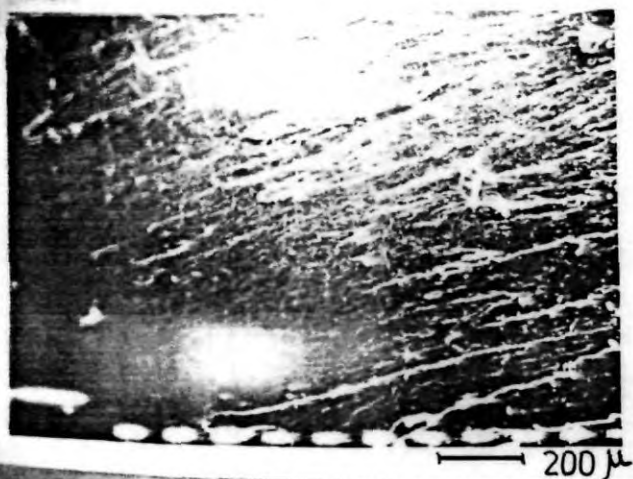


FIG. IV.25 : Tensile fracture after aging, black-filled EV mix; general surface.

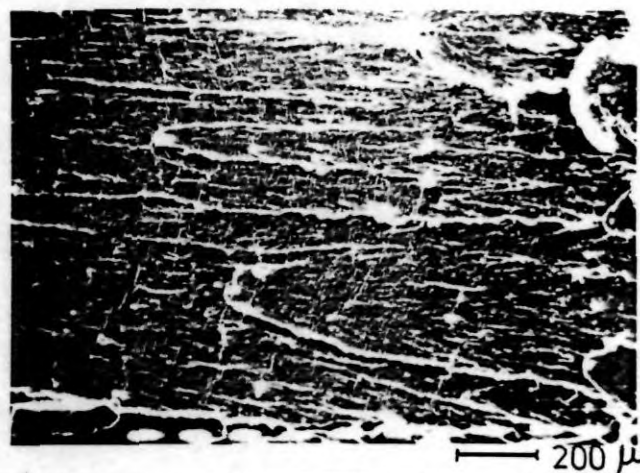


FIG. IV.26 : Tensile fracture after aging, black-filled EV mix with PBNA; rough surface.

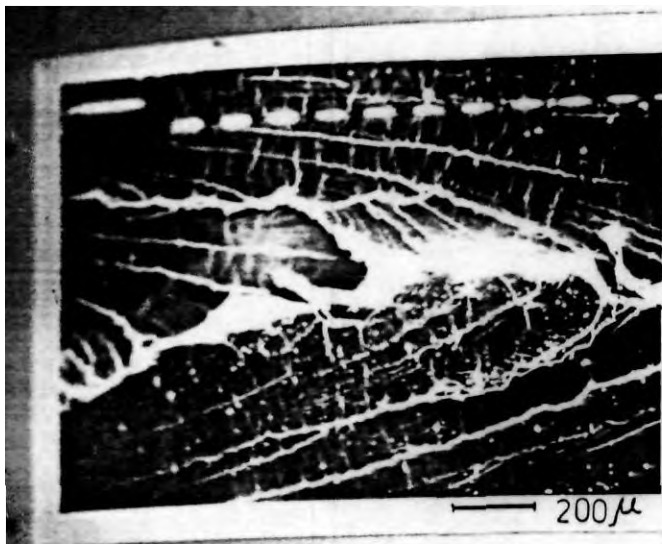


FIG. IV.27 : Tear fracture before aging, unfilled Conv. mix; tear path and secondary tear lines.

(6)



FIG. IV.28 : Tear fracture before aging, unfilled Conv. mix; tear path magnified.



FIG. IV.29 : Tear fracture before aging, unfilled EV mix; tear lines on the surface.

(7)

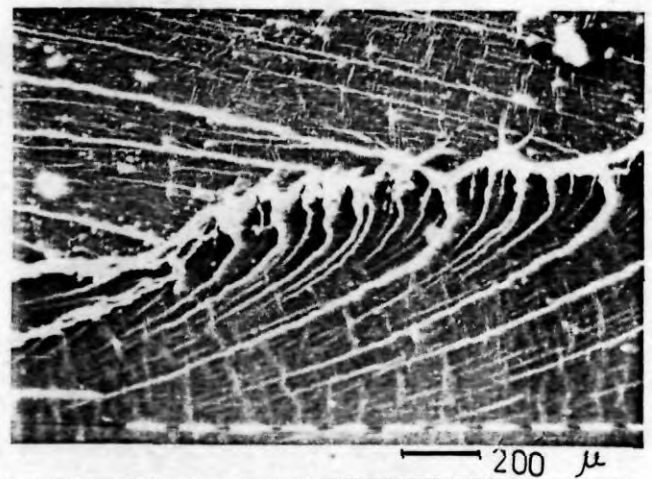


FIG. IV.30 : Tear fracture after aging, unfilled Conv. mix; tear path and secondary tear lines.

(8)

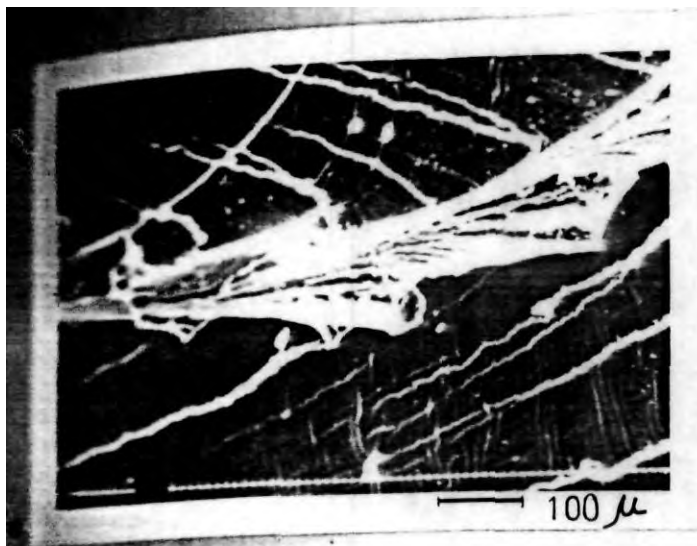


FIG. IV.31 : Tear fracture after aging, unfilled Conv. mix; stick-slip tear.

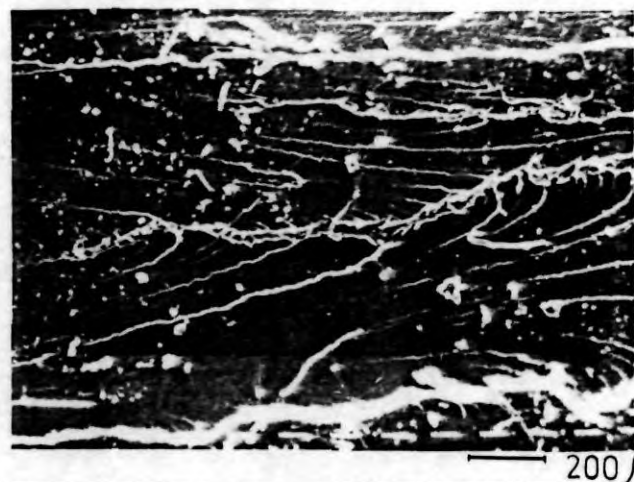


FIG. IV.32 : Tear fracture after aging, unfilled Conv. mix with PBNA; general surface.



FIG. IV.33 : Tear fracture after aging, unfilled EV mix; tear path.

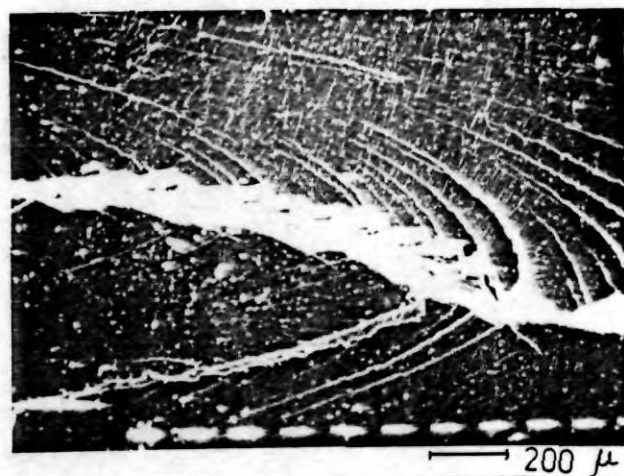


FIG. IV.34 : Tear fracture after aging, unfilled EV mix with PBNA; stick-slip tear.



FIG. IV.35 : Tear fracture before aging, black-filled Conv. mix; short curved tear lines.

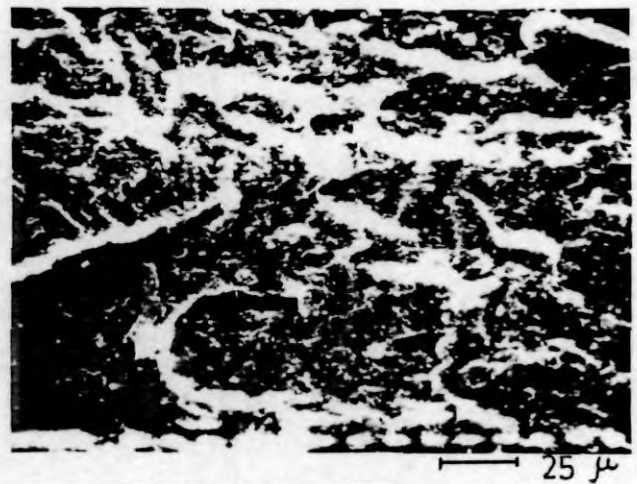


FIG. IV.36 : Tear fracture before aging, black-filled Conv. mix; layered structure.

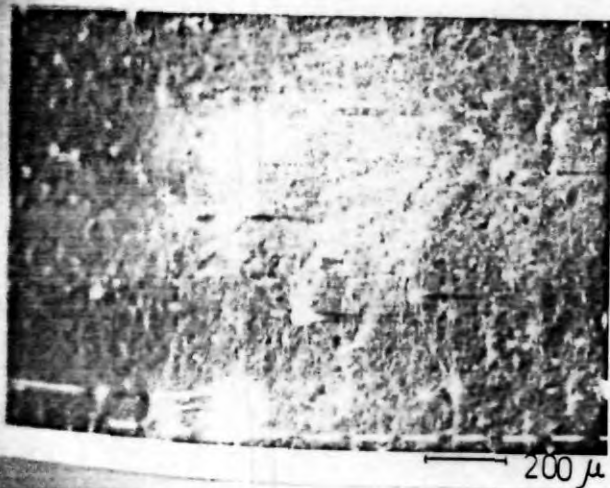


FIG. IV.37 : Tear fracture after aging, black-filled Conv. mix; smooth surface.

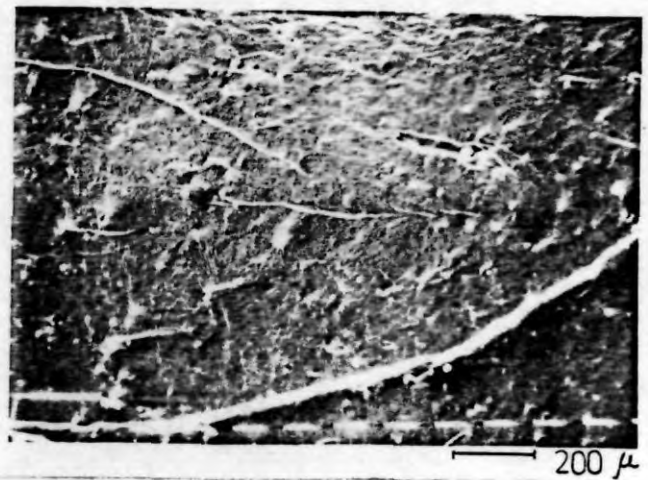


FIG. IV.38 : Tear fracture after aging, black-filled Conv. mix with PBNA; scattered tear lines.

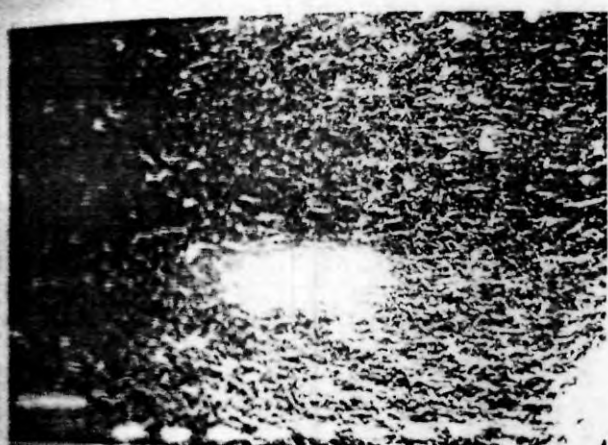


FIG. IV.39 : Tear fracture after aging, black-filled EV mix; general surface.

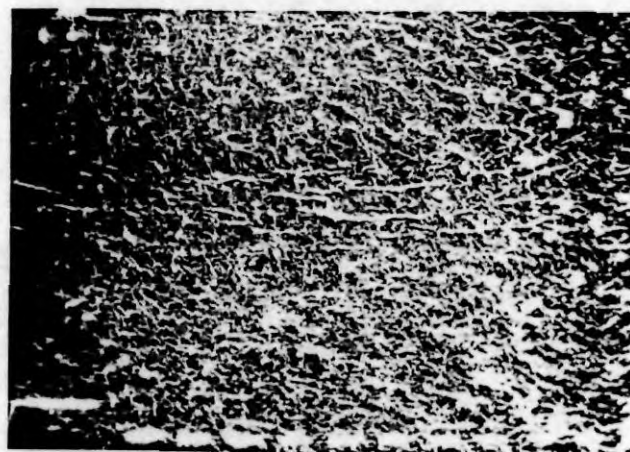


FIG. IV.40 : Tear fracture after aging, black-filled EV mix with PBNA; general surface.

**PART B. SCANNING ELECTRON MICROSCOPIC STUDIES
ON OZONE CRACKING OF RUBBER**

**This part has been communicated to Journal of
Polymer Science (Polymer Letters Edition).**

Protection of unsaturated rubbers against ozone attack is achieved by using waxes, flexible coatings⁵⁰ and chemical antiozonants⁵¹. The first two provide a physical barrier against ozone, while chemical antiozonants raise the critical strain. The physical antiozonants are not suitable for dynamic applications and chemical antiozonants are highly staining and are likely to be lost during processing and service^{52,53}.

Blending with ozone inert rubbers such as EPR has been reported to be effective in improving the ozone resistance of natural rubber⁵⁴. In this part studies on the ozone resistance of NR and NR/EPDM blends and on the nature of ozone cracking observed in such rubbers are reported. The formulations of the mixes are given in Table IV.3 and the physical properties in Table IV.4.

The mix D' was of the same formulation as that of D, but the mixing of the ingredients other than accelerator and sulfur was done separately. The masterbatches were then blended in the desired proportion and then the mixing was completed by adding accelerator and sulfur. The rheographs of the Mixes C, D and D' are given in Figure IV.41 and those of A and B were already given in Figures IV.1 and IV.2.

Ozone resistance of the samples has been measured in terms of the critical stress-strain parameters by the method described by Wilchinsky and Kresge¹⁷⁴. The critical stress-strain parameters of the different vulcanizates are given in Table IV.5. As the elastic modulus of the vulcanizates is different, the critical stored elastic energy density (W_c) is the best criterion for ozone resistance. From Table IV.5 it is seen that W_c of the unfilled NR/EPDM blend is three times higher than that of the unfilled NR vulcanizate. Carbon black improves the ozone resistance both in NR and NR/EPDM vulcanizates. It is also observed that when the black is incorporated separately into the rubbers like in Mix D', the ozone resistance improves remarkably. When black is added to a blend of polymers, it goes more into the polymer which is having a higher affinity for black¹⁷⁵. EPDM is having less affinity for carbon black with respect to natural rubber¹⁷⁵ and hence the EPDM phase in the blend remains less reinforced. This reduces the capacity of EPDM rubber to prevent the propagation of crack. This explains the lower ozone resistance of mix D compared to mix D'.

The SEM photomicrographs of the cracked specimens are shown in Figures IV.42 to IV.49. The specimens for the SEM observations were taken from the lower most portion of the tapered test piece. Figures IV.42 and IV.43 are the SEM photomicrographs of the unfilled NR and NR/EPDM blend respectively. As the specimens were no longer under strain, the cracks were not open while being observed in SEM and the horizontal lines represent the cracks. The figures show that the cracking pattern is almost the same for both NR and NR/EPDM blend. However the black-filled vulcanizates show differences in the cracking behavior. In the case of NR, the filled vulcanizates show shorter cracks than the unfilled one. Figures IV.44 and IV.45 are the SEM photomicrographs of the black-filled NR. Figure IV.45 shows that the cracks propagate straight without much deviation. Figures IV.46 and IV.47 are the SEM photomicrographs of the black-filled NR/EPDM blend. Compared to the black-filled NR vulcanizate, here the crack density is less, but the cracks are longer. The cracks do not propagate straight as seen in Figure IV.47. The ozone resistant EPDM zones in the blend prevent the cracks from proceeding straight. A similar explanation had been put forward by Andrews⁵⁴ in the case of NR/EPR blends. Figures IV.48 and IV.49 are the SEM photomicrographs of vulcanizates from Mix D', in which carbon black was separately mixed with the individual polymers before blending. Although the ozone resistance of this blend was much better than that of Mix D, the crack density remains almost the same. However, the cracks are shorter. Crack deviation is observed in this case also.

TABLE IV.3

FORMULATIONS OF THE MIXES

| MIX | A | B | C | D and D' |
|-------------------------------------|-----|-----|-----|----------|
| Natural rubber | 100 | 100 | 70 | 70 |
| EPDM rubber | - | - | 30 | 30 |
| Zinc oxide | 5 | 5 | 5 | 5 |
| Stearic acid | 2 | 2 | 2 | 2 |
| HAF black (N 330) | - | 50 | - | 50 |
| Naphthenic oil | - | 5 | - | 5 |
| CBS | 3.5 | 3.5 | 3.5 | 3.5 |
| Sulfur | 0.5 | 0.5 | 0.5 | 0.5 |
| Optimum cure time at 150°C, min. | 18 | 9 | 19 | 9 |

TABLE IV.4

PROPERTIES OF THE VULCANIZATES

| | A (NR-gum) | B (NR-filled) | C (NR/EPDM-gum) | D (NR/EPDM-filled) | D' (Same as D-master batches) |
|---------------------------------|---------------|------------------|--------------------|-----------------------|--|
| 300% Modulus, MPa | 0.3 | 8.5 | 2.3 | 8.8 | 8.0 |
| Tensile strength, MPa | 13.1 | 20.9 | 16.2 | 13.6 | 14.2 |
| Elongation at break, % | 740 | 560 | 850 | 560 | 480 |
| Hardness, Shore A | 35 | 35 | 47 | 66 | 67 |
| Resilience, % | 72 | 44 | 64 | 48 | 48 |
| Compression set, % | 11 | 24 | 31 | 26 | 29 |
| Heat buildup, ΔT , °C | 8 | 63 | 52* | 63 | 66 |
| Tear resistance, kN/m | 19 | 62 | 35 | 94 | 85 |
| V_T (original) | 0.175 | 0.200 | 0.166 | 0.207 | 0.201 |
| V_T (after exposure to ozone) | 0.176 | 0.202 | 0.174 | 0.206 | 0.204 |

* Sample blown out after 5 minutes.

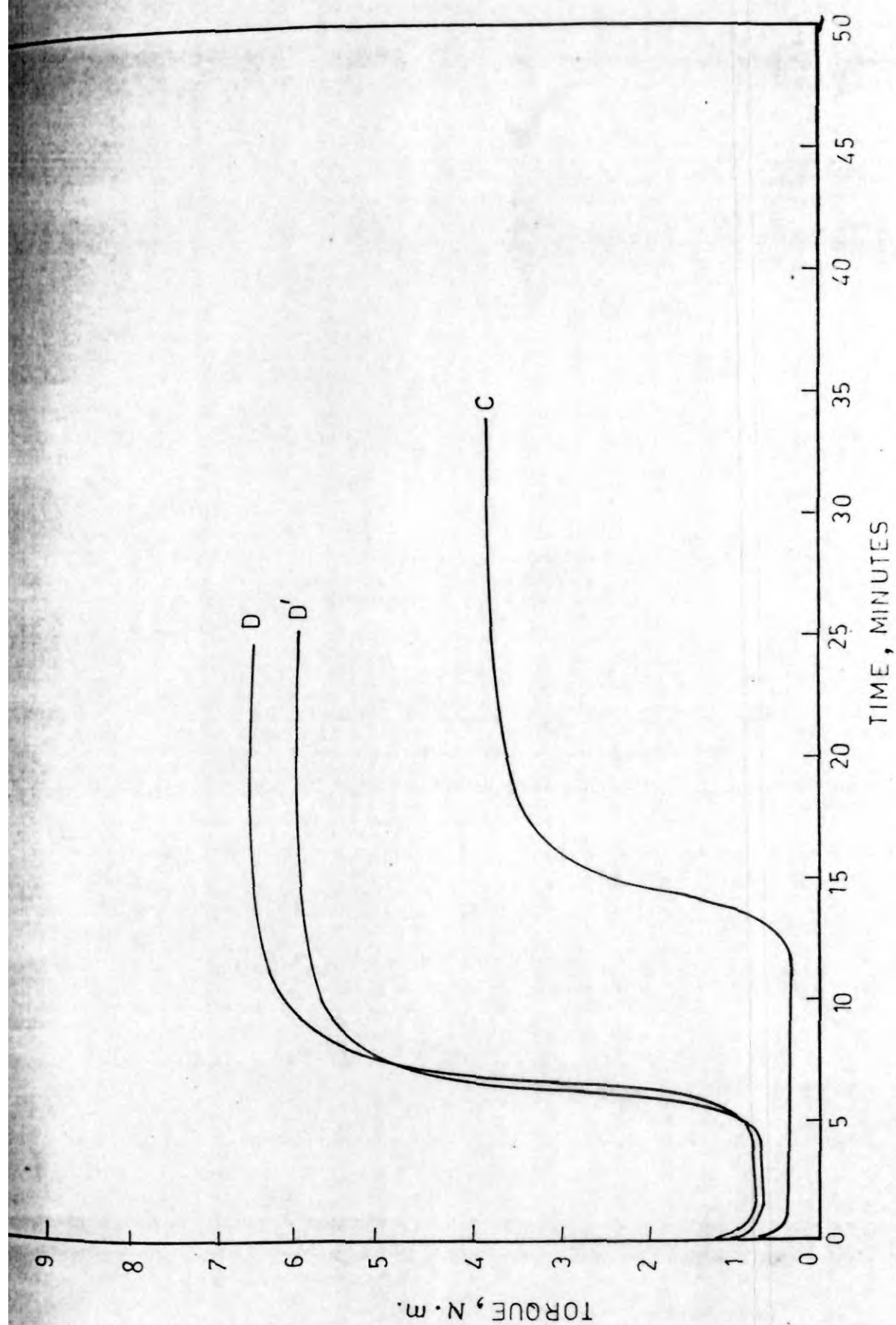


FIG. IV-41. RHEOGRAPHS OF MIXES C, D AND D'.

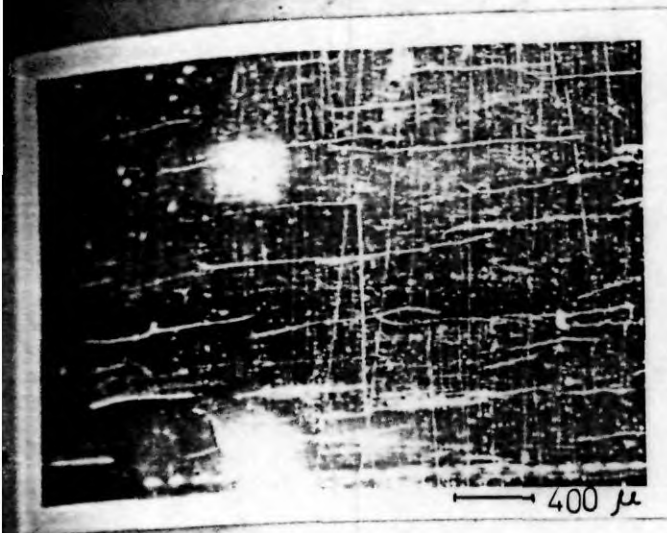


FIG. IV.42 : Ozone cracks in unfilled NR.

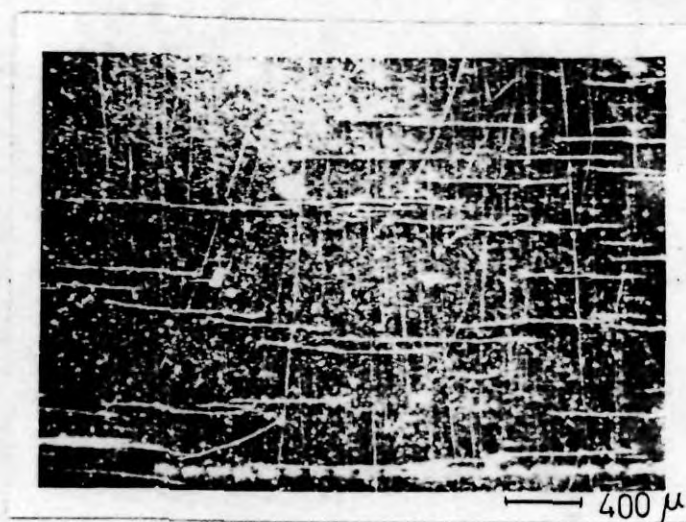


FIG. IV.43 : Ozone cracks in unfilled NR/EPDM blend.

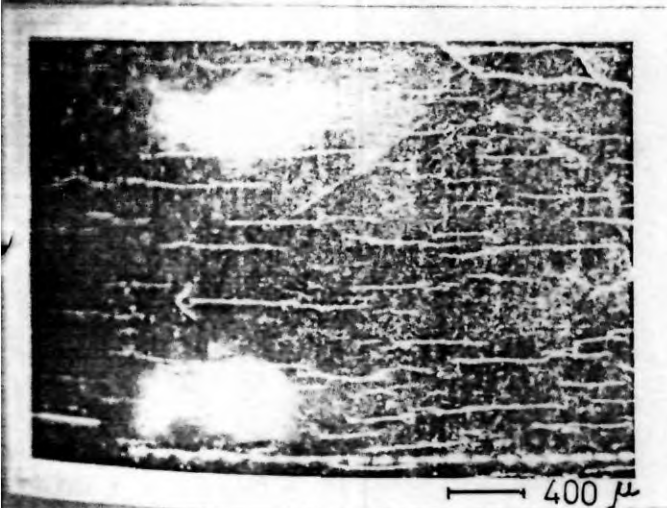


FIG. IV.44 : Ozone cracks in black-filled NR.

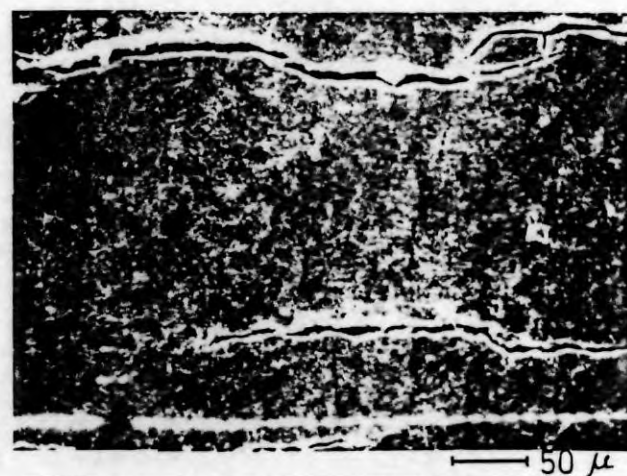


FIG. IV.45 : Straight cracks in black-filled NR.

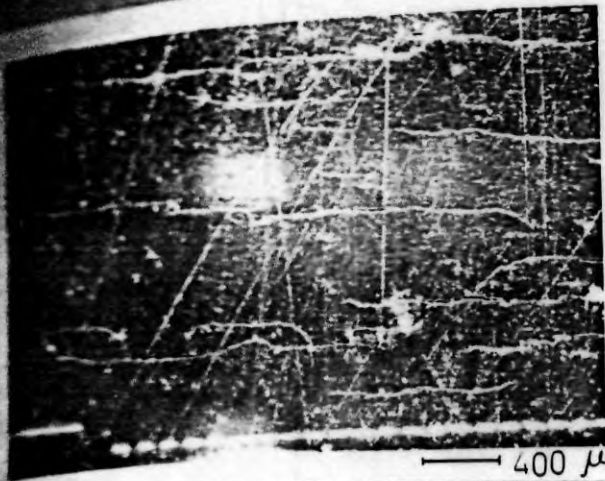


FIG. IV.46 : Ozone cracks in black-filled NR/EPDM blend.

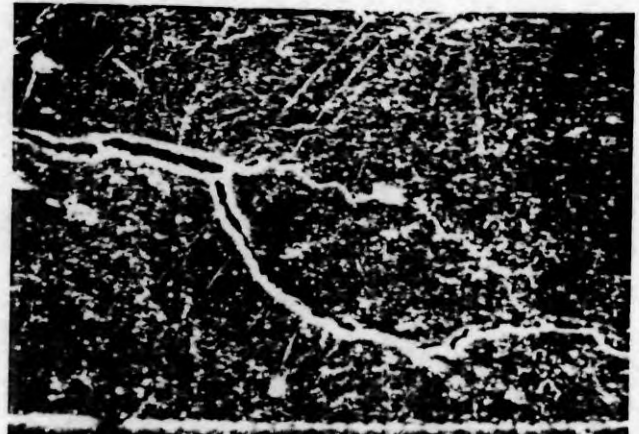


FIG. IV.47 : Crack deviation in black-filled NR/EPDM blend. .

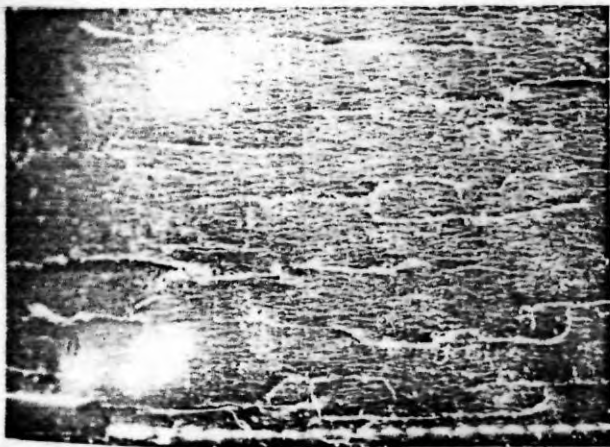


FIG. IV.48 : Ozone cracks in black-filled NR/EPDM blend (Mix D').

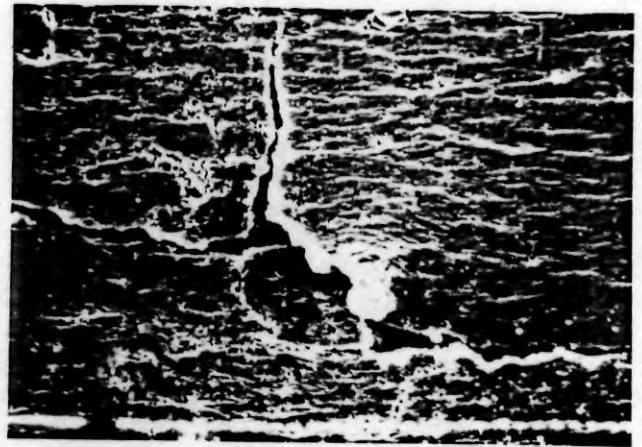


FIG. IV.49 : Crack deviation in black-filled NR/EPDM blend (Mix D').

CHAPTER V

**PART A. CHEMICAL AND SCANNING ELECTRON MICROSCOPIC
STUDIES ON FATIGUE FAILURE OF NATURAL
RUBBER VULCANIZATES.**

**PART B. SCANNING ELECTRON MICROSCOPIC STUDIES ON
FLEXING AND TENSION FATIGUE FAILURE OF RUBBER.**

**PART A. CHEMICAL AND SCANNING ELECTRON MICROSCOPIC STUDIES
ON FATIGUE FAILURE OF NATURAL RUBBER VULCANIZATES**

This part has been published in Rubber Chemistry
and Technology, 55, 51 (1982).

Fatigue is an important factor causing failure of rubber vulcanizates. It is defined as the decay caused by cyclic deformations at an amplitude less than that is necessary for fracture in one cycle⁵⁵. The deformation can be caused by tension, compression, flexing or shear. Various testing methods have been developed to determine the resistance of rubber vulcanizates to fatigue occurring under different types of deformation. A number of studies have been made by different authors to explain the mechanism of fatigue failure of rubbers⁵⁶⁻⁵⁹ and to correlate the

fatigue resistance with the chemical and physical characteristics of the vulcanizates^{29,167,168}. It is also known that network changes in rubber samples taken from failure surfaces cannot always explain failure behavior of rubber vulcanizates⁸⁸⁻⁹⁰. Hence in this part results of SEM studies and studies on the changes in network structure of natural rubber vulcanizates which have undergone fatigue failure in a De Mattia flexing machine are reported. The following parameters have been included in this study : (a) effect of vulcanizing system, (b) effect of fillers, (c) effect of antioxidant, (d) effect of test temperature.

The formulations of the mixes are given in Table V.1. The rheographs of mixes A to D have already been given in Chapter IV (Figures IV.1 and IV.2) and those of mixes E and F are given in Figure V.1. Physical properties of the mixes are given in Table V.2. The shape of the test specimen and the portion from where the fracture surface has been taken for SEM observations are shown in Figure V.2A.

Results of De Mattia fatigue tests are shown in Figure V.2B. The results can be summarized as follows.

(a) The Conv. system gives more flex resistance than EV system.

- (b) Addition of reinforcing carbon black reduces flex resistance.
- (c) Addition of antioxidant enhances flex resistance.
- (d) Increase of testing temperature to 100°C increases flex resistance. This increase is only an apparent one as it is mainly due to the increased set and the consequent reduction in strain in the grooves as observed by Cox and Parks¹⁶⁸.

Table V.3 summarizes the results of chemical characterization. Mix A has a slightly higher crosslink density and, as expected, registers a higher proportion of polysulfidic crosslinks than Mix B. Addition of HAF black slightly decreases the crosslink density. Addition of antioxidant does not have any considerable effect on the total crosslink density and polysulfidic crosslinks. These observations are true in both the original samples and those fatigue-tested at room temperature.

From the values of $[Sc]$, $[S^{--}]$, E and F it is found that there are only marginal changes in the network structure due to flexing at room temperature. But at 100°C, the mixes with the Conv. system show significant changes in the network structure. The higher $[Sc]$ and E values of the gum and black-filled Conv. mixes indicate extensive main chain modifications. The higher F values of these mixes after testing indicate

LIBRARY
No. : T 19
: 28/6/2000
: Rg

crosslink destruction reactions. However, the fact that the total chemical crosslink density remains almost constant, indicates that new crosslinks were formed as a result of post-curing. But the mixes containing antioxidant show a significant increase in total chemical crosslink density owing to postcuring and minimum crosslink destruction reaction as is evident from the constant value of F . Main chain modifications are also minimized by the presence of the antioxidant. These changes in the network structure are mostly the effect of temperature and not due to flexing.

From the foregoing discussion it is seen that the difference in the resistance to fatigue failure of different mixes cannot be explained from chemical characterization alone. Results of the SEM observations are summarized below.

Figures V.3 and V.4 show the photomicrographs of the Conv. and EV gum vulcanizates respectively. Ductile failure with dimples resulting in higher flex resistance is evident in the case of these gum mixes. The mix with Conv. system shows smaller dimples. Photomicrographs of samples from the black-filled Conv. mix are given in Figures V.5 and V.6 and that of the EV mix in Figure V.7. Addition of HAF black makes the mixes more brittle and this changes the failure mode to shear fracture in both the systems. Cracks on the surface are evident and there occurs a drastic drop in flex resistance.

Rubber balling is observed in these samples, which has been reported earlier by De and coworkers¹⁶³. But at 100°C flow of the matrix is more predominant as may be seen in Figures V.8 and V.9 which are the photomicrographs of the black-filled Conv. and EV mixes respectively. Moreover, there are fewer cracks which are thinner than those occurred at room temperature. Rubber balling is not observed in the Conv. mix and only a slight amount is seen in the EV mix. The EV mix, which gives poor flex resistance, shows larger number of cracks and less flow.

Addition of antioxidant changes the fracture mode. Figures V.10 and V.11 show the effect of antioxidant on the nature of fracture in the case of the black-filled Conv. and EV mixes respectively. Figures V.12 and V.13 show the effect at 100°C in the case of the Conv. mix and Figure V.14 that in the case of the EV mix. The photomicrographs show that, with addition of antioxidant, the brittle failure nature of the filled vulcanizates changes to quasi-ductile; the result is higher flex resistance. A few cracks were visible near the edge of the samples. It is likely that the antioxidant reacts chemically with the free radicals formed, and this makes the matrix resistant to fatigue failure and hence causes a transition from brittle to quasi-ductile failure.

TABLE V.1
FORMULATIONS OF THE MIXES

| MIX | A | B | C | D | E | F |
|--------------------|-----|-----|-----|-----|-----|-----|
| Natural rubber | 100 | 100 | 100 | 100 | 100 | 100 |
| Zinc oxide | 5 | 5 | 5 | 5 | 5 | 5 |
| Stearic acid | 2 | 2 | 2 | 2 | 2 | 2 |
| Antioxidant (IPPD) | - | - | - | - | 1 | 1 |
| HAF black (N 330) | - | - | 50 | 50 | 50 | 50 |
| Naphthenic oil | - | - | 5 | 5 | 5 | 5 |
| CBS | 0.6 | 3.5 | 0.6 | 3.5 | 0.6 | 3.5 |
| Sulfur | 2.5 | 0.5 | 2.5 | 0.5 | 2.5 | 0.5 |

TABLE V.2

PHYSICAL PROPERTIES OF THE MIXES

| PROPERTY | A | B | C | D | E | F |
|-------------------------|-----------|--------|-----------|--------|--------------|------------|
| | GUM-CONV. | GUM-EV | HAF-CONV. | HAF-EV | HAF-CONV-A/O | HAF-EV-A/O |
| Optimum cure time, min. | 11.0 | 18.0 | 10.5 | 9.0 | 12.0 | 8.0 |
| Modulus 300%., MPa | 0.7 | 0.3 | 9.4 | 7.4 | 9.2 | 7.4 |
| Tensile strength, MPa | 16.4 | 13.1 | 21.5 | 20.6 | 23.3 | 22.4 |
| Elongation at break, % | 730 | 740 | 460 | 510 | 530 | 550 |

TABLE V.3

CHEMICAL CHARACTERISTICS BEFORE AND AFTER FIXING FAILURE

| MIX. NO. | SYSTEM | NATURE OF VULCANIZATE | TOTAL CROSS-LINK DENSITY (2Mc, chem) mmol/kg RH | POLYSULFIDIC CROSS-LINKS, % | COMBINED SULFUR, [Sc] mmol/kg RH | FREE SULFUR, mmol/kg RH | E, ATOMS/CHEM. CROSSLINK | F, SULFIDE ION/CHEM. CROSSLINK |
|----------|--------------|-----------------------|---|-----------------------------|----------------------------------|-------------------------|--------------------------|--------------------------------|
| A | Gum-conv. | | 29.3 | 67 | 531 | 211 | 18.1 | 1.32 |
| B | Gum-EV | | 24.0 | 33 | 151 | 5 | 6.3 | a |
| C | HAF-conv. | Original | 25.0 | 53 | 447 | 311 | 17.9 | 0.94 |
| D | HAF-EV | | 20.5 | 40 | 145 | 9 | 7.1 | 0.11 |
| E | HAF-conv-A/O | | 27.6 | 48 | 445 | 295 | 16.1 | 1.49 |
| F | HAF-EV-A/O | | 21.7 | 33 | 144 | 12 | 6.6 | a |

TABLE V.3

CHEMICAL CHARACTERISTICS BEFORE AND AFTER FIXING FAILURE

| MIX. NO. | SYSTEM | NATURE OF VULCANIZATE | TOTAL CROSS-LINK DENSITY (2Mc, chem) $\frac{1}{\text{mmol/kg RH}}$ | POLYSULFIDIC CROSS-LINKS, % | COMBINED SULFUR, [Sc], $\frac{\text{mmol}}{\text{kg RH}}$ | FREE SULFUR, $\frac{\text{mmol}}{\text{kg RH}}$ | E, ATOMS/CHEM. CROSSLINK | F, SULFIDE ION/CHEM. CROSSLINK |
|----------|--------------|-----------------------|--|-----------------------------|---|---|--------------------------|--------------------------------|
| A | Gum-conv. | | 29.3 | 67 | 531 | 211 | 18.1 | 1.32 |
| B | Gum-EV | | 24.0 | 33 | 151 | 5 | 6.3 | a |
| C | HAF-conv. | Original | 25.0 | 53 | 447 | 311 | 17.9 | 0.94 |
| D | HAF-EV | | 20.5 | 40 | 145 | 9 | 7.1 | 0.11 |
| E | HAF-conv-A/O | | 27.6 | 48 | 445 | 295 | 16.1 | 1.49 |
| F | HAF-EV-A/O | | 21.7 | 33 | 144 | 12 | 6.6 | a |

TABLE V.3 (CONTD.)

| MIX. NO. | SYSTEM | NATURE OF VULCANIZATE | TOTAL CROSS-LINK DENSITY (2Mc, chem) mmol/kg RH | POLYSULFIDIC CROSS-LINKS, % | COMBINED SULFUR, [Sc], mmol/kg RH | FREE SULFUR, mmol/kg RH | E, ATOMS/CHEM. CROSSLINK | F, SULFIDE ION/CHEM. CROSSLINK |
|----------|--------------|-----------------------|---|-----------------------------|-----------------------------------|-------------------------|--------------------------|--------------------------------|
| A | Gum-conv. | Flexed | 28.6 | 66 | 539 | 191 | 18.8 | 1.80 |
| B | Gum-EV | at | 22.7 | 34 | 149 | 5 | 6.6 | 0.06 |
| C | HAF-conv. | room | 26.8 | 49 | 478 | 273 | 17.8 | 1.12 |
| D | HAF-EV | temp. | 22.2 | 40 | 147 | 9 | 6.6 | a |
| E | HAF-conv-A/O | (30°C) | 31.1 | 56 | 470 | 266 | 15.1 | 1.46 |
| F | HAF-EV-A/O | | 22.2 | 36 | 145 | 11 | 6.5 | a |
| A | Gum-conv. | Flexed | 28.9 | 61 | 680 | 26 | 23.5 | 2.78 |
| B | Gum-EV | at | 30.6 | 21 | 149 | 5 | 4.9 | 0.05 |
| C | HAF-conv. | 100°C | 28.3 | 56 | 691 | 47 | 24.4 | 1.52 |
| D | HAF-EV | | 24.6 | 41 | 144 | 10 | 5.9 | 0.09 |
| E | HAF-conv-A/O | | 48.7 | 61 | 694 | 16 | 14.3 | 1.46 |
| F | HAF-EV-A/O | | 26.2 | 28 | 144 | 10 | 5.5 | 0.08 |

a = negligible.

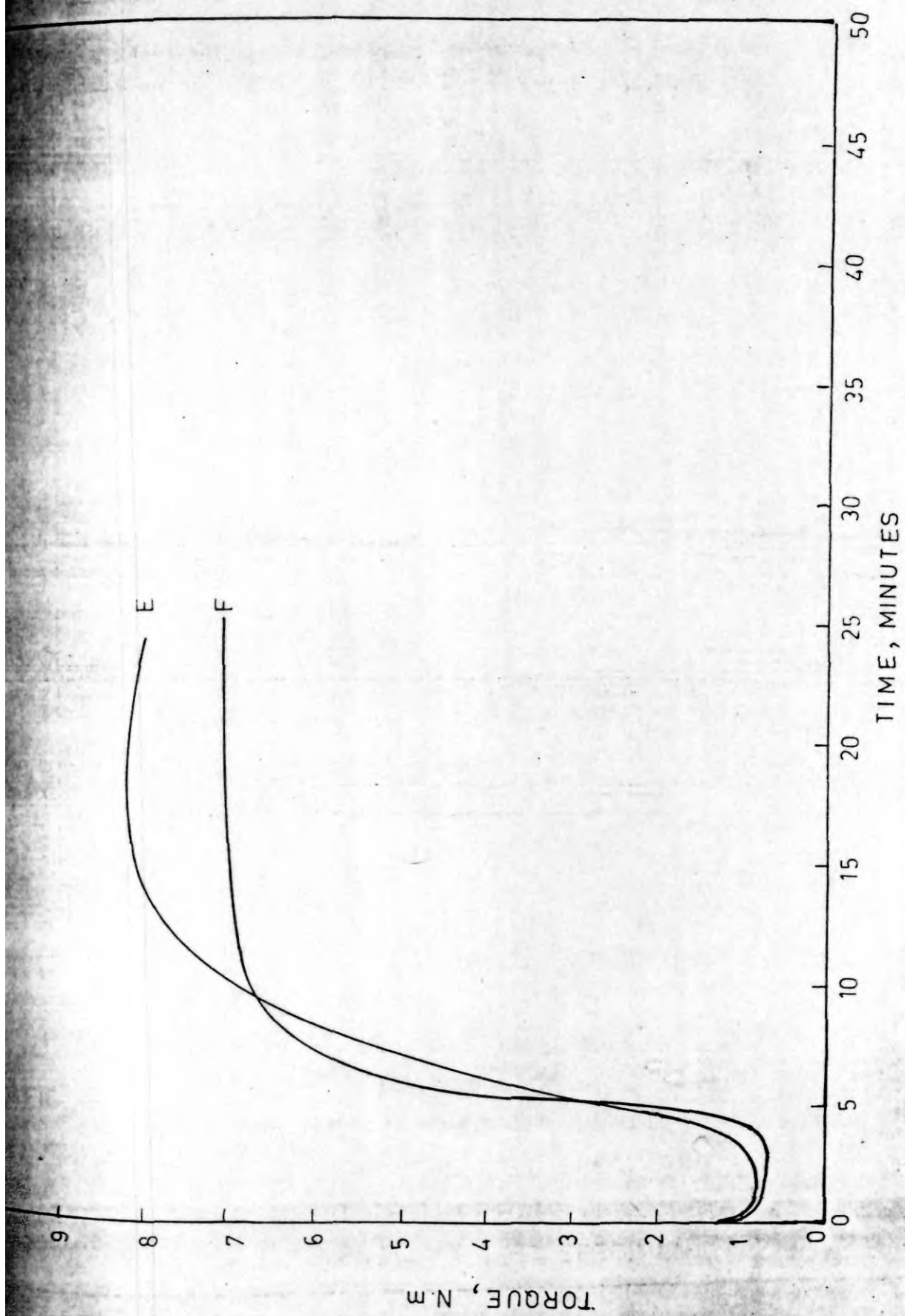


FIG. V.1. RHEOGRAPHS OF MIXES E AND F

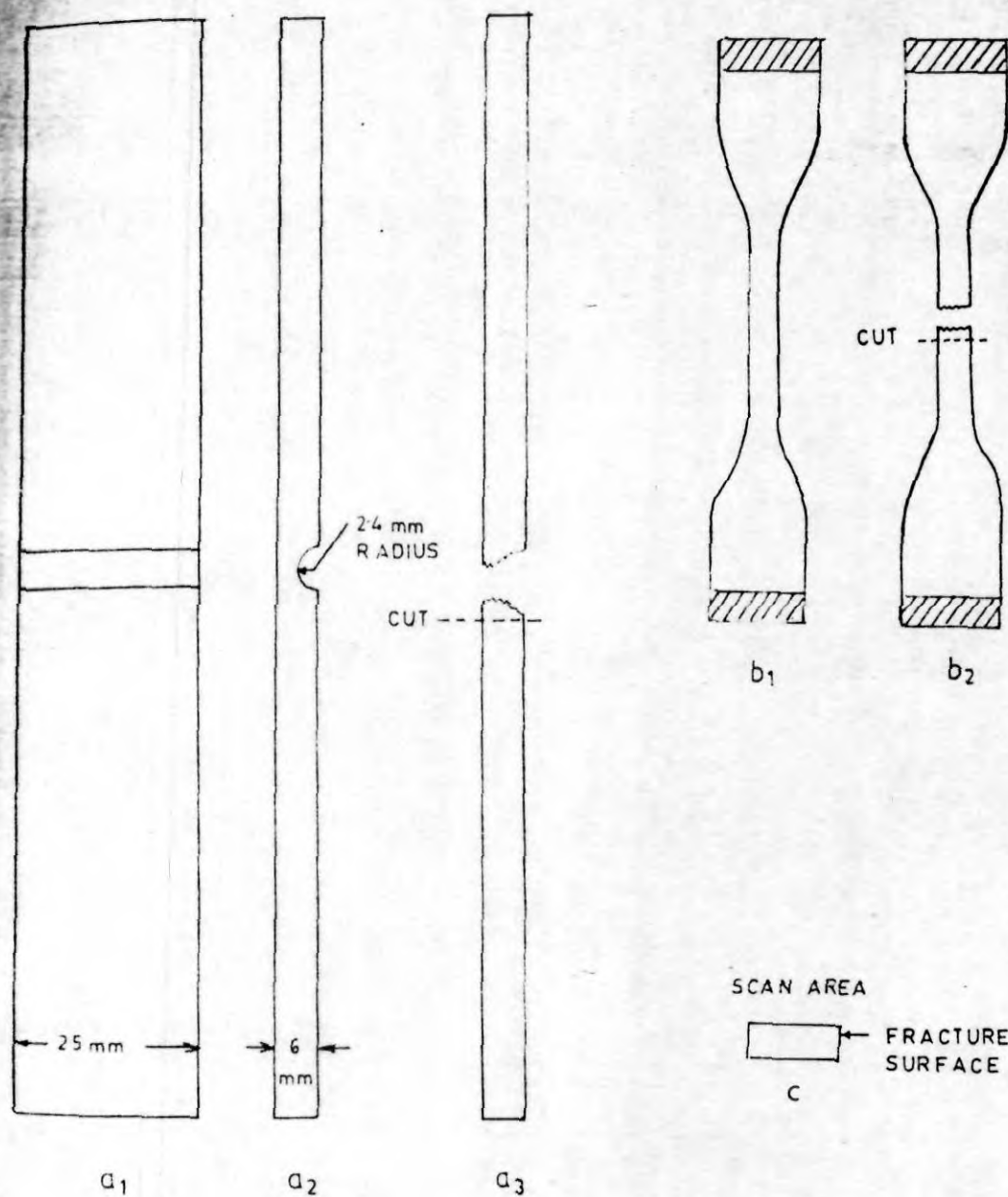


FIG. V-2 A. a₁-DE MATTIA TEST SPECIMEN,
a₂-DE MATTIA TEST SPECIMEN (SIDE VIEW),
a₃-FAILED DE MATTIA TEST SPECIMEN,
b₁-MONSANTO TEST SPECIMEN,
b₂-FAILED MONSANTO TEST SPECIMEN.

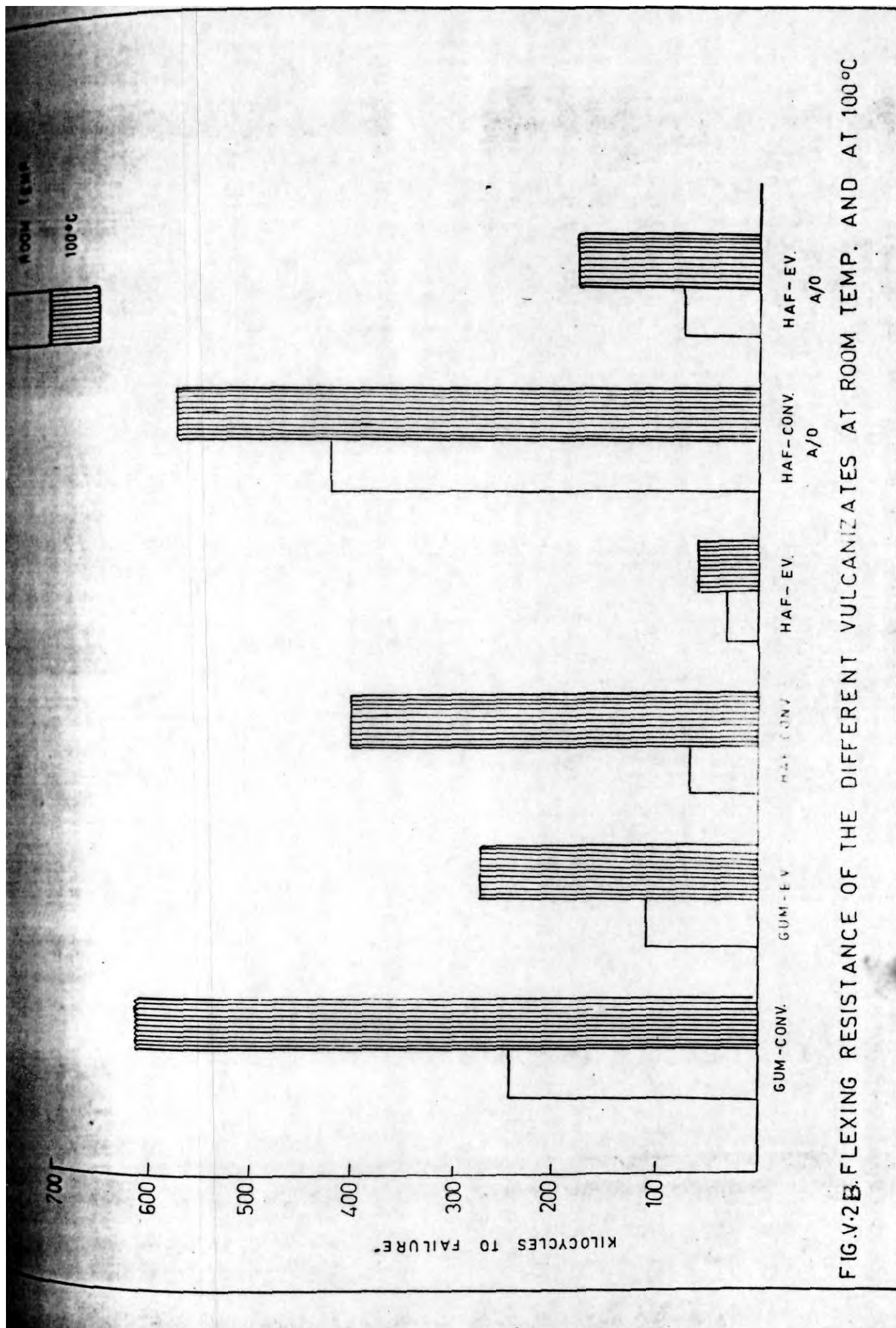


FIG.V.2B.FLEXING RESISTANCE OF THE DIFFERENT VULCANIZATES AT ROOM TEMP. AND AT 100°C

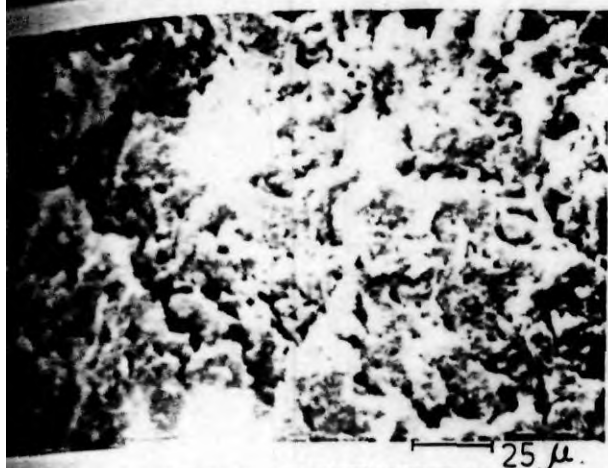


FIG. V.3 : Flex fatigue failure of unfilled Conv. mix; ductile failure with small dimples.

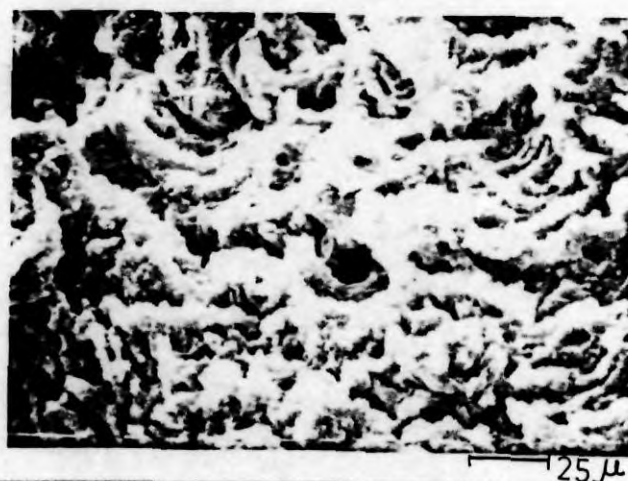


FIG. V.4 : Flex fatigue failure of unfilled EV mix; ductile failure with larger dimples.

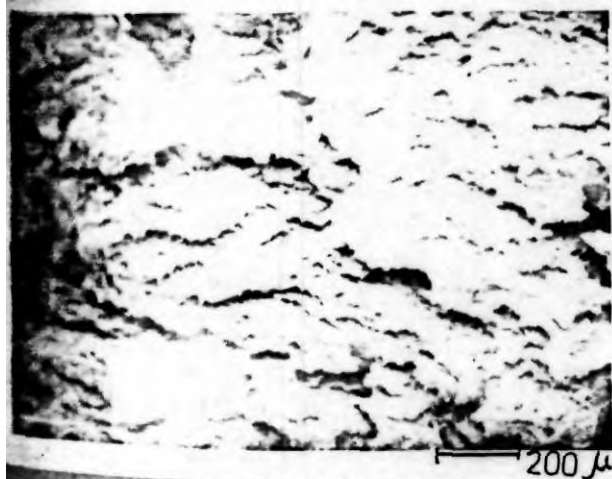


FIG. V.5 : Flex fatigue failure of black-filled Conv. mix; bare fracture.



FIG. V.6 : Flex fatigue failure of black-filled Conv. mix; rubber balling.



FIG. V.7 : Flex fatigue failure of black-filled EV mix; brittle fracture.

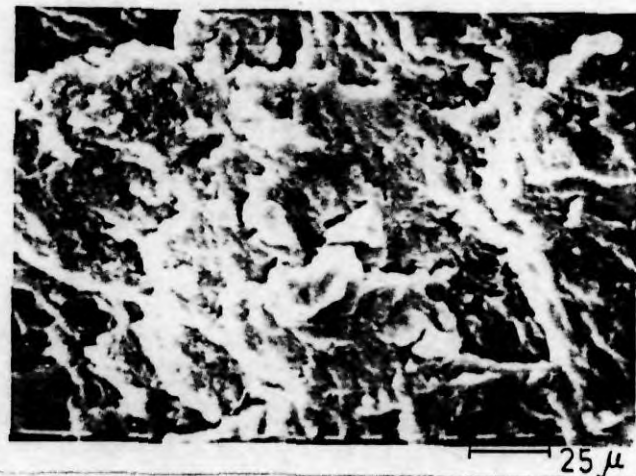


FIG. V.8 : Flex fatigue failure of black-filled Conv. mix at 100°C; matrix flow.

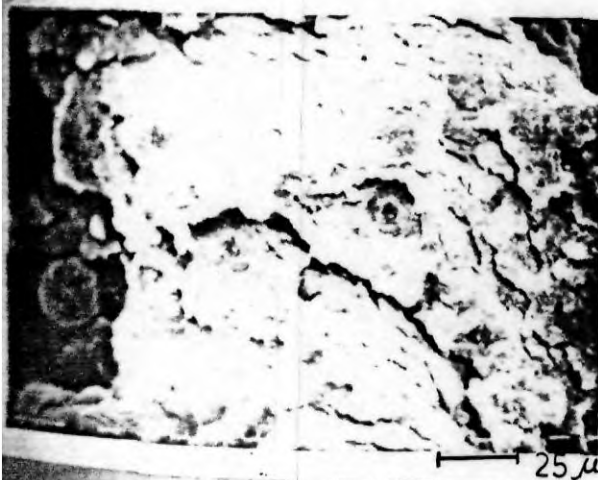


FIG. V.9 : Flex fatigue failure of black-filled EV mix at 100°C; thinner cracks and lesser balling.

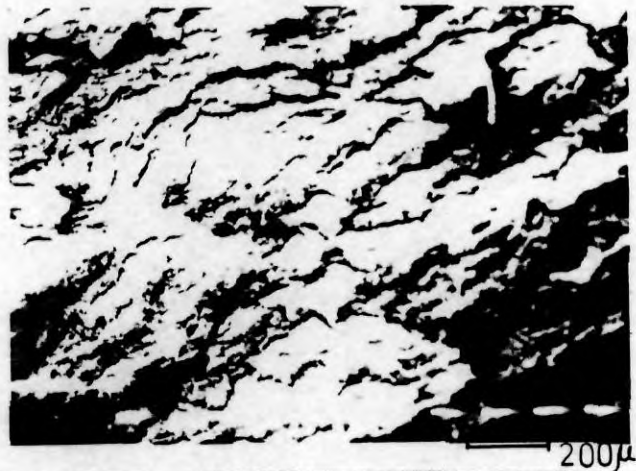


FIG. V.10 : Flex fatigue failure of black-filled Conv. mix with IPPD; quasi-ductile fracture.

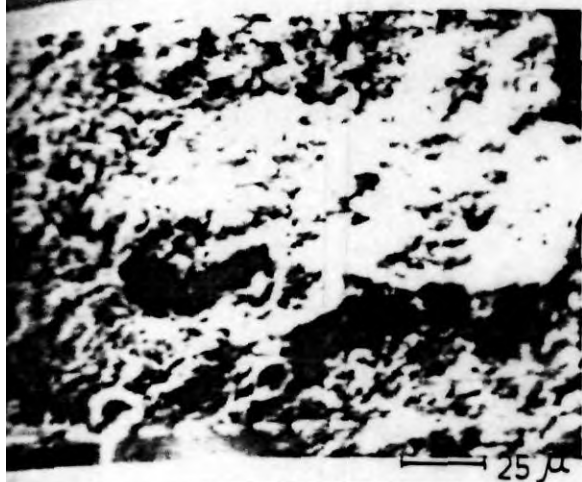


FIG. V.11 : Flex fatigue failure of black-filled EV mix with IPPD at 100°C; flow of matrix.

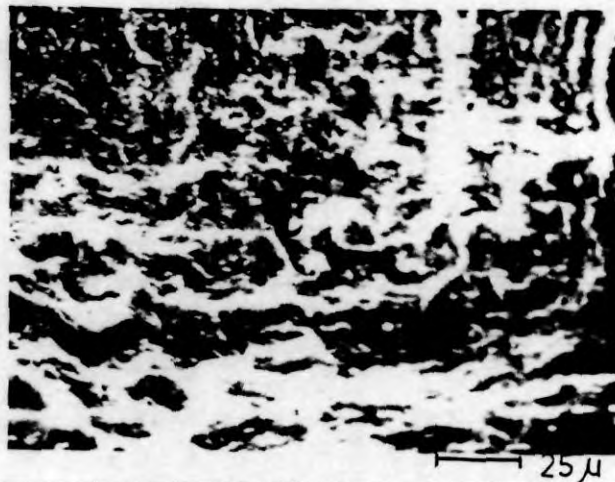


FIG. V.12 : Flex fatigue failure of black-filled Conv. mix with IPPD at 100°C; zone between ductile and brittle fracture.

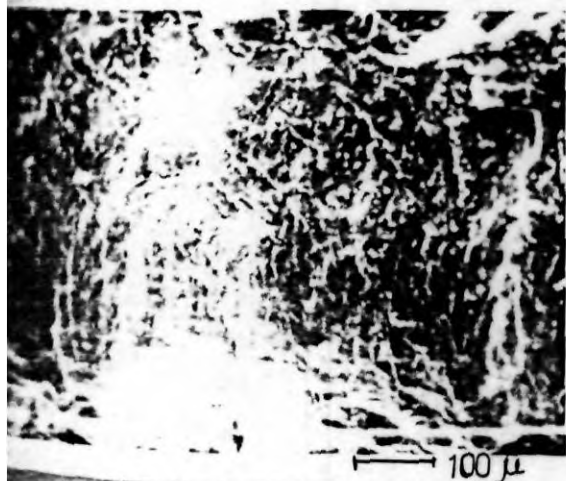


FIG. V.13 : Flex fatigue failure of black-filled Conv. mix with IPPD at 100°C; flow of matrix.



FIG. V.14 : Flex fatigue failure of black-filled EV mix with IPPD at 100°C; tiny cracks on the surface.

PART B.

SCANNING ELECTRON MICROSCOPIC STUDIES ON
FLEXING AND TENSION FATIGUE FAILURE OF RUBBER

This part has been published in International Journal
of Fatigue, January, 1983.

Chemical and SEM studies on flex fatigue failure of natural rubber vulcanizates have been reported in Part A. It was found that the fatigue failure is not accompanied by any major change in the network structure, but is mostly a physical phenomenon. In this part SEM observations on the nature of fatigue failure occurring in natural rubber and natural rubber/polybutadiene rubber (NR/BR) blends, when tested separately under tension and flexing, are reported. The parameters included in the study are the effect of blend ratio and the effect of filler. The formulations of the mixes are given in Table V.4. The physical properties of the vulcanizates are summarized in Table V.5. The experimental conditions in the

two types of fatigue tests are given in Table V.6. The rheographs of the mixes B, C, E and F are given in Figure V.15. The rheographs of mixes A and D are already given in Chapter IV (Figure IV.1). The shape of the test specimens and the portion from where the fracture surface has been removed for SEM observations are shown in Figure V.2A.

The fatigue life of the different vulcanizates, as obtained from the De Mattia and the Monsanto fatigue testing machines are given in Table V.7. Although the absolute values obtained from the two machines are different, the relative ranking of the unfilled vulcanizates is almost the same. The results show that in the case of the unfilled mixes the fatigue life of the 75/25 NR/BR blend is better than that of NR itself. But when the proportion of BR in the blend is increased to 50 percent, the fatigue life is reduced considerably. It may be noted that unlike natural rubber, BR is not a strain-crystallizing rubber and hence its unfilled vulcanizates possess only poor strength properties. Therefore, the presence of a high proportion of this rubber in an unfilled blend with NR is expected to cause poor strength properties. This is evident from the physical properties of the vulcanizates given in Table V.5. Earlier, Lake and Thomas⁶¹ suggested that crack growth and hence fatigue of a strain crystallizing rubber are retarded by the formation of crystallites near the growing end of the crack, which causes a higher dissipation of strain energy through hysteresis. The improvement in fatigue life

observed in the case of the unfilled 75/25 NR/BR blend is believed to be due to the presence of a lightly crosslinked BR in the matrix. As BR is slower curing than NR, in blends with NR, at optimum cure levels, the BR component is expected to attain only a lower state of cure (Table V.4).

Addition of reinforcing carbon black reduces the fatigue life in the case of NR and the 75/25 NR/BR blend and the reduction is not prominent in the case of tension fatigue. In the case of 50/50 NR/BR blend the fatigue life increases. Thus, the effect of blending BR with NR on the fatigue life becomes less marked in the filled vulcanizates, as compared to the unfilled vulcanizates.

Addition of reinforcing carbon black affects fatigue life in two ways : the increased tensile strength and tear resistance tend to increase the fatigue life, while the enhanced stiffness tends to reduce it. In the case of NR the unfilled vulcanizates have reasonably high strength, because of strain crystallization. Hence the effect of the enhanced stiffness, due to carbon black, on fatigue life predominates. However, in the case of BR the effect of the improvement in strength brought about by carbon black may overshadow or balance the effect of the increased stiffness. Hence the effect of filler on the fatigue life of NR/BR blends is not as marked as in the case of NR.

Figure V.16 is the SEM photograph of the flex fatigue failure surface of the unfilled NR vulcanizate. The surface shows a dimple structure. But the corresponding fractographs of the unfilled 75/25 and 50/50 NR/BR blends (Figures V.17 and V.18) show increased brittleness. This is supported by the physical properties (Table V.5). Presence of BR in blends increases the stiffness and hardness and lowers the elongation at break. Figure V.19 is an observation in the case of the unfilled 75/25 NR/BR blend, where a flaw in the matrix is seen initiating brittle fracture.

Addition of reinforcing filler makes the matrix stiffer and during flexing it undergoes brittle fracture as seen in Figure V.20, which is the SEM fractograph of the HAF black-filled NR vulcanizate. More or less similar fracture surfaces were observed in the case of the black-filled blend vulcanizates (Figure V.21). The surfaces show a large number of small cracks, which are less in the case of the blends. Table V.7 shows that the flex fatigue life of the black-filled NR/BR blend vulcanizates is slightly higher than that of the filled NR vulcanizate.

The nature of the fracture surfaces obtained from the Monsanto Fatigue-to-Failure tester is different from that obtained from the De Mattia machine. While the De Mattia machine gives rise to a fracture surface which is almost

uniform throughout, in the Monsanto tester the fracture surface of the unfilled vulcanizates can be divided into two zones : a rough zone similar in nature to the fracture surface obtained from the De Mattia machine and a comparatively smooth surface similar to the tear fracture surface of unfilled NR vulcanizates reported in Chapter III. The rough region is the region where the failure starts and from where the crack propagates in slow increments during each cycle of deformation. But when the crack grows to a reasonable size, the deformation causes tear fracture at a faster rate. The fracture surface in the tear zone shows tear paths. Figures V.22 and V.23 show the rough zone and smooth zone respectively in the case of the unfilled NR vulcanizates. These observations are in line with those of Bader and Johnson¹⁶⁹ and Prakash¹⁷⁰ who have reported the presence of two zones in the fatigue-failed surfaces of carbon fiber-reinforced polymer composites. An interesting observation made on this rubber fracture surface is the presence of a large number of small cracks in the matrix, which are found predominantly in the smooth zone and is shown in Figures V.23 and V.24. It is believed that the formation of these small cracks is a mode of dissipation of stress caused by cyclic tension. The fracture surface of the unfilled 75/25 NR/BR blend is similar to that of NR. Here also the surface consisted of a rough zone and a smooth zone. Also a number of small cracks were

observed in the smooth zone, a magnified image of which is shown in Figure V.24. On a closer examination of this figure, it is observed that the cracks are formed near small tear lines which are the regions of stress concentration in the matrix. Figure V.25 is the SEM fractograph of the unfilled 50/50 NR/BR blend. The figure clearly shows the two zones on the fracture surface. Here also the presence of small cracks was observed in both zones, but was not as widespread as in the case of NR and the 75/25 NR/BR blend.

With the addition of carbon black the fatigue life of NR and 75/25 NR/BR vulcanizates is reduced and the nature of fracture surface is also changed. Unlike the unfilled vulcanizates, here the whole surface appears to be uniform in nature. Figure V.26 is the fractograph of the black-filled NR which shows cracks all along the surface. This type of cracks has been observed in the flex fatigue failed surface also. Figure V.27 is the SEM fractograph of the black-filled 75/25 NR/BR blend. Cracks are less prominent in this case. In the case of the 50/50 NR/BR blend cracks are much less prominent as shown in Figure V.28 and the tension fatigue life is also higher (Table V.7).

In general it is found that the fracture surfaces obtained from the two types of tests are different in the case of the unfilled vulcanizates while they have more or less the same features in the case of the filled vulcanizates.

TABLE V.4

FORMULATIONS OF THE MIXES

| MIX | A | B | C | D | E | F |
|-------------------------------------|------|-----|-----|------|------|------|
| Natural rubber | 100 | 75 | 50 | 100 | 75 | 50 |
| Polybutadiene rubber | - | 25 | 50 | - | 25 | 50 |
| Zinc oxide | 5 | 5 | 5 | 5 | 5 | 5 |
| Stearic acid | 2 | 2 | 2 | 2 | 2 | 2 |
| HAF black (N 330) | - | - | - | 50 | 50 | 50 |
| Naphthenic oil | - | - | - | 5 | 5 | 5 |
| CBS | 3.5 | 3.5 | 3.5 | 3.5 | 3.5 | 3.5 |
| Sulfur | 0.5 | 0.5 | 0.5 | 0.5 | 0.5 | 0.5 |
| Optimum cure time at 150°C, min. | 16 | 18 | 22 | 9 | 10 | 11 |
| Cure rate index | 11.1 | 8.8 | 6.1 | 19.0 | 19.0 | 18.2 |

TABLE V.5

PHYSICAL PROPERTIES OF THE VULCANIZATES

| PROPERTIES | A | B | C | D | E | F |
|--|-------|-------|-------|-------|-------|-------|
| 300% Modulus, MPa | 1.3 | 1.5 | 1.6 | 9.5 | 9.7 | 10.1 |
| Tensile strength, MPa | 14.2 | 14.1 | 6.2 | 22.8 | 22.1 | 19.4 |
| Elongation at break, (%) | 740 | 690 | 550 | 540 | 510 | 440 |
| Tear resistance, kN/m | 19 | 20 | 18 | 63 | 54 | 43 |
| Hardness, Shore A | 35 | 40 | 44 | 62 | 64 | 66 |
| Resilience, % | 67 | 77 | 83 | 48 | 53 | 58 |
| Heat buildup, ΔT at 50°C, °C | 10 | 9 | 9 | 33 | 33 | 34 |
| Compression set, % | 11 | 18 | 13 | 22 | 28 | 22 |
| Crack growth resistance, Kilocycles to 12.5 mm length | 40.0 | 19.0 | 1.5 | 12.0 | 10.0 | 3.0 |
| V_r , volume fraction of rubber | 0.156 | 0.188 | 0.206 | 0.193 | 0.206 | 0.227 |

TABLE V.6

EXPERIMENTAL CONDITIONS IN TIE FATIGUE TESTS

| SL.NO. | PARAMETER | DE MATTIA | MONSANTO |
|--------|--|---|---|
| 1 | Mode of deformation | Flexing (bending) | Tension |
| 2 | Extent of deformation | 180° | Extension ratio, 2 |
| 3 | Test piece | Rectangular moulded slab with groove at the centre. | Dumbbell, die stamped from moulded sheet, thickness 1 mm. |
| 4 | Frequency of deformation, cycles/minute. | 300 | 100 |
| 5 | Temperature of test, °C | 30 | 30 |

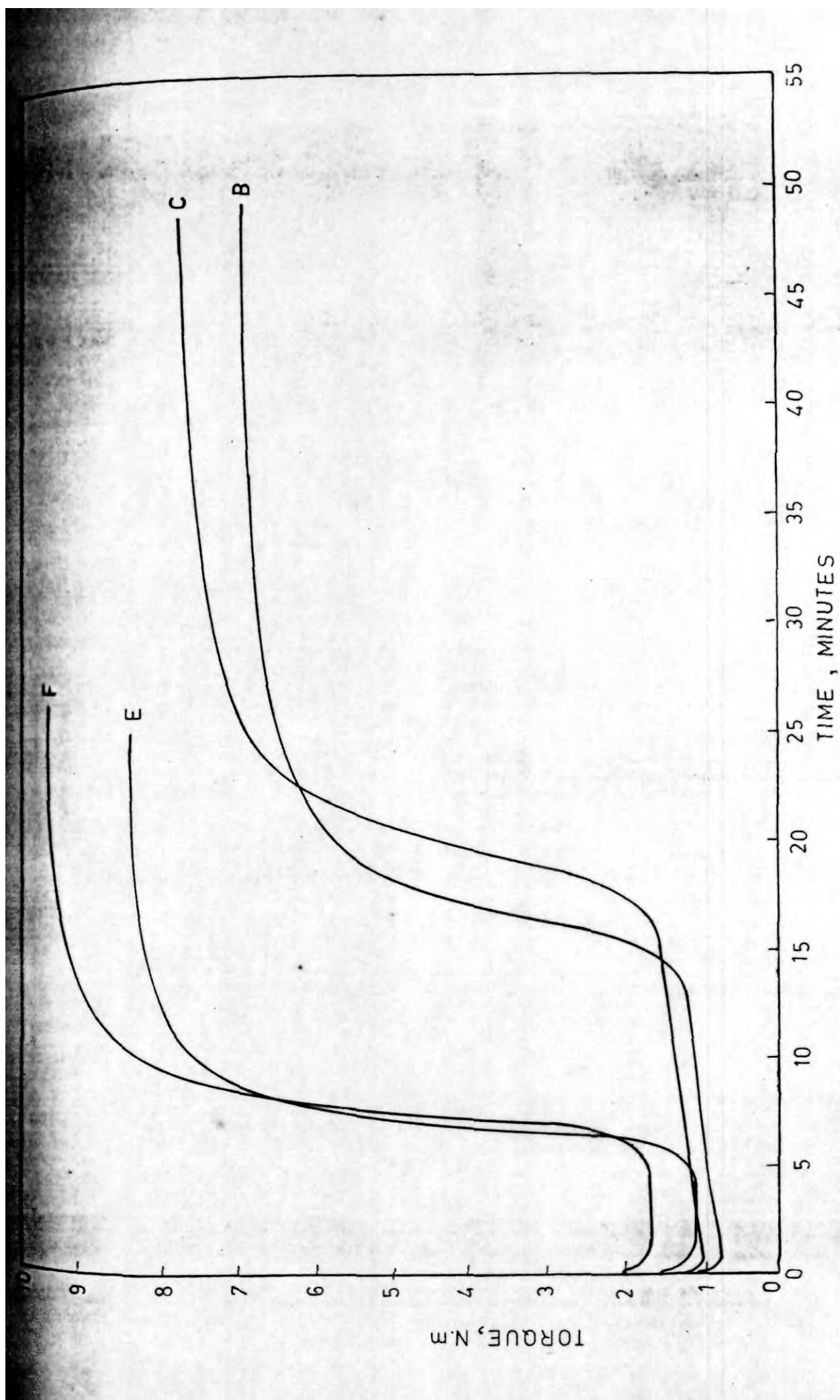


FIG. V.15. RHEOGRAPHS OF MIXES B, C, E AND F



FIG. V.16 : Flex fatigue failure of unfilled NR; dimple structure.

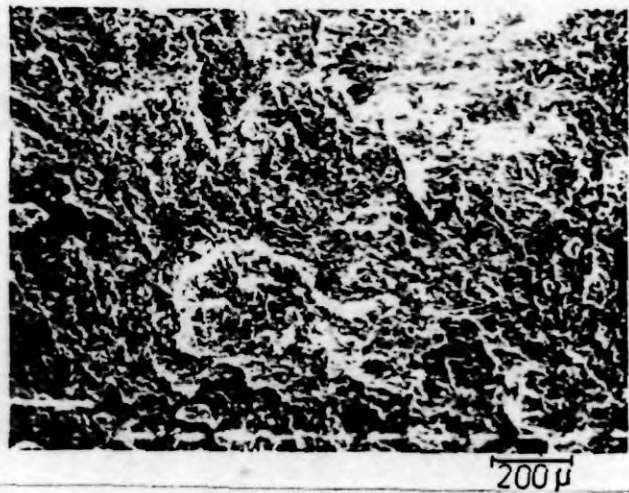


FIG. V.17 : Flex fatigue failure of unfilled 75/25 NR/BR blend; brittle failure.

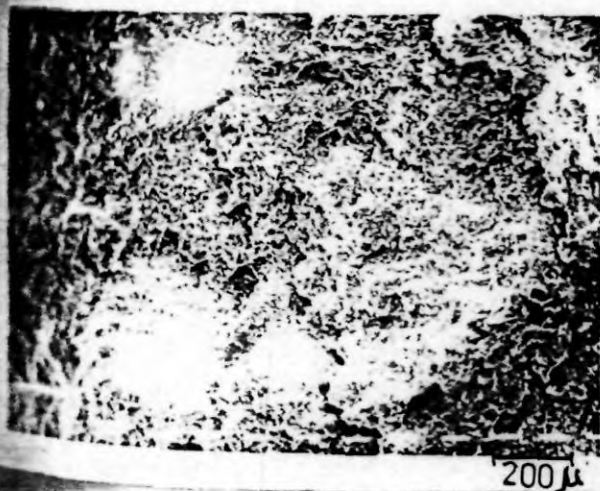


FIG. V.18 : Flex fatigue failure of unfilled 50/50 NR/BR blend; brittle failure.

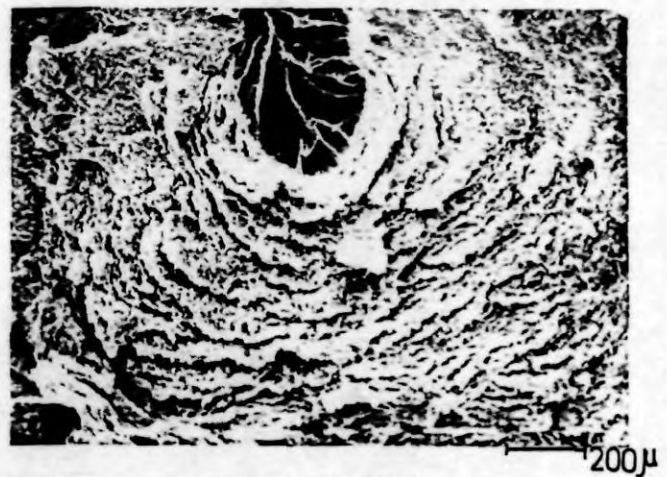


FIG. V.19 : Flex fatigue failure of unfilled 75/25 NR/BR blend; flaw initiating fracture.

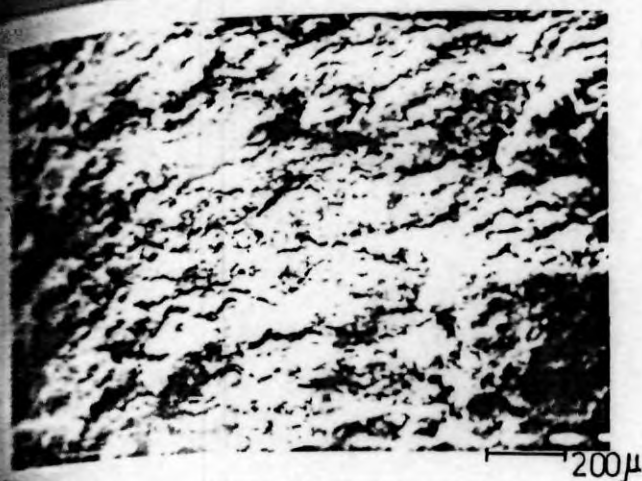


FIG. V.20 : Flex fatigue failure of black-filled NR; brittle failure with cracks.

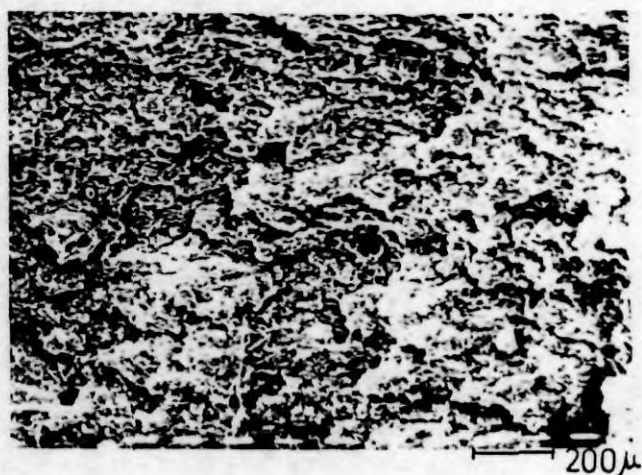


FIG. V.21 : Flex fatigue failure of black-filled 50/50 blend; general surface.

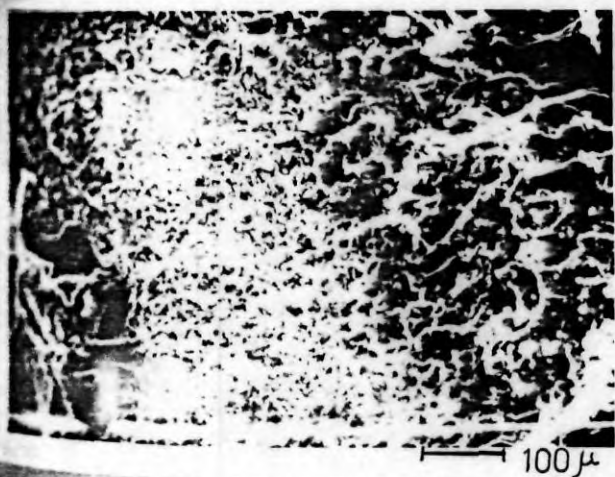


FIG. V.22 : Tension fatigue failure of unfilled NR; rough zone.

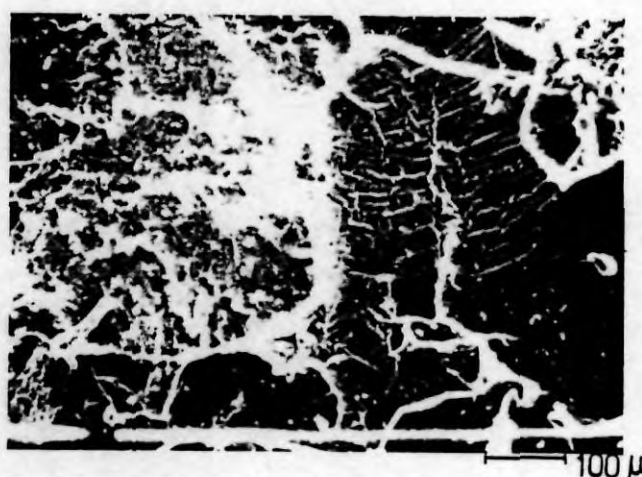


FIG. V.23 : Tension fatigue failure of unfilled NR; tear zone.

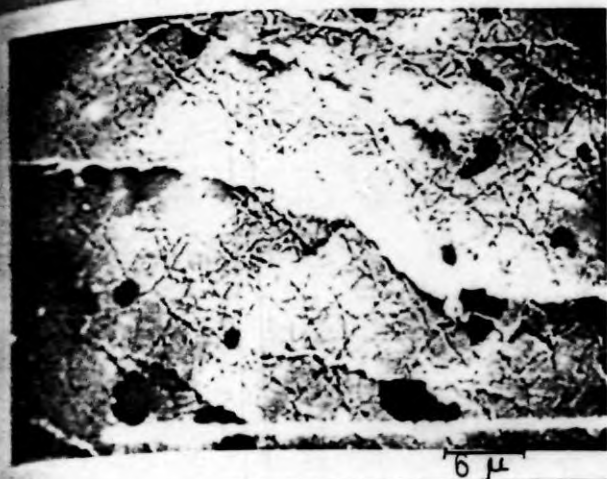


FIG. V.24 : Tension fatigue failure of unfilled 75/25 NR/BR blend; microcracks.

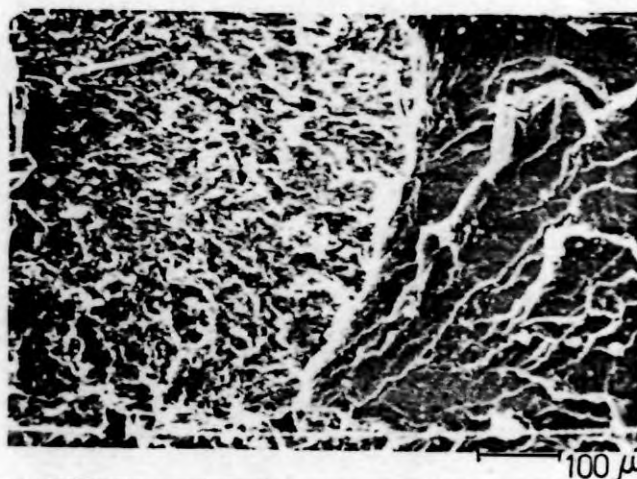


FIG. V.25 : Tension fatigue failure of unfilled 50/50 NR/BR blend; rough and tear zones.

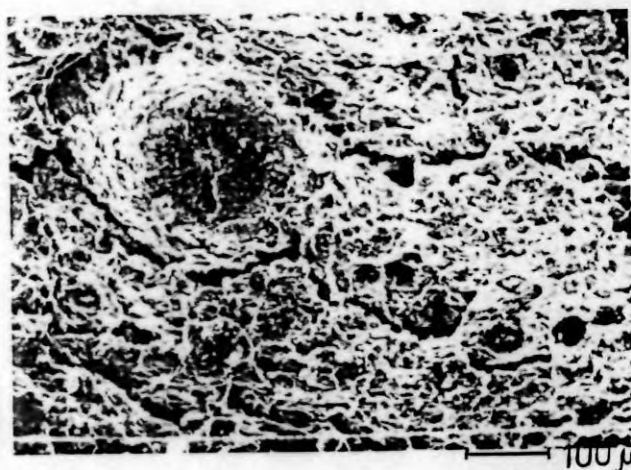


FIG. V.26 : Tension fatigue failure of black-filled NR; cracks on the surface.

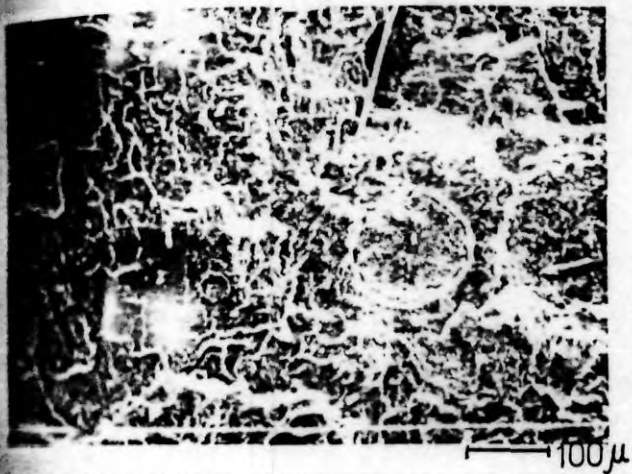


FIG. V.27 : Tension fatigue failure
of black-filled 75/25 NR/ER blend;
general surface.

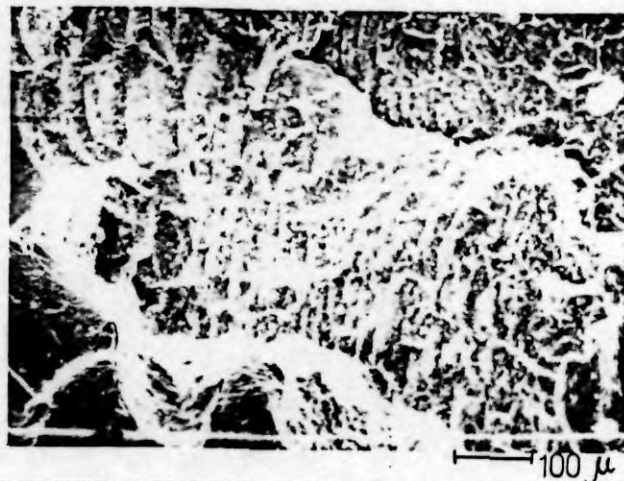


FIG. V.28 : Tension fatigue failure
of black-filled 50/50 NR/ER blend;
general surface.

CHAPTER VI

STUDIES ON ABRASION

**SCANNING ELECTRON MICROSCOPIC STUDIES ON ABRASION OF
NR/BR BLENDS UNDER DIFFERENT TEST CONDITIONS**

**Results of this Chapter have been published in
Journal of Materials Science, 17 (1982).**

Abrasion is an important factor leading to the failure of a number of rubber products including tires. It is, perhaps, the least understood among the various types of failure of rubber. A number of studies have been made by several authors to understand the abrasion process in detail. Schallamach⁶² was the first to study the abrasion pattern on abraded rubber surfaces, which is believed to play a significant role in the abrasion process. Later studies by the same author⁶³⁻⁶⁵ have given more information on the phenomenon. But the exact mechanism of formation of the abrasion pattern and the extent of its influence on abrasive wear are not clearly known. Reznikovskii and Brodskii⁶⁶⁻⁶⁹ have described the different types of wear occurring during abrasion of elastic materials and attempted to find out the influence of

non-mechanical factors on abrasion as well as the relation between mechanical properties of rubber and its abrasion resistance. A recent study by Southern and Thomas⁷³ described the application of fracture mechanics to explain abrasion of rubber. According to these authors, the formation of the abrasion pattern is followed by crack growth which plays an important role in the abrasion process. Laboratory tests for abrasion resistance are used mainly to rank materials. Usually these tests are used to control manufacturing uniformity. Over the years a number of tests have been developed to test the abrasion resistance of rubbers⁷⁴. None of these tests can predict precisely the behavior of rubbers under actual service conditions and even the ranking obtained from one test method may not hold good in another. This shows the complex nature of abrasion of rubber and that the mechanism of abrasion under different test conditions is quite different.

The superior abrasion resistance of polybutadiene rubber is well known¹⁷¹. Blends of BR with natural rubber, which combine the superior abrasion resistance of the former with the excellent processing and physical properties of the latter, are now popularly used in areas like tire treads and conveyor belts. However, studies on the mechanism of abrasion of these blends, especially when tested under different conditions, have not been made. Recently Bhowmick, Basu and De¹³⁹ have studied the abraded surfaces of BR and styrene-butadiene rubber using scanning electron microscope, with a view to study the mechanism of wear of these rubbers.

In this Chapter an attempt is made to study the abrasion of IR/ER blends, in different abrasion test machines, using SEM. The parameters studied include : (a) effect of test conditions, (b) effect of blend ratio and (c) effect of reinforcing carbon black. The formulations of the mixes are given in Table VI.1. The rheographs of these mixes were already given in Chapter V. (Figure V.15). The physical properties of the mixes are furnished in Table VI.2. The test conditions were varied by using three different testing machines, namely Croydon-Akron abrader, DIN abrader and Du Pont abrader, details of which are summarized in Table VI.3. The shape and size of the test specimens and the direction of abrasion are shown in Figure VI.1. In the case of the DIN abrader the direction is changing continuously.

In the Akron abrader the contour of the circular test specimen, mounted on a motor-driven spindle, is brought into contact with the periphery of an abrasive wheel, which is mounted on another spindle. Rotation of the specimen causes the abrasive wheel to rotate and the two are held together under a force of 4.5 kg. The axis of the specimen and the axis of the abrasive wheel are at an angle of 20° , which causes a rubbing action. The abrasion resistance of the specimen is calculated from its weight loss after a specified number of revolutions of the abrasive wheel. During the test, the abrasive wheel was cleaned manually with a brush and the specimen surface was continuously cleaned with a circular brush which was running in contact with the

specimen. In the Du Pont machine two test pieces, each having 2 cm. square surfaces, are simultaneously held against an abrasive paper disc rotating at a speed of 40 rpm. The two are held together under a load of 3.62 kg and the abrasive paper disc used was silicon carbide type having a grain size of 325. The specimens were abraded for 10 minutes and the abrasion loss was calculated in terms of volume loss. During the test the abrasive surface was continuously cleaned with a compressed air jet. The DIN abrader differs from the other two in that the direction of abrasion changes continuously. This is achieved by rotating the specimen on its own axis while undergoing abrasion. The cylindrical specimen, 16 mm in diameter, is brought into contact with the abrasive surface (emery cloth No. 60 mounted on a drum) under a normal load of 1.0 kg. The specimen is made to travel from one end of the drum to the other. The drum rotates at a speed of 40 rpm so that by the time the specimen reaches the other end of the drum, it traverses a distance of 40 meters. The abrasion is calculated in volume loss in one run of 40 meters. The specimens for SEM study were carefully cut from the abraded surfaces (after 500 revolutions in the case of Akron, after 10 minutes of abrasion in Du Pont and after 1 run of 40 meters in DIN) and were gold shadowed in a sputter coater within 72 hrs of testing.

Akron abrader : Figures VI.2 and VI.3 show the plots of abrasion loss of the unfilled and filled vulcanizates against the number of revolutions in the Akron abrader. The unfilled 75/25 NR/BR

blend shows a slow rate of abrasion initially which increases and again slows down as the abrasion is continued. But the unfilled 50/50 NR/BR blend shows a different behavior, showing a rapid rate of abrasion right from the beginning. It may be assumed that abrasion in Akron abrader is governed by the tensile and fatigue properties. From Table VI.2 it is seen that tensile strength, flexing resistance and crack growth resistance are higher for the 75/25 NR/BR blend. Southern and Thomas⁷³ have shown that crack growth plays an important role in abrasion. The initial slow rate of abrasion observed in the case of the 75/25 NR/BR blend is believed to be caused by the delay in the formation of the abrasion pattern. Schallamach⁶² found earlier that the rate of abrasion is slow till the abrasion pattern is well developed and from then onwards the rate increases rapidly. The decrease in the rate of abrasion as the abrasion is continued for a longer time, can be attributed to smearing as reported by Schallamach¹⁷². Smearing is caused by the thermo-oxidative degradation of the surface layer of rubber accelerated by high mechanical action and results in a sticky surface layer.

Figures VI.4 and VI.5 are the SEM photographs of the abraded surfaces of the unfilled 75/25 NR/BR blend vulcanizates. Figure VI.4 shows a coarse abrasion pattern. The ridges are large but are wide apart. It is interesting to note that, contrary to earlier reports, here the ridges are not perpendicular to the direction of abrasion. This is caused by two factors : the slip angle of 20° and the deformation of the sample in the contact area. In the case

of soft unfilled vulcanizates, the deformation is so large that the direction of abrasion is believed to be turned almost by 90° . Thus the actual direction of abrasion in those samples is more or less across the circumference of the specimen, giving rise to a pattern with ridges running along the circumference. Therefore, the contradiction regarding the direction of the abrasion pattern, as mentioned above, is only an apparent one. Figure VI.5 is a magnified image of one of the ridges. The intense mechanical action on the ridges produces folding on the surface which is clearly seen in Figure VI.5. When the proportion of BR is increased as in 50/50 NR/BR blend, the unfilled vulcanizate shows much higher abrasion loss as is evident from Figure VI.2 and Table VI.4. Figures VI.6 and VI.7 are the SEM photographs of the abraded surface of the unfilled 50/50 NR/BR blend vulcanizate. The abrasion pattern which was observed in the case of the 75/25 NR/BR blend is not prominent in this case. Though ridges are formed during abrasion, the strength of the matrix is so poor that the ridges get torn off soon after their formation, thereby giving rise to an apparently ridge-free surface. From figure VI.7 it appears that material from the surface has been chipped off by the hard asperities on the abrasive surface.

Addition of reinforcing carbon black makes the matrix stronger, as is evident from Table VI.2. Abrasion resistance is improved remarkably. Figure VI.3 shows that the 75/25 NR/BR blend gives slightly lower abrasion loss initially but as the abrasion is continued it registers a higher loss than the 50/50

NR/BR blend. The tensile strength of these vulcanizates are more or less the same. However, the fatigue resistance of the filled 75/25 NR/BR blend is less than that of the 50/50 NR/BR blend. This might account for the slightly higher abrasion loss of the 75/25 NR/BR blend, when the abrasion is continued for a longer period. Figure VI.8 is the SEM photograph of the abraded surface of the black-filled 75/25 NR/BR blend. Here the ridges are much closer and they are formed at an angle of about 45° to the circumference of the specimen. The difference in the direction of the ridges in the unfilled and filled vulcanizates may be due to the difference in the extent of deformation that the specimen surface undergoes when it slides against the abrasive wheel. Figures VI.9 and VI.10 are the SEM photographs in the case of the black-filled 50/50 NR/BR blend. Figure VI.9 shows a pattern which is almost identical to that obtained in the case of the 75/25 NR/BR blend. Figure VI.10 shows material being removed from the ridges.

DIN abrader : In the DIN abrader the results obtained are different from that from the Akron abrader. This is especially true in the case of the unfilled vulcanizates. The abrasion loss of the 50/50 NR/BR blend is almost a half of that of the 75/25 NR/BR blend. Under the conditions of testing in the DIN abrader, coefficient of friction is believed to play the major role in determining abrasion loss. Grosch and Schallanach¹⁷³ have reported that the coefficient of friction of BR is lower

than that of NR and that carbon black reduces it still further. The coefficient of friction of NR/BR blends may be assumed to decrease with increase in the proportion of BR. This might account for the lower abrasion loss of the 50/50 blend in the DIN abrader. The SEM photographs in the case of the unfilled 75/25 NR/BR blend vulcanizates (Figures VI.11 and VI.12) are different from those obtained from the same vulcanizate tested in the Akron abrader. The ridges are not continuous and do not form a well defined pattern. This is evidently due to the continuous change in the direction of abrasion during the test. Deformation of the ridges is clearly seen in Figure VI.12. The abrasion pattern is still less defined in the case of the unfilled 50/50 NR/BR blend, as shown in Figures VI.13 and VI.14. Ridges are not observed at all. Here, material removal is found to occur in small lumps. Two such lumps are magnified and shown in Figure VI.14. The structure of the lumps are very similar to that of the ridges found in samples obtained from Akron abrader. As expected, the reinforcing black-filled vulcanizates show lower abrasion loss, the 50/50 NR/BR blend being better than the 75/25 NR/BR blend. The abraded surface of the 75/25 NR/BR blend vulcanizate does not show any clear pattern, although a few coarse ridges are seen (Figure VI.15). However, a more or less well defined pattern is formed in the case of the 50/50 NR/BR blend (Figure VI.16). Here the ridges are not continuous as in the case of the Akron abrader.

Du Pont abrader : Results obtained from the Du Pont abrader are more or less similar to those obtained from the DIN abrader, except for the fact that unfilled 50/50 NR/BR blend vulcanizate shows remarkably low abrasion loss. Here also it is believed that the coefficient of friction plays the major role in determining the abrasion loss. It may be noted here that the abrasive surface used in the Du Pont abrader (silicon carbide paper, grain size 325) was quite fine as compared to those in the other two machines. But unlike in those machines, the abrasive action in the present case is continuous and in the same direction. Figures VI.17 and VI.18 show the abraded surface of the unfilled 75/25 NR/BR vulcanizate. A pattern of ridges formed at right angle to the direction of rotation is clearly visible. Unlike in the case of the Akron abrader, here the ridges are finer. Material removal from the ridge is shown in Figure VI.18. The abraded surface of the unfilled 50/50 NR/BR blend, as shown in Figures VI.19 and VI.20 shows a very different picture. Only some scratch marks are observed on the surface. Possibly due to the continuous rubbing action, some sort of ball formation is observed on the surface, which is clearly shown in Figure VI.20. As pointed out earlier, abrasion loss in this case is abnormally low. The abrasion loss in the case of black-filled blend vulcanizates, as expected, is low, but the difference between the unfilled and filled vulcanizates of the 50/50 NR/BR blend is not significant. The abraded surface of the black-filled 75/25

NR/BR blend, as shown in Figure VI.21, gives a very fine and well defined pattern with ridges running perpendicular to the direction of abrasion. But in the case of the black-filled 50/50 NR/BR blend, the pattern is not well developed, as shown in Figure VI.22. But there is a definite tendency towards the formation of a pattern.

TABLE VI.1

FORMULATIONS OF THE MIXES

| MIX | A | B | C | D |
|----------------------|-----|-----|-----|-----|
| Natural rubber | 75 | 75 | 50 | 50 |
| Polybutadiene rubber | 25 | 25 | 50 | 50 |
| Zinc oxide | 5 | 5 | 5 | 5 |
| Stearic acid | 2 | 2 | 2 | 2 |
| HAF black (N 330) | - | 50 | - | 50 |
| Naphthenic oil | - | 5 | - | 5 |
| CBS | 3.5 | 3.5 | 3.5 | 3.5 |
| Sulfur | 0.5 | 0.5 | 0.5 | 0.5 |

TABLE VI.2

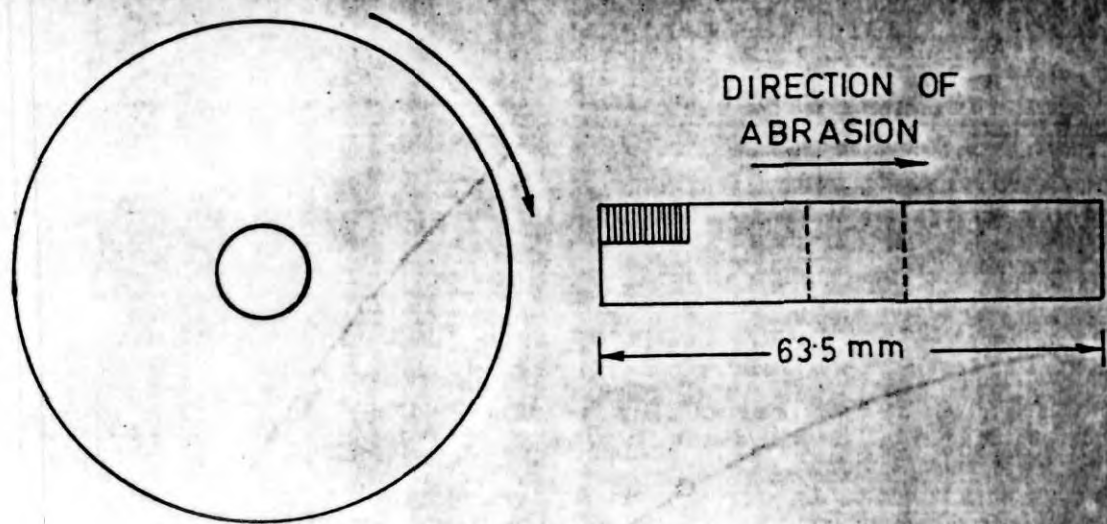
PHYSICAL PROPERTIES OF THE MIXES

| MIX | A | B | C | D |
|---|-------|------|-----|------|
| Optimum cure time at 150°C, min. | 18 | 10 | 22 | 11 |
| 300% Modulus, MPa | 1.5 | 9.7 | 1.6 | 10.1 |
| Tensile strength, MPa | 14.1 | 22.1 | 6.2 | 19.4 |
| Elongation at break, % | 690 | 510 | 550 | 440 |
| Tear resistance, kN/m | 20 | 54 | 18 | 43 |
| Hardness, Shore A | 40 | 64 | 44 | 66 |
| Resilience, % | 77 | 53 | 83 | 58 |
| Heat buildup, ΔT , °C | 9.0 | 33 | 9 | 34 |
| Permanent set, % | 0.6 | 2.8 | 0.8 | 2.1 |
| Compression set, % | 18 | 28 | 13 | 22 |
| Flexing resistance, kilocycles to failure | > 130 | 22 | 10 | 30 |
| Crack growth resistance, kilocycles | 19 | 10 | 1.5 | 3.0 |

TABLE VI.3

TEST CONDITIONS IN DIFFERENT ABRASERS

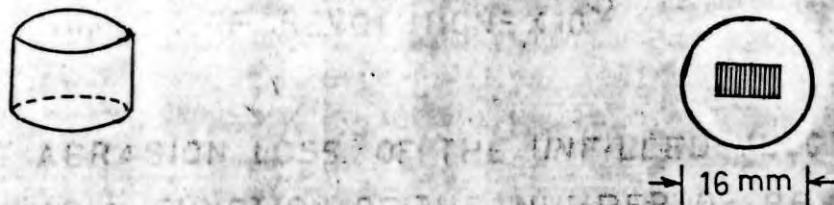
| | AKRON | DIN | DU PONT |
|---|---------------------------|---|---|
| 1 | Nature of abrasive action | Discontinuous | Continuous |
| 2 | Temperature of test | 30°C | 30°C |
| 3 | Test specimen | Circular in shape, 1.37 cm thick, 6.35 cm outside dia., with a central hole of 1.27 cm dia. | Cylindrical in shape with 1.6 cm dia. 2 cm square, 1 cm thick with provision for easy insertion of the specimen in the clamp. |
| 4 | Abrasive | Aluminum oxide wheel Grade A, 36-PS-V, 15 cm dia, 2.54 cm, thick. | Emery cloth No. 60 Silicon carbide paper, grain size 225. |
| 5 | Slip angle | 20° | 0° |
| 6 | Normal load, kg. | 4.5 | 1.62 |
| 7 | Speed of testing | Specimen rotates at 250 rpm; corresponding speed of the abrasive wheel is 104 rpm. | Drum rotates at 40 rpm. speed. Abrasive disc rotates at 40 rpm speed. |
| 8 | Sliding velocity, cm/sec. | 83 | 27 |



a AKRON



b DU PONT



c DIN RACER

FIG. VI-1. SHAPE AND SIZE OF THE TEST SPECIMENS AND THE DIRECTION OF ABRASION. THE SHADED AREA IS THE PORTION REMOVED FOR SEM OBSERVATIONS

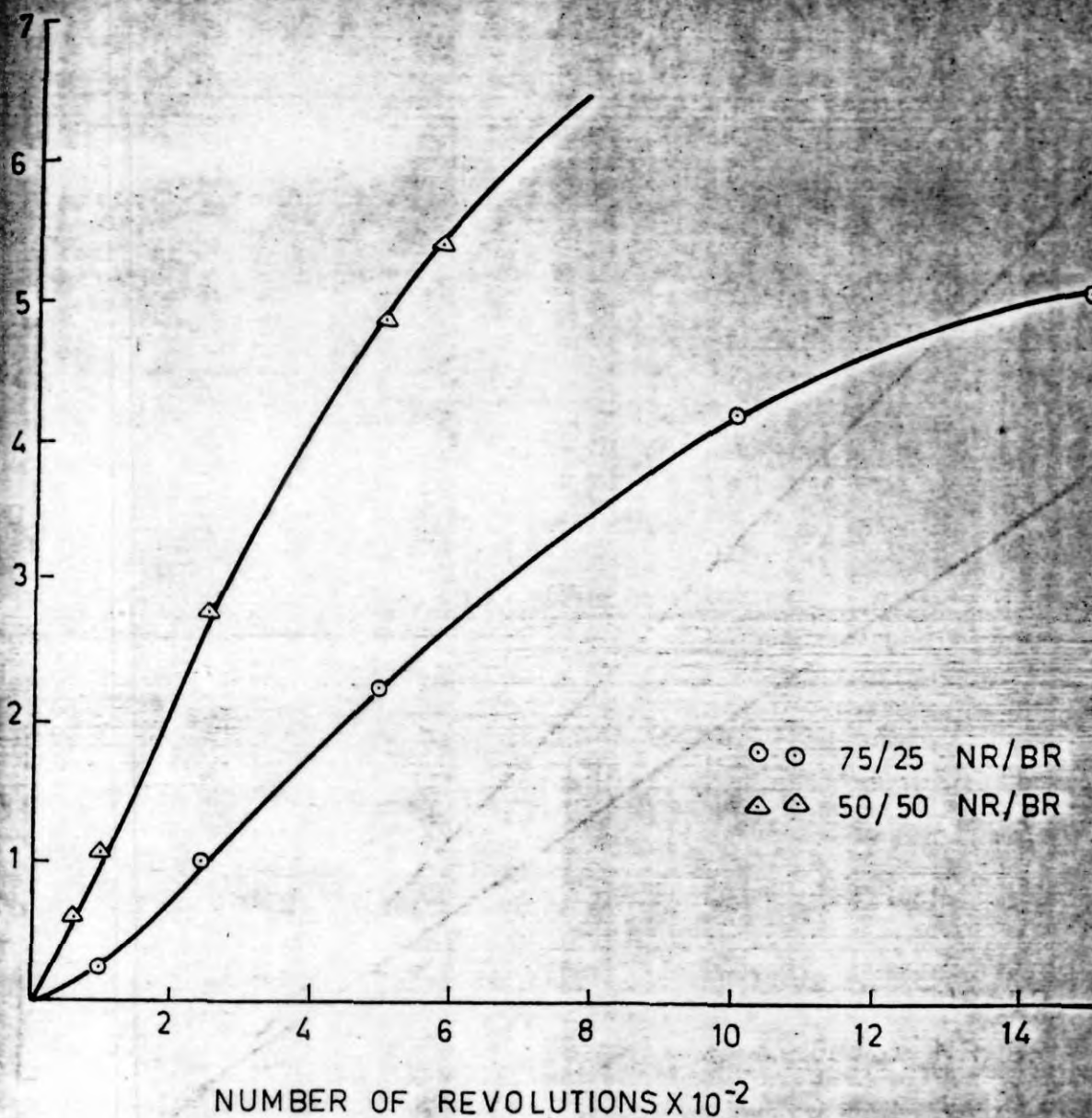


FIG. VI.2. ABRASION LOSS OF THE UNFILLED VULCANIZATES AS A FUNCTION OF THE NUMBER OF REVOLUTIONS IN THE AKRON ABRADER

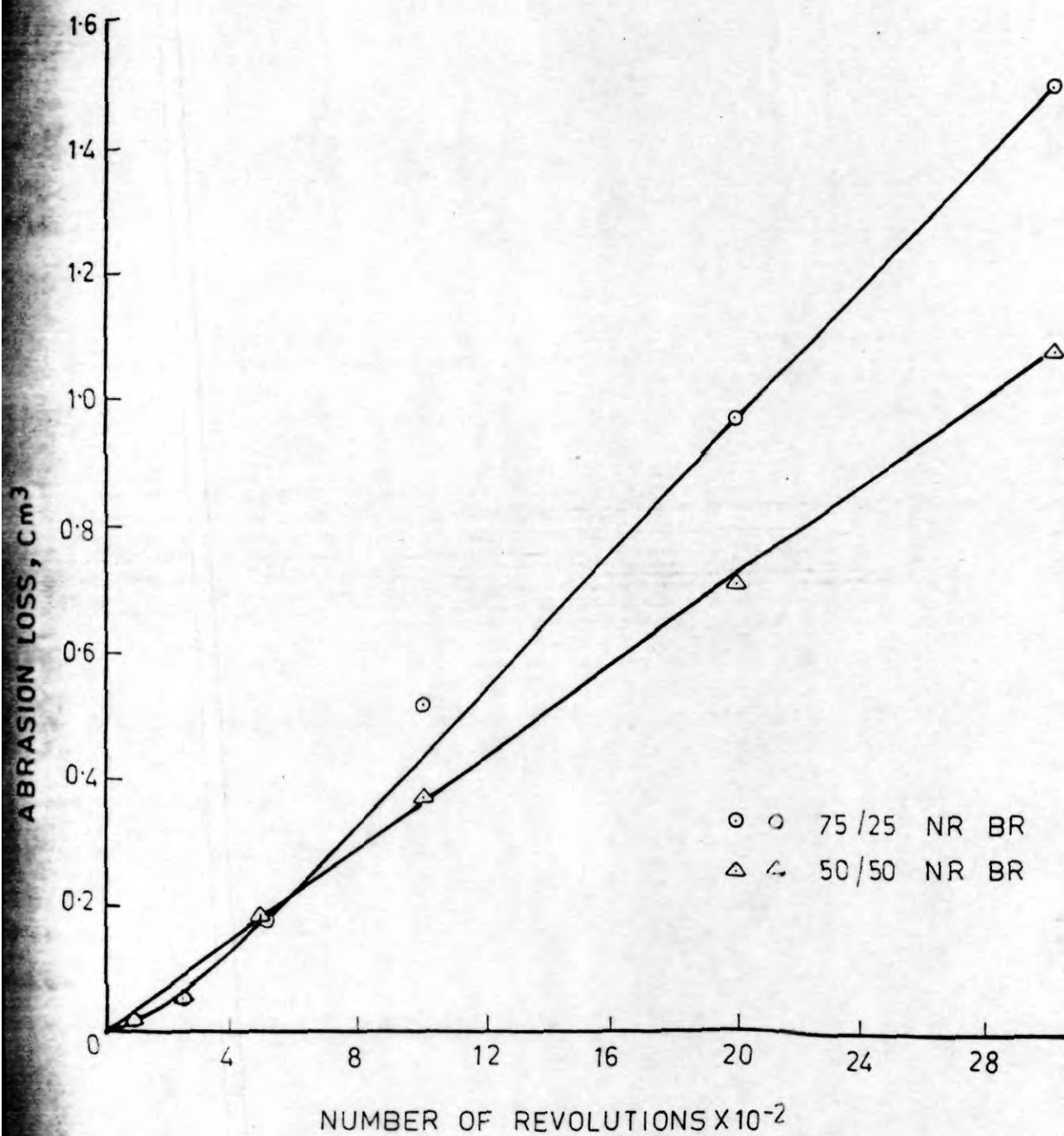


FIG. VI. 3. ABRASION LOSS OF THE FILLED VULCANIZATES AS A FUNCTION OF THE NUMBER OF REVOLUTIONS IN THE AKRON ABRADER.

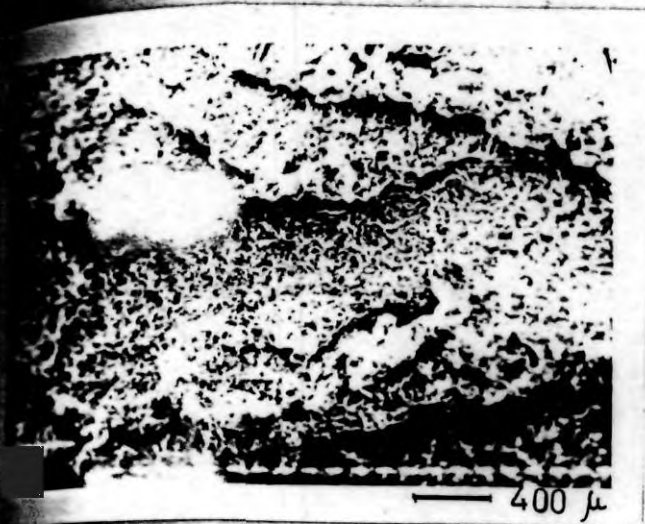


FIG. VI.4 : Abraded surface of the filled 75/25 NR/BR blend in the Akron abrader; coarse abrasion pattern.

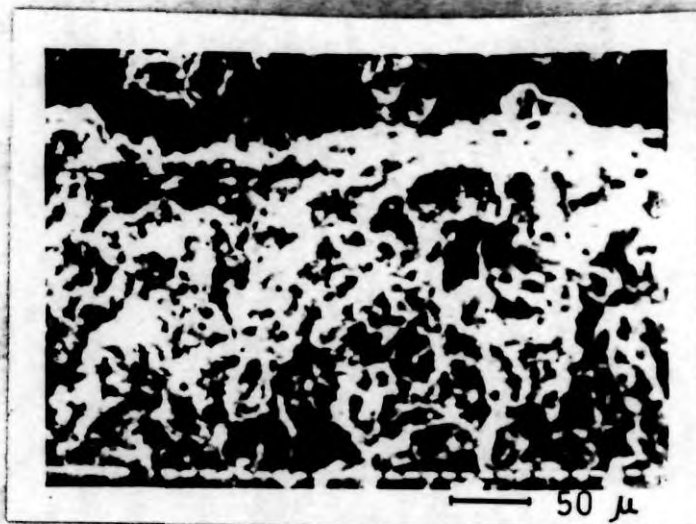


FIG. VI.5 : Abraded surface of the unfilled 75/25 NR/BR blend in the Akron abrader; magnified image of the ridge.

(18)

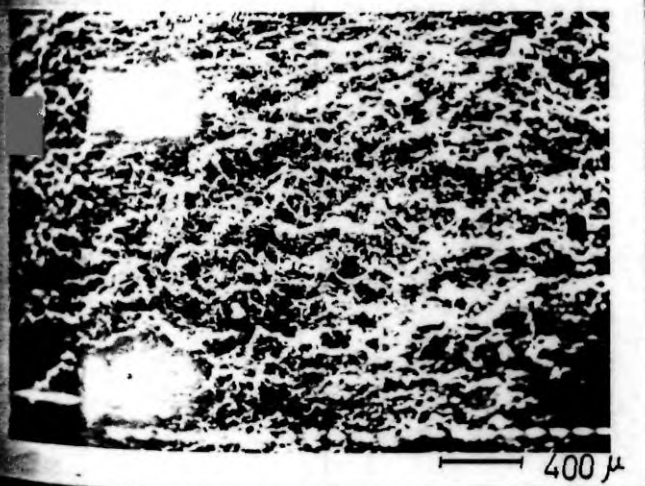


FIG. VI.6 : Abraded surface of the filled 50/50 NR/BR blend in the Akron abrader; ridge-free surface.

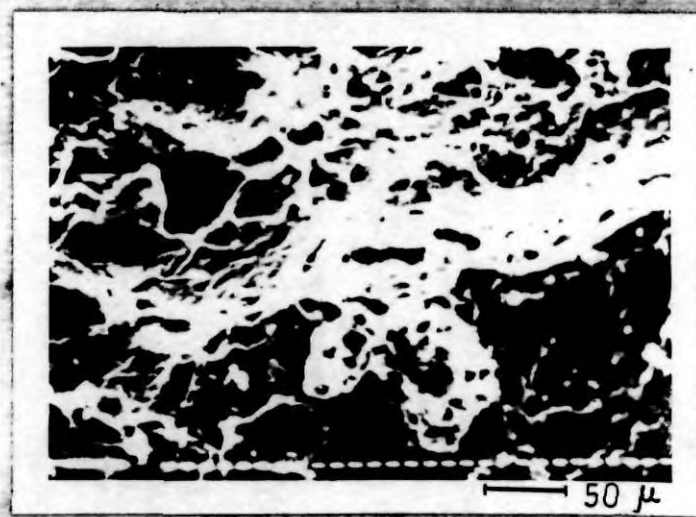


FIG. VI.7 : Abraded surface of the unfilled 50/50 NR/BR blend in the Akron abrader, material removal from the surface.

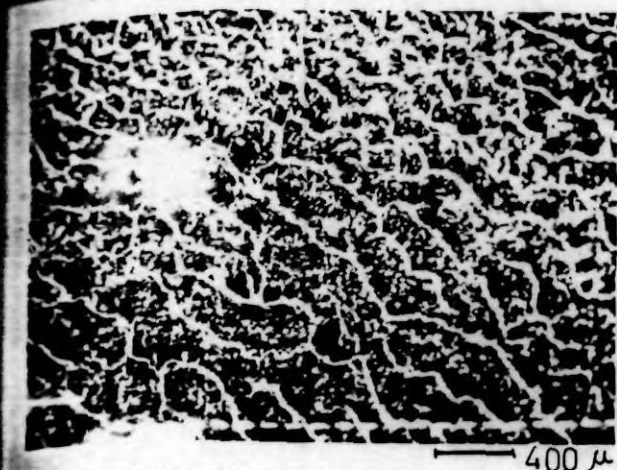


FIG. VI.8 : Abraded surface of the black-filled 75/25 NR/BR blend in the Akron abrader; pattern forming an angle with the direction of abrasion.

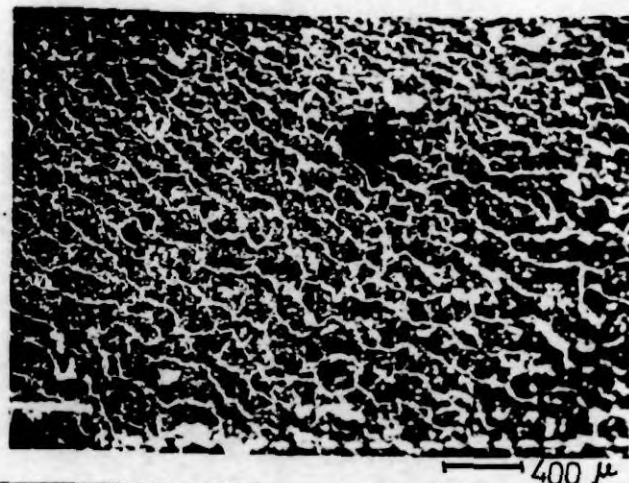


FIG. VI.9 : Abraded surface of the black-filled 50/50 NR/BR blend in the Akron abrader; finer abrasion pattern.

(19)



FIG. VI.10 : Abraded surface of the black-filled 50/50 NR/BR blend in the Akron abrader; material removal.

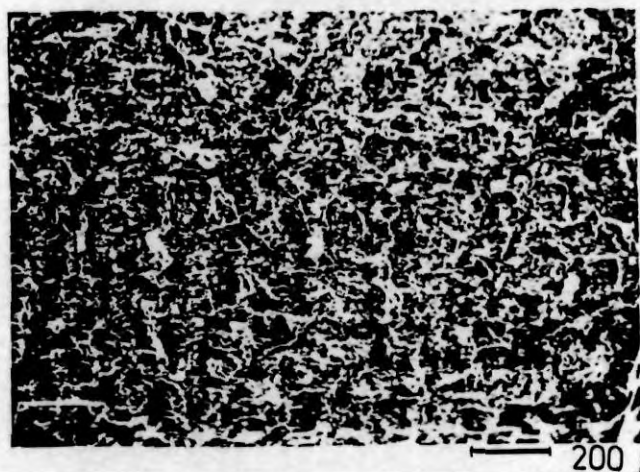


FIG. VI.11 : Abraded surface of the unfilled 75/25 NR/BR blend in the DIN abrader; discontinuous ridges.

(20)

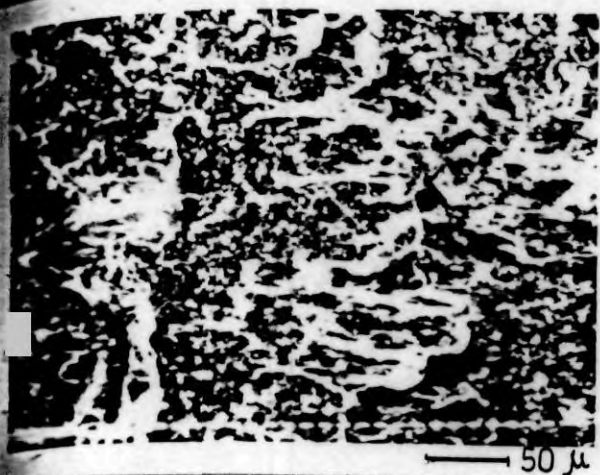


FIG. VI.12 : Abraded surface of the unfilled 75/25 NR/BR blend in the DIN abrader; deformed ridges.

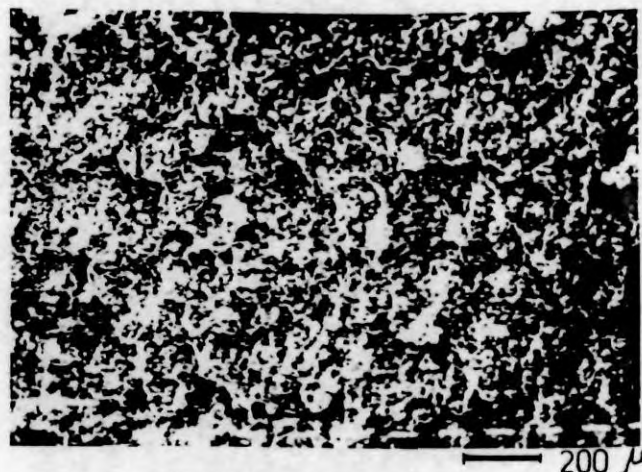


FIG. VI.13 : Abraded surface of the unfilled 50/50 NR/BR blend in the DIN abrader; ridge-free surface.

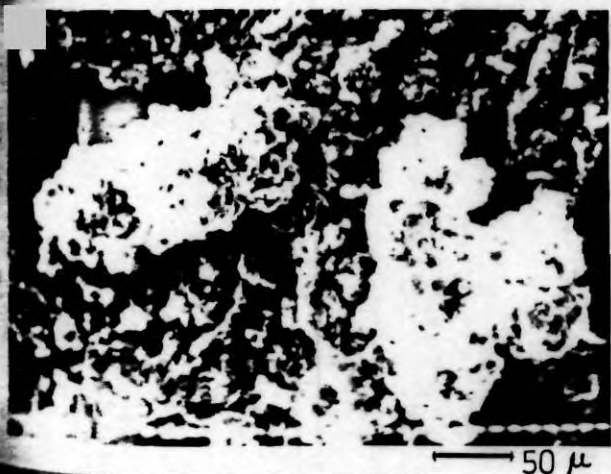


FIG. VI.14 : Abraded surface of the unfilled 50/50 NR/BR blend in the DIN abrader; lumps of abraded rubber.

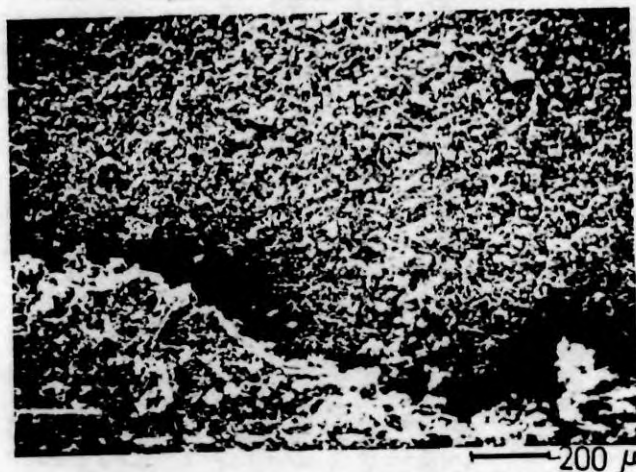


FIG. VI.15 : Abraded surface of black-filled 75/25 NR/BR blend in the DIN abrader; coarse ridges.

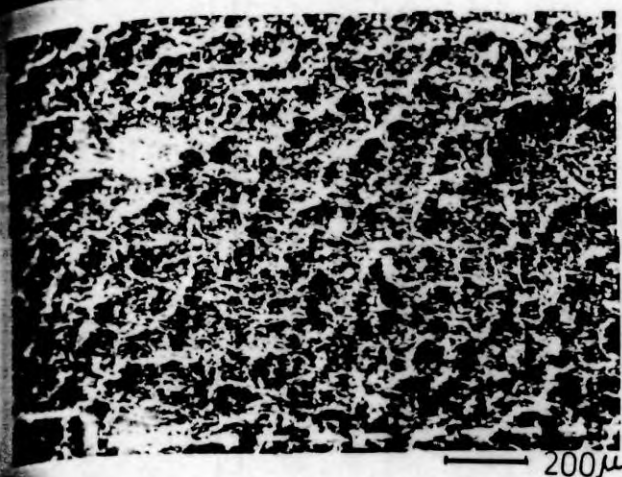


FIG. VI.16 : Abraded surface of the black-filled 50/50 NR/BR blend in the DIN abrader; discontinuous ridges.



FIG. VI.17 : Abraded surface of the unfilled 75/25 NR/BR blend in the Du Pont abrader; ridges running perpendicular to the direction of abrasion.

22

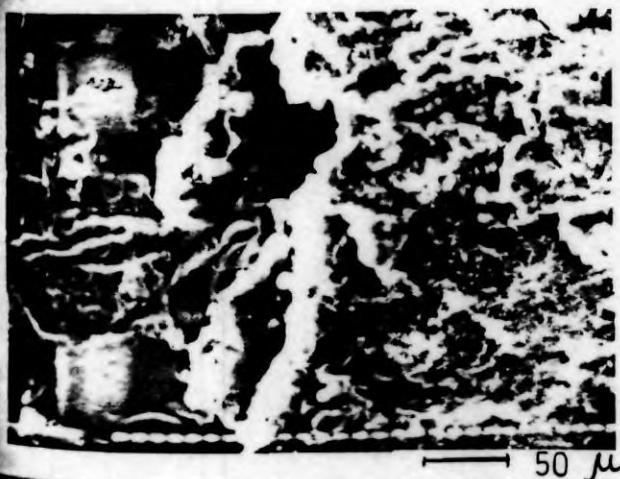


FIG. VI.18 : Abraded surface of the unfilled 75/25 NR/BR blend in the Du Pont abrader; material removal from the ridges.

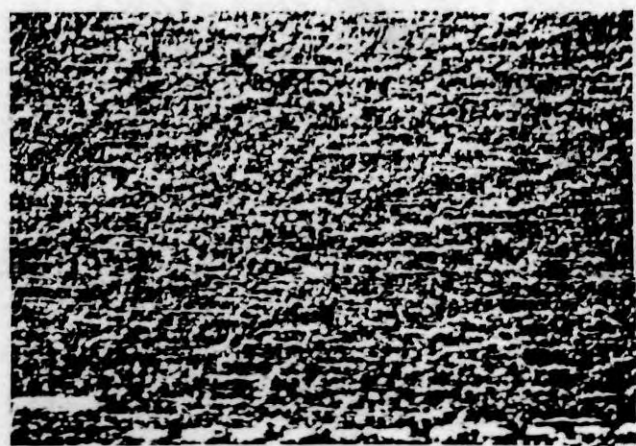


FIG. VI. 19 : Abraded surface of the unfilled 50/50 NR/BR blend in the Du Pont abrader; scratch marks on the surface.



FIG. VI.20 : Abraded surface of the unfilled 50/50 NR/BR blend in the Du Pont abrader; ball formation on the surface.



FIG. VI.21 : Abraded surface of the black-filled 75/25 NR/BR blend in the Du Pont abrader; fine pattern.

(23)

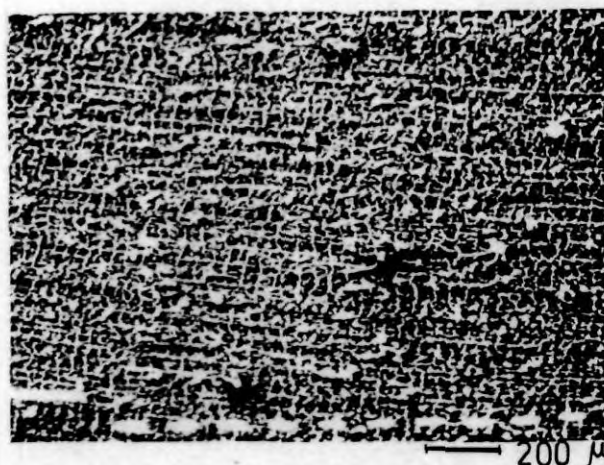


FIG. VI.22 : Abraded surface of the black-filled 50/50 NR/BR blend in the DU Pont abrader; abrasion pattern in the early stages of formation.

CHAPTER VII

**PART A. NETWORK CHANGES IN NATURAL RUBBER
VULCANIZATES UNDER COMPRESSION.**

**PART B. NETWORK CHANGES IN V-BLET RUBBER BASE
DURING SIMULATED SERVICE TESTING.**

**PART. A. NETWORK CHANGES IN NATURAL RUBBER
VULCANIZATES UNDER COMPRESSION.**

**This part has been published in Journal of Applied
Polymer Science, 27, 1827 (1982).**

Rubber products are subjected to various forms of mechanical and thermal strains during service and it is likely that their network structure undergoes changes during service. Such structural changes contribute considerably towards the deterioration of rubber products. A sound knowledge about the structural changes that are likely to occur in vulcanizates under service conditions will help in understanding their failure phenomena. Nando and De^{88,89} studied changes in the network structure of natural rubber vulcanizates subjected to different physical tests, since these tests, either singly or in combination, simulate at least a few service conditions. Stuckey and coworkers⁹⁰

recently reported decrease in the proportion of polysulfidic linkages in NR vulcanizates during De Mattia flexing. Cunneen and Russel⁹¹ reported changes in chemical structure of NR tire tread vulcanizates during simulated and actual service conditions. They found marked reduction in the concentration of polysulfidic linkages and increase in main chain modifications. Increase in crosslink density in tire treads during service was observed by Howard and Wilder⁹². But the extent of increase depends on the curative system and the nature of the base polymer. However, more extensive studies in this line are required to understand the failure phenomena in detail.

During service life a number of rubber products are subjected to compression at elevated temperature. In this part an attempt is made to study the changes occurring in NR vulcanizates under compression at elevated temperature. The study gives an idea whether the network changes, if they occur at all, are due to compression or aging or both. For this a Conv. vulcanizing system has been chosen in gum, whiting-, black- and silica-filled mixes. The effects of using EV system and a higher test temperature were also studied in the gum mix. It is generally known that rubber products can be protected from aging by the use of antioxidants. Hence, the effect of an antioxidant, phenyl- β -naphthylamine (PBNA), in the above compounds has also been investigated. The formulations of the

various mixes are given in Table VII.1. The rheographs of mixes C and E are given in Figure VII.1. The rheographs of the other mixes are already given in Chapter IV. (Figures IV.1 and IV.2). The compression set test was done at 25% strain and for 22 hours at 70°C. The test was done also at 100°C in the case of the gum vulcanizates. In order to study the effect of aging alone, samples were kept simultaneously at the same temperature, but without compression. The compressed as well as the aged samples were subjected to chemical analysis.

Samples for determining the network characteristics were taken from the inside middle sections of all the specimens. The extent of scatter in experimental results was assessed by carrying out estimations on samples taken from the surface and core of three different test pieces, selected at random. Table VII.3 gives the mean of three estimations and the standard deviation.

Physical properties of the vulcanizates : The optimum cure times and the physical properties of the mixes are given in Table VII.2. The higher strength properties of the Conv. gum mixes, in comparison to the EV gum mixes, may be attributed to the higher proportion of polysulfidic linkages in the former as shown in Table VII.4. For the same reason they show higher resilience and flexing resistance. Whiting is a

non-reinforcing filler and hence its addition causes reduction in strength properties. However, there is a slight improvement in modulus and hardness. The reinforcing capacity of HAF black is very much evident from the physical properties of the black-filled mixes. But the reinforcing potential of precipitated silica is not reflected in the properties of the mixes containing it. The low crosslink density of the silica-filled mixes, caused by the adsorption of the curatives, is responsible for their poor properties. Addition of 1 phr of PENA to the mixes causes a slight improvement in physical properties like modulus, tensile strength, tear resistance and resilience. The improvement in these properties can be correlated to the higher proportion of polysulfidic linkages as may be seen from Tables VII.4 and VII.5. The marked improvement in flex resistance resulting from the addition of antioxidant is reported in Chapter V.

Changes in network structure of gum vulcanizates after compression : The results of chemical characterization of the Conv. gum vulcanizates are given in Table VII.4. At 70°C these vulcanizates show either the same or higher V_r after testing. The change is more in the case of the compressed sample. The increase in V_r is due to the formation of new crosslinks through the unused curatives present in the samples. The change in the proportion of polysulfidic linkages is not systematic, but the

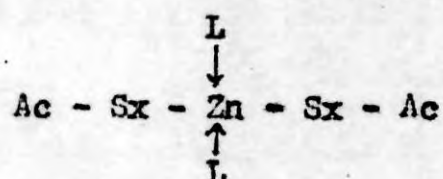
concentration of zinc sulfide increases during the testing. As ZnS formation may occur through crosslink destruction¹, it can be assumed that crosslink destruction occurs during the test. However, its effect is more than compensated by crosslink formation during testing. With the addition of PBNA, compression set increases and this can be correlated to the higher proportion of polysulfidic linkages in these samples. The lower concentration of zinc sulfide in these samples indicates that crosslink destruction reactions are minimised by the antioxidant and hence the effect of post-curing is more pronounced. Table VII.5 gives the network characteristics of the EV gum vulcanizates. As expected, set is much lower. The EV system gives rise to a more stable network and this is evident from the minimum changes in V_r , polysulfidic linkages and zinc sulfide concentration. In the EV system also the effect of PBNA is similar to that in the case of the Conv. gum mix, giving rise to a higher proportion of polysulfidic linkages and a higher set.

Table VII.5 also gives the results of chemical characterization of the gum mixes tested at 100°C. As expected, the set value is higher than that at 70°C. The V_r values are reduced remarkably, indicating the predominance of crosslink destruction during testing. This is further evident from the large increase in the concentration of zinc sulfide and the reduction in polysulfidic linkages. Here again, the changes

are less in the case of the EV mix.

Changes in network structure of filled vulcanizates after compression: In the case of the whiting-filled vulcanizates, at 70°C, the changes are similar to those in the gum mixes. The changes in V_r and in zinc sulfide concentration are slightly more in the samples under compression. In the case of the black-filled vulcanizates the changes in V_r and polysulfidic linkages are not significant. However, the increase in zinc sulfide concentration indicates crosslink destruction during the testing. It is assumed that in black-filled vulcanizates postcuring and crosslink destruction reactions occur to the same extent resulting in an almost constant V_r value. The increase in V_r and zinc sulfide concentration in silica-filled vulcanizates indicates that a larger number of new crosslinks are being formed than those undergoing destruction.

In all the filled vulcanizates, as in the case of the gum mixes, antioxidant causes an increase in the proportion of polysulfidic linkages and consequently in a higher set. The increase in polysulfidic linkages is abnormally large in the silica-filled mix. But as the set values are very high in these mixes, the effect of antioxidant on set is not notable. It is known that zinc forms a sulfurating complex¹ as shown below.



where L is a basic group, Ac is the accelerator moiety and x is the number of sulfur atoms. The effectiveness of this complex is enhanced by the addition of PBNA especially in the Conv. mixes. It is known that this complex forms initially unstable polysulfidic crosslinks which then breaks into mono- and disulfidic links. Since the conversion of polysulfides into mono- and disulfides is minimized by PBNA, the mixes containing it show a higher proportion of polysulfidic crosslinks and less crosslink destruction during the test.

TABLE VII.1
FORMULATIONS OF THE MIXES*

| MIX | A | B | C | D | E |
|---------------------|-----|-----|-----|-----|-----|
| Natural rubber | 100 | 100 | 100 | 100 | 100 |
| Zinc oxide | 5 | 5 | 5 | 5 | 5 |
| Stearic acid | 2 | 2 | 2 | 2 | 2 |
| Whiting | - | - | 50 | - | - |
| HAF black (N-330) | - | - | - | 50 | - |
| Precipitated silica | - | - | - | - | 50 |
| Naphthenic oil | - | - | - | 5 | 5 |
| Ethylene glycol | - | - | - | - | 2 |
| CBS | 0.6 | 3.5 | 0.6 | 0.6 | 0.6 |
| Sulfur | 2.5 | 0.5 | 2.5 | 2.5 | 2.5 |

* Mixes containing phenyl- β -naphthylamine (1 phr) are numbered
A₁ to E₁ against the respective base mixes.

TABLE VII.2
PHYSICAL PROPERTIES OF THE MIXES

| MIX | OPTIMUM CURE TIME, MIN. | MODULUS 300%., MPa | TENSILE STRENGTH, MPa | ELONGATION AT BREAK, % | TEAR RESIS- TANCE, kN/m |
|----------------|-------------------------------|--------------------------|-----------------------------|------------------------------|-------------------------------|
| A | 11.0 | 0.71 | 16.4 | 730 | 25 |
| B | 18.0 | 0.31 | 13.1 | 740 | 19 |
| C | 12.0 | 0.85 | 15.0 | 720 | 21 |
| D | 10.5 | 9.42 | 21.5 | 460 | 56 |
| E | 30.0 | 1.18 | 11.0 | 725 | 14 |
| A ₁ | 12.0 | 0.68 | 21.7 | 725 | 30 |
| B ₁ | 17.0 | 0.29 | 18.1 | 700 | 20 |
| C ₁ | 11.5 | 0.87 | 19.3 | 700 | 21 |
| D ₁ | 12.0 | 9.23 | 23.3 | 530 | 77 |
| E ₁ | 28.5 | 1.27 | 12.5 | 710 | 16 |

TABLE VII.2 (CONTD.)

| MIX | HARDNESS, SHORE A | RESILIENCE, % | HEAT BUILD- UP, ΔT , $^{\circ}\text{C}$ | FLEXING RESISTANCE, kg. TO FAILURE | COMPRE- SSION SET, % | ABRASION LOSS, cm ³ /1000 rev. |
|----------------|----------------------|------------------|--|---|-------------------------------|---|
| A | 40 | 78 | 8.5 | 130 | 35 | 1.95 |
| B | 35 | 72 | 8.0 | 108 | 11 | 1.37 |
| C | 45 | 74 | 15.0 | 14 | 37 | 3.18 |
| D | 62 | 51 | 25.5 | 120 | 47 | 0.67 |
| E | 64 | 31 | a | 148 | 97 | 2.74 |
| A ₁ | 40 | 85 | 6.0 | > 260 | 41 | 2.59 |
| B ₁ | 35 | 75 | 8.0 | 240 | 18 | 2.02 |
| C ₁ | 46 | 77 | 13.0 | 63 | 51 | 3.02 |
| D ₁ | 62 | 51 | 23.5 | > 230 | 72 | 0.58 |
| E ₁ | 64 | 30 | a | > 230 | 96 | 2.17 |

a The dynamic set was very high and the samples slipped from the anvils.

TABLE VII.3
EXPERIMENTAL SCATTER IN DETERMINATION V_r , POLYSULFIDIC LINKAGE
AND ZINC SULFIDE SULFUR

| CONV. SYSTEM | | V_r | | POLYSULFIDIC LINKAGE, % | | $[S^{2-}]$ mmol/kg RH | |
|----------------------------------|-----------------------|---------|--------|----------------------------|------|-----------------------|------|
| | | SURFACE | CORE | SURFACE | CORE | SURFACE | CORE |
| A (Gum mix) | Mean | 0.2039 | 0.2071 | 41 | 43 | 106 | 117 |
| | Standard deviation | 0.0014 | 0.0025 | NIL | 0.7 | 1.7 | 0.7 |
| C (Whiting- filled mix) | Mean | 0.1844 | 0.1840 | 50 | 52 | 38 | 44 |
| | Standard deviation | 0.0019 | 0.0043 | 1.2 | 0.7 | 2.3 | 2.3 |
| D (Black- filled mix) | Mean | 0.2274 | 0.2297 | 33 | 35 | 78 | 94 |
| | Standard deviation | 0.0049 | 0.0027 | 1.2 | 3.2 | 6.1 | 12.9 |

TABLE VII.4

CHEMICAL CHARACTERIZATION OF VULCANIZATES BEFORE AND AFTER
TESTING. TEMPERATURE OF TESTING 70°C, CONV. VULCANIZING SYSTEM

| MIX | SET, %. | V_r | POLYSULFIDIC LINKAGES, %. | $[s^{2-}]$ mmol/kg RH |
|--|---------|--------|------------------------------|--------------------------|
| A (gum) | a | 0.2109 | 39 | 95 |
| | b | 0.2083 | 37 | 131 |
| | c | 0.2225 | 39 | 129 |
| A ₁ (gum with PBNA) | a | 0.1996 | 55 | 27 |
| | b | 0.2212 | 43 | 48 |
| | c | 0.2228 | 44 | 73 |
| C (Whiting) | a | 0.1756 | 48 | 41 |
| | b | 0.1801 | 35 | 47 |
| | c | 0.1866 | 41 | 81 |
| C ₁ (Whiting with PBNA) | a | 0.1995 | 55 | 16 |
| | b | 0.2139 | 48 | 30 |
| | c | 0.2165 | 46 | 30 |

TABLE VII. 4 (CONTD.)

| MIX | SET, % | V_r | POLYSULFIDIC LINKAGES, % | $[s^2]$ mmol/kg RH |
|---|--------|--------|--------------------------|-----------------------|
| D (Black) | a | 0.2425 | 28 | 52 |
| | b | 0.2364 | 26 | 90 |
| | c | 0.2383 | 25 | 97 |
| D ₁ (Black with PBNA) | a | 0.2462 | 39 | 24 |
| | b | 0.2542 | 39 | 53 |
| | c | 0.2501 | 38 | 62 |
| E (Silica) | a | 0.1382 | 26 | 140 |
| | b | 0.1461 | 18 | 131 |
| | c | 0.1445 | 25 | 140 |
| E ₁ (Silica with PBNA) | a | 0.1424 | 100 | 47 |
| | b | 0.1680 | 100 | 54 |
| | c | 0.1671 | 100 | 58 |

a Original sample

b Sample kept without compression at 70°C for 22 hrs.

c Sample kept under 25% compression at 70°C for 22 hrs.

TABLE VII.5

EFFECT OF CHANGES IN VULCANIZING SYSTEM AND TEST TEMPERATURE
ON COMPRESSION SET AND NETWORK CHANGES*

| MIX | TEST TEMP., °C | SET, % | V_r | POLYSUL- FIDIC LINKAGES, % | $[s^{2-}]$ mmol/kg RH |
|---|----------------------|--------|--------|-------------------------------------|--------------------------|
| B (Gum EV) | | | | | |
| a | 70 | | 0.1715 | 3 | 15 |
| b | 70 | 11 | 0.1742 | 4 | 20 |
| c | 70 | | 0.1791 | 6 | 30 |
| B ₁ (Gum EV with PENA) | | | | | |
| a | 70 | | 0.1739 | 8 | Negligible |
| b | 70 | 18 | 0.1850 | 12 | 1 |
| c | 70 | | 0.1871 | 5 | 2 |
| A (Gum Conv.) | | | | | |
| a | 100 | | 0.2109 | 39 | 95 |
| b | 100 | 78 | 0.1624 | 11 | 148 |
| c | 100 | | 0.1849 | 8 | 137 |
| B (Gum EV) | | | | | |
| a | 100 | | 0.1715 | 3 | 15 |
| b | 100 | 39 | 0.1725 | 3 | 21 |
| c | 100 | | 0.1723 | 1 | 52 |

* Results of Conv. gum vulcanizates are given in Table VII.4

a Original sample.

b Sample kept without compression at 70°C for 22 hrs.

c Sample kept under 25% compression at 70°C for 22 hrs.

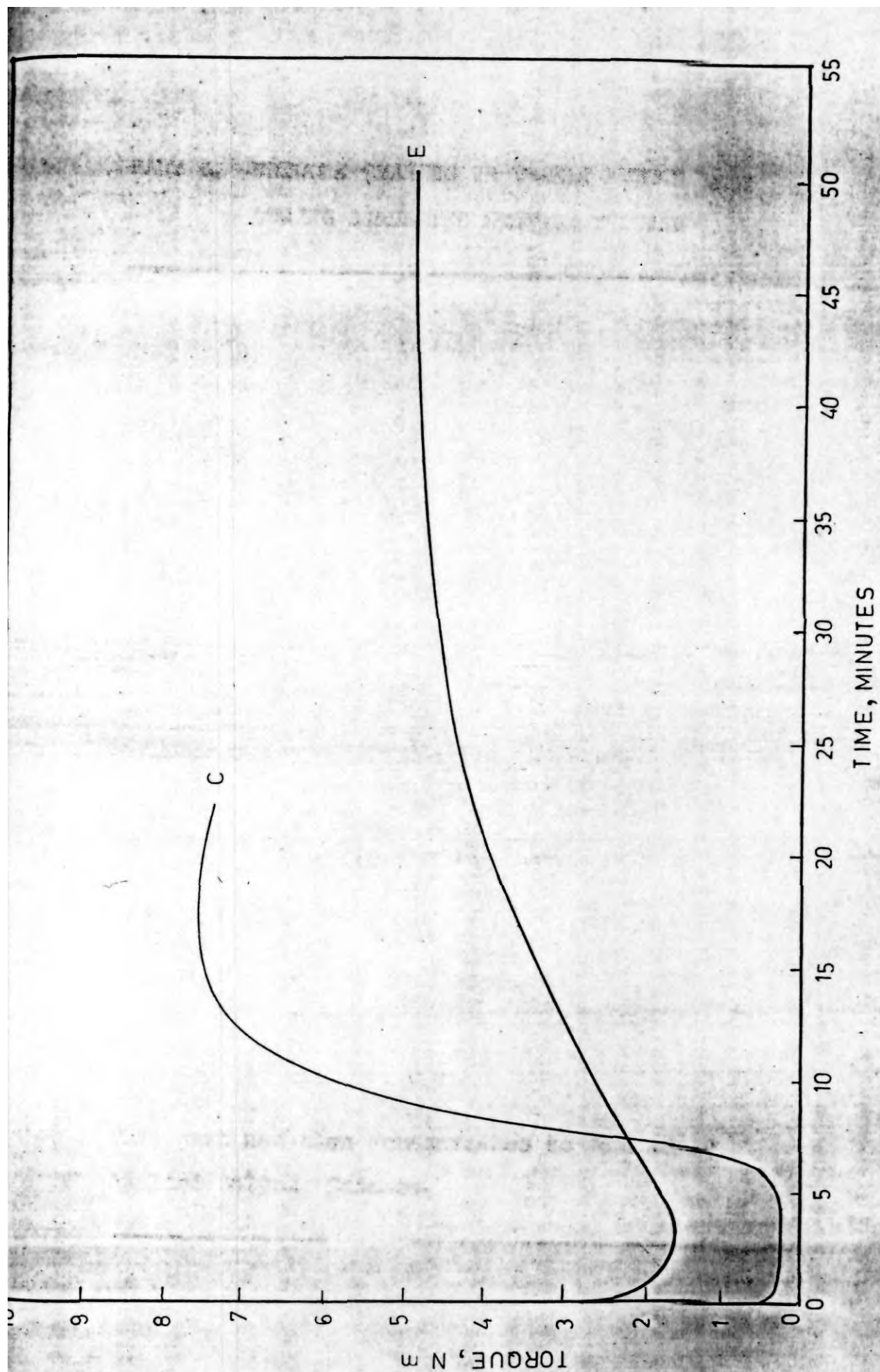


FIG. VII.1. RHEOGRAPHS OF MIXES C AND E

PART B. NETWORK CHANGES IN V-BELT RUBBER BASE DURING SIMULATED SERVICE TESTING

The popularity of rubber V-belts in the field of power transmission has been increasing in recent years and this has led to an intensive development work on belt design and the use of new materials. The all straight V-belt has been replaced by the semi-V-belt or the wide V-belt. The wide V-belt has a wider base and a shallower angle. The semi-V-belt has a wider base and a shallower angle. The wide V-belt has a wider base and a shallower angle. The semi-V-belt has a wider base and a shallower angle.

This part has been communicated to Journal of
Applied Polymer Science.

(2) *Journal of Applied Polymer Science*

(3) *Journal of Applied Polymer Science*

The popularity of rubber V-belts in the field of power transmission has been increasing in recent years and this has resulted in extensive development work on belt design and the use of new materials. Use of stronger materials like rayon, steel wire and polyester fibers as tension member demands proportionate improvements in the rubber components of transmission belts. The major technical requirements of the rubber components of V-belts are :

- (1) Good dynamic properties (high resilience, low heat buildup).
- (2) Good heat resistance.
- (3) Excellent resistance of flex cracking.

Moreover these compounds should possess other desirable characteristics like resistance to oils and ozone.

Studies on the failure mechanism of V-belts are very scanty. The different ways in which V-belts fail have been outlined by Johnson and Hornung¹⁷⁶. According to these authors breakage of jacket, separation between cord and rubber or that between cushion rubber and reinforced compression rubber, breakage of cord and cracks in rubber resulting from alternating tension and compression, are the main types of plane-base belt failure. The influence of metal oxide dispersion on neoprene V-belt fatigue failure has been studied by Vickery, Fullman and Snyder¹⁷⁷. Walter¹⁷⁸ also reviewed the different types of failure in V-belts. However more fundamental studies on the different aspects are required to understand the failure of V-belts. In the present work the chemical changes in V-belt base rubber vulcanizates during simulated service testing has been studied. The effect of antioxidant under these conditions has been included in the study.

The formulations of the base mixes are given in Table VII.6. A blend of NR and polybutadiene rubber has been chosen for these mixes. Mixing of the ingredients other than the curatives was carried out in a Shaw Intermix size K₄. The mixing cycle is shown in Table VII.7. The curatives were added in an open mill. The rheographs are given in

Figure VII.2. The optimum cure time of the compounds are given in Table VII.8. The mixes were used for the base of V-belts of size A 57. The tension member used was Resorcinol-Formaldehyde-Latex treated rayon monocord. A natural rubber based compound, suitable for bonding to rayon cord was used as the cushion rubber. The jacket used was from polychloroprene rubber based cotton fabric. Building of the belt was done on a collapsible drum and the cut sections were jacketed and then cured in a steam pot for 30 minutes at 5.5 kg steam pressure.

Rig testing : The belts were rig tested upto failure. The test conditions are given in Table VII.8. As the belt from Mix F failed after 108 hr, one belt from Mix G was run under the same conditions for a period of 108 hr to find out the changes occurring during the same period of testing in the two different base vulcanizates. Samples for chemical testing were taken from the base.

The physical properties of the base vulcanizates are given in Table VII.8. The higher compression set, heat buildup and tear resistance and the lower resilience and abrasion loss show that the vulcanizate. F is having a lower crosslink density compared to the vulcanizate G. Similar observations have been made earlier¹⁷⁹. This is confirmed by the lower V_r values of vulcanizate F (Table VII.9). It is also seen from Table VII.8 that the test life of the belt

made from Mix F, in rig testing, is only half of that of the belt made from Mix G. Although this is quite unexpected, it is believed that the antioxidants have affected the state of cure of the vulcanizate¹⁸⁰. The lower state of cure leads to higher heat buildup during rig testing, which in turn, might have contributed to bond failure between the jacket and rubber and then between cord and rubber and ultimately to failure of the belt.

The chemical characterization of the optimum cured vulcanizates and that of the base vulcanizates are given in Table VII.9. The lower values of free sulfur and higher values of combined sulfur and V_r of the base vulcanizates show that the belts are over cured compared to the test specimens cured in the laboratory.

Results of rig testing : Although the percentage change in the concentration of free sulfur and ZnS sulfur are quite considerable, the actual quantities involved are very small and hence not significant. This is also confirmed by the constant value of combined sulfur Sc . The major changes in the chemical characteristics of the vulcanizates include an increase in V_r and in sol content and a decrease in the polysulfidic linkages. The changes in V_r can be attributed to the occurrence of postcuring and crosslink destruction reactions as discussed in Part A of this chapter. Both these

reactions are activated by the heat generated during the testing. In the case of base F the postcuring reactions are more predominant and hence the percentage increase in V_T is more. In the case of base G the V_T value increases first and then decreases. This is due to the predominance of crosslink destruction over postcuring as the testing is continued. The concentration of polysulfidic linkages decreases with testing. The reduction is more in base B which contains no antioxidant. The extent of chain scission occurring during the testing period is not remarkable. Also during the rig testing because of the presence of the jacket, the base rubber has no direct access to oxygen and hence oxidative chain scission does not occur to any significant level.

TABLE VII.6

FORMULATIONS OF THE MIXES

| MIX | F | G |
|----------------------------------|------|------|
| Natural rubber | 75 | 75 |
| Polybutadiene rubber | 25 | 25 |
| Peptiser (Renacit VII) | 0.1 | 0.1 |
| Zinc oxide | 10 | 10 |
| Stearic acid | 1.2 | 1.2 |
| Phenyl- β -naphthylamine | 1.25 | - |
| Acetone-diphenylamine condensate | 1.25 | - |
| HAF black (N 330) | 75 | 75 |
| SRF black (N 770) | 25 | 25 |
| CI resin | 2.5 | 2.5 |
| Aromatic oil (Dutrex R) | 10 | 10 |
| Retarder (Santoguard PVI-50) | 0.43 | 0.43 |
| CBS | 0.68 | 0.68 |
| MBTS | 0.11 | 0.11 |
| Sulfur | 1.36 | 1.36 |

TABLE VII.7
MIXING CYCLE IN INTERNAL MIXER

| TIME, MIN. | CHARGE |
|------------|--------------|
| 0 | NR + BR |
| 1 | Chemicals |
| 2 | Carbon black |
| 3 | Oil |
| 5.5 | Dump |

TABLE VII.8

PROPERTIES OF THE VULCANIZATES^a

| PROPERTIES | F | G |
|--|------|------|
| 300% modulus, MPa | 14.2 | 15.0 |
| Tensile strength, MPa | 16.9 | 17.1 |
| Elongation at break, % | 340 | 340 |
| Tear resistance, kN/m | 77 | 71 |
| Resilience, % | 29 | 38 |
| Hardness, Shore A | 74 | 75 |
| Heat buildup, ΔT , °C | 56 | 42 |
| Compression set, % | 54 | 47 |
| Flexing resistance, kilocycles to failure | 125 | 65 |
| Abrasion loss, cc/1000 rev. | 0.23 | 0.33 |
| Performance of the belt in the rig test ^b , No. of hours to failure | 108 | 220 |

^a Cured to optimum cure at 150°C (A, 7.5 min; B, 7 min.)

^b Load, 65 kg; Speed, 1400 rpm.

TABLE VII.9

CHEMICAL CHARACTERIZATION OF THE VULCANIZATES. VALUES GIVEN IN PARENTHESES ARE THE PERCENT CHANGE AFTER RIG TESTING.

| SAMPLE DESCRIPTION | MIX | FREE SULFUR, mmol/kg RH | ZnS SULFUR, mmol/kg RH | COMBINED SULFUR, [Sc], mmol/kg RH | V _r | POLYSULFIDIC LINKAGES, % | SOL CONTENT mmol/kg RH |
|---|-----------------------|-------------------------|------------------------|-----------------------------------|----------------|--------------------------|------------------------|
| Optimum cured samples, prepared in the laboratory | F | 73 | 5 | 347 | 0.211 | 26 | 672 |
| | G | 68 | 8 | 349 | 0.227 | 29 | 566 |
| V-belt base, original | F | 15 | 27 | 383 | 0.225 | 24 | 275 |
| | G | 27 | 18 | 379 | 0.248 | 30 | 440 |
| V-belt base, after rig testing. | F | 7 | 29 | 390 | 0.277 | 17 | 347 |
| | (failed after 108 hr) | (53) | (7) | (1.8) | (23) | (29) | (26) |
| | G | 20 | 23 | 383 | 0.288 | 16 | 463 |
| | (run for 108 hr) | (26) | (27) | (1.1) | (16) | (46) | (5) |
| | G | 13 | 28 | 384 | 0.266 | 9 | 609 |
| | (failed after 220 hr) | (52) | (56) | (1.3) | (7) | (70) | (38) |

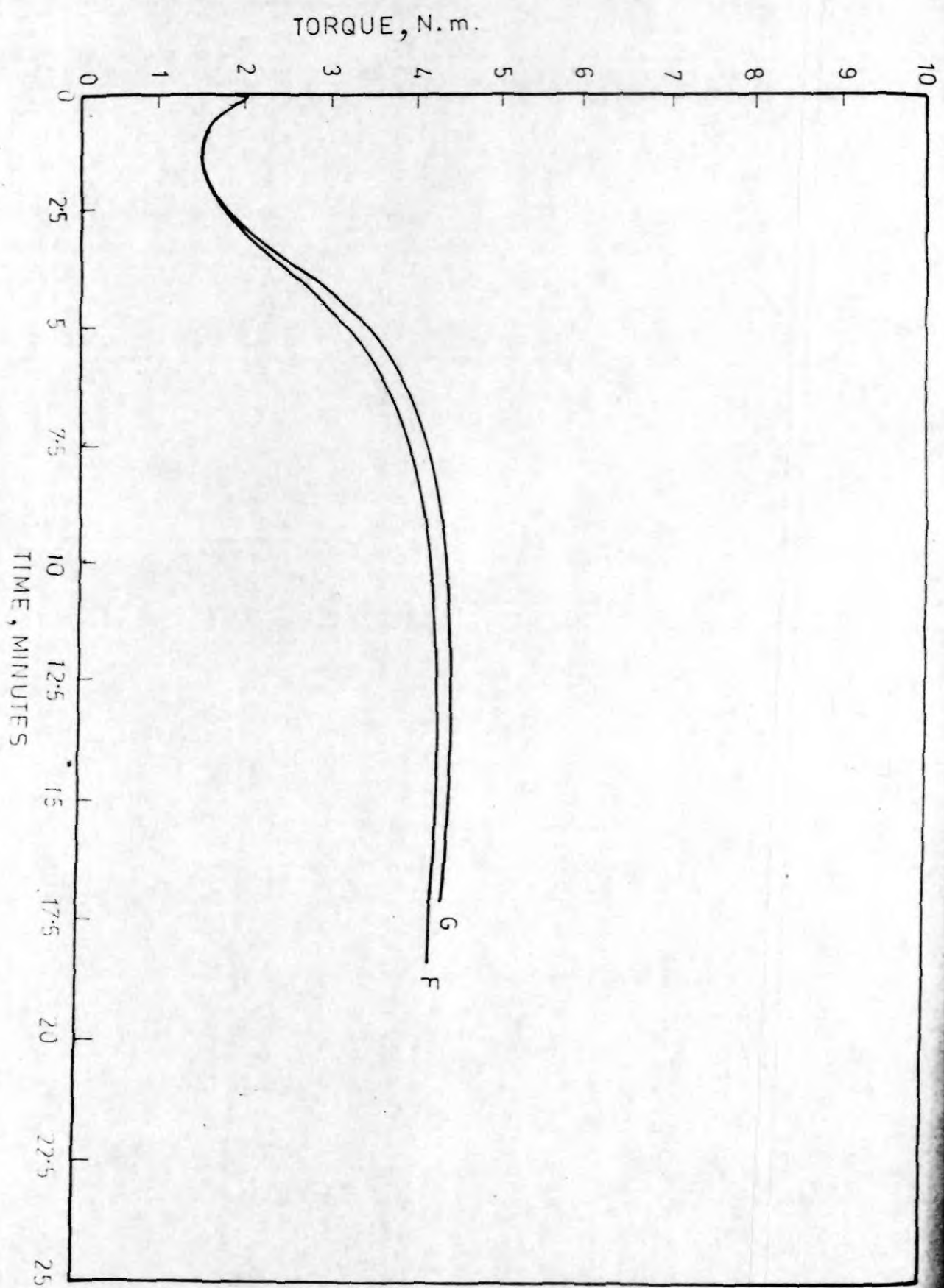


FIG VII 2 RHEOGRAPHS OF MIXES F AND G

SUMMARY AND CONCLUSIONS

The results of the study of the effect of the concentration of the solution of the polymer on the rate of the reaction of the polymer with the reagent are presented in Table I. It is seen from the data that the rate of the reaction increases with increasing concentration of the solution of the polymer. This is due to the fact that the rate of the reaction is determined by the rate of the diffusion of the reagent into the polymer solution. The rate of the diffusion increases with increasing concentration of the solution of the polymer. The results of the study of the effect of the concentration of the solution of the polymer on the rate of the reaction of the polymer with the reagent are presented in Table II. It is seen from the data that the rate of the reaction increases with increasing concentration of the solution of the polymer. This is due to the fact that the rate of the reaction is determined by the rate of the diffusion of the reagent into the polymer solution. The rate of the diffusion increases with increasing concentration of the solution of the polymer.

Failure of rubber is accompanied by changes in its chemical structure. Therefore studies on the changes in chemical structure of vulcanizates during failure are expected to give informations on the mechanism of failure. Also the failure surface, wherever available, offers a good area of research on failure mechanism. The present thesis consists of studies on the chemical changes associated with failure of rubber and scanning electron microscopic studies of failure surfaces. The different modes of failure like tensile and tear fracture, fatigue, aging, abrasion and set have been included in the study. The effect of using different rubbers and rubber blends and the effects of fillers and vulcanizing system on the failure properties have also been studied.

Part B consists of SEM studies on tensile rupture of rubber. The fracture surfaces of unfilled natural rubber show evidence of strain-induced crystallization which is absent in styrene-butadiene rubber. The fracture surface of filler-reinforced NR and SBR vulcanizates are characterized by their roughness and by the presence of short and curved tear lines. Increase of crosslink density changes the fracture mode. Peroxide-cured SBR undergoes brittle fracture, whereas the sulfur-cured one shows smooth surface with a few tear lines.

Chemical and SEM studies on thermo-oxidative aging and its effect on network structure and fracture mode of NR vulcanizates are described in part A of Chapter IV. The fall in properties during aging is caused mainly by chain scission. The increase in crosslink density during the initial periods of aging causes an increase in modulus and tensile strength. Carbon black accelerates aging, probably by surface catalysis. The simple network structure of efficiently vulcanized NR results in better retention of properties during aging. Antioxidant retards aging. The extent of degradation of vulcanizates is reflected in the nature of the fracture surfaces. The roughness of the tensile fracture surface is affected to varying degrees depending upon the aging resistance of the vulcanizates. However, in tear it is the mode of fracture propagation that is affected by aging.

Part B consists of SEM studies on tensile rupture of rubber. The fracture surfaces of unfilled natural rubber show evidence of strain-induced crystallization which is absent in styrene-butadiene rubber. The fracture surface of filler-reinforced NR and SBR vulcanizates are characterized by their roughness and by the presence of short and curved tear lines. Increase of crosslink density changes the fracture mode. Peroxide-cured SBR undergoes brittle fracture, whereas the sulfur-cured one shows smooth surface with a few tear lines.

Chemical and SEM studies on thermo-oxidative aging and its effect on network structure and fracture mode of NR vulcanizates are described in part A of Chapter IV. The fall in properties during aging is caused mainly by chain scission. The increase in crosslink density during the initial periods of aging causes an increase in modulus and tensile strength. Carbon black accelerates aging, probably by surface catalysis. The simple network structure of efficiently vulcanized NR results in better retention of properties during aging. Antioxidant retards aging. The extent of degradation of vulcanizates is reflected in the nature of the fracture surfaces. The roughness of the tensile fracture surface is affected to varying degrees depending upon the aging resistance of the vulcanizates. However, in tear it is the mode of fracture propagation that is affected by aging.

Part B of Chapter IV consists of chemical and SEM studies on ozone cracking of rubber. Ozone resistance of NR and BR/EPDM vulcanizates have been quantitatively assessed. Blending of EPDM with NR improves the ozone resistance of the latter, as indicated by higher values for the critical stress-strain parameters. Presence of carbon black improves the ozone resistance. Addition of black to the individual rubbers prior to blending improves the ozone resistance of the blend. SEM observations show that the cracking pattern in the unfilled vulcanizates is the same in both NR and the blend. However, crack deviation observed in the black-filled NR/EPDM blends, was less marked in the black-filled NR.

Chapter V consists of two parts. Part A is the chemical and SEM studies on fatigue failure of NR vulcanizates. Unfilled and filled vulcanizates with both conventional and EV systems were tested in a De Mattia flexing machine at two temperatures and the fracture surfaces were subjected to chemical analyses and SEM studies. The study shows that flexing failure is not accompanied by any major change in network structure. SEM studies show ductile failure of gum mixes. HAF black-filled mixes show brittle failure which changes to quasi-ductile with the addition of antioxidants. At 100°C flow of the matrix is more important.

In Part B of Chapter V SEM studies on flexing and tension fatigue failure of natural rubber/polybutadiene rubber blends

are described. The ranking of the vulcanizates on the basis of fatigue resistance, obtained from both types of tests is almost the same. However, the mode of fracture varies depending upon the type of strain. In the case of flexing failure, the dimple structure as observed in unfilled NR was absent in the case of the blends. Presence of carbon black filler causes brittle fracture in both NR and the blends. In the case of tension fatigue, the fracture surface of the unfilled vulcanizates shows two zones, a rough zone and a tear zone. Brittleness observed in the black-filled NR vulcanizates was less prominent in the case of the blends.

Chapter VI consists of SEM studies on the abraded surfaces of NR/BR blends under different test conditions. The ranking of the unfilled blends obtained from the Akron abrader is different from that obtained from the Du Pont and the DIN abraders, while in the case of the black-filled vulcanizates the same ranking can be obtained from all the three machines. Tensile and fatigue properties are believed to play major roles in determining abrasion loss in the Akron abrader, while the effect of friction is more pronounced in the other two machines. The slip angle and the deformation of the surface layer of rubber during abrasion account for the difference in the direction of the abrasion pattern observed in the case of the Akron abrader. The carbon black-reinforced vulcanizates give rise to a fine abrasion pattern.

Because of the continuous change in the direction of abrasion in the DIN abrader, a well defined pattern was not observed. The 50/50 NR/BR blend vulcanizates showed very high abrasion resistance in the Du Pont abrader and this is reflected in the nature of their abraded surfaces as observed in SEM.

Chapter VII is divided into two parts. Part A deals with the changes in network structure of NR vulcanizates under compression. When vulcanizates are kept under compression at elevated temperature, two types of changes occur : postcuring and crosslink destruction. At 70°C the former is predominant, while at 100°C crosslink destruction occurs to a larger extent. These changes are less in the EV mixes. The addition of antioxidant (phenyl- β -naphthylamine) increases the proportion of polysulfidic linkages in the vulcanizates and consequently increases the compression set. Antioxidant minimizes crosslink destruction reactions as well. The changes in network structure are mainly the effect of aging although in many cases compressive strain accelerates the changes occurring due to temperature.

Part B of the Chapter VII deals with studies on the changes in network structure of V-belt base vulcanizates during simulated service testing. It has been observed that the V-belt made from the base compound containing antioxidant failed more quickly than that without antioxidant, possibly due to a lower state of cure in the former. The crosslink density of the base

vulcanizate in the failed belts is higher than that of the original belt. The sol content also increases. There is a reduction in the concentration of polysulfidic crosslinks during the rig testing.

REFERENCES

1. R. J. Ceresa, S. G. Pinner, L. Walling and J. H. Duerksen, "The Chemistry of Vinyl Monomers and Polymers", Int. Rev. Phys. Chem., 1963, p. 15.
2. R. J. Ceresa and A. A. Watson, Rubber Chem. Technol., 46, 164 (1973).
3. R. J. Ceresa and R. E. Tidd, Progress in Rubber Technol., 1972-74, Rubber Publ. Ind., London, p. 78, 81.
4. R. J. Ceresa and A. G. Thomas, J. Polym. Sci., 12(3), 291 (1953).
5. R. J. Ceresa, J. Polym. Sci., 21, 137 (1955).

1. L. Bateman, J.I. Cunneen, C.G. Moore, L. Mullins and A.G. Thomas, 'The Chemistry and Physics of Rubber-like Substances', L. Bateman Ed., MacLaren and Sons Ltd., London, 1963, p. 715.
2. B. Saville and A.A. Watson, Rubber Chem. Technol., 40, 100 (1967).
3. D.J. Elliot and B.K. Tidd, Progress in Rubber Technology 1973-74 Inst. Rubb. Ind., London, p. 37, 83.
4. R.S. Rivlin and A.G. Thomas, J. Polym. Sci., 10(3), 291 (1953).
5. H.W. Greensmith, J. Polym. Sci., 21, 175 (1955).

6. A.G. Thomas, J. Polym. Sci., 28, 177 (1955).
7. A.G. Thomas, J. Appl. Polymer Sci., 3, 168 (1960).
8. A.G. Veith, Rubber Chem. Technol., 38, 700 (1965).
9. A. Ahagon and A.N. Gent, J. Polym. Sci., Polymer Physics edition, 13, 1903 (1975).
10. J. Glucklich and R.F. Landel, J. Appl. Polymer Sci., 20, 121 (1976).
11. M.L. William, R.E. Landel and F.D. Ferry, J. Amer. Chem. Soc., 77, 3701 (1955).
12. L. Mullins, Trans. Inst. Rubb. Ind., 35(4), 213 (1959).
13. H.W. Greensmith, L. Mullins and A.G. Thomas, Trans. Soc. Rheology, 4, 179 (1960).
14. L. Mullins, Rubber Chem. Technol., 33, 315 (1960).
15. E.H. Andrews, J. Appl. Physics, 32(3), 542 (1961).
16. A.M. Borders and R.D. Juve, Ind. Eng. Chem., 39, 1066 (1947).
17. T.L. Smith, J. Polym. Sci., 32, 99 (1958).
18. H.W. Greensmith, J. Appl. Polymer Sci., 3, 175 (1960).
19. A.G. Thomas and J.M. Whittle, Rubber Chem. Technol., 43, 222 (1970).
20. C.L.M. Ball, D. Stinson and A.G. Thomas, Rubber Chem. Technol., 55, 66 (1982).

21. A.S. Kuzminskii, Rubber Chem. Technol., 39, 88 (1966).
22. J.I. Cunneen, Rubber Chem. Technol., 41, 182 (1968).
23. J.R. Dunn, Rubber Chem. Technol., 51, 686 (1978).
24. T. Colclough, J.I. Cunneen and G.M.C. Higgins, J. Appl. Polymer Sci., 12, 295 (1968).
25. A.G. Veith, J. Polym. Sci., 25, 355 (1957).
26. A.V. Tobolsky, J. Appl. Polymer Sci., 27, 673 (1956).
27. M.M. Horikx, J. Polym. Sci., 19, 445 (1956).
28. J.R. Dunn and J. Scanlan, Trans. Faraday Soc., 57, 160 (1961).
29. E.J. Blackman and E.B. McCall, Rubber Chem. Technol., 43, 651 (1970).
30. E.M. Bevilacqua and W.J. Wenisch, J. Appl. Polymer Sci., 9, 267 (1965).
31. J.R. Dunn and J. Scanlan, J. Appl. Polymer Sci., 41, 84 (1959).
32. C.L.M. Ball and R. Tiller, J. Appl. Polymer Sci., 9, 3091 (1965).
33. G. Scott, Chem. Ind., 7, 271 (1963).
34. J.R. Shelton, Rubber Chem. Technol., 45, 359 (1972).
35. T. Colclough and J.I. Cunneen, J. Chem. Soc., 4790 (1964).

36. C.L.M. Bell and J.I. Cunneen, J. Appl. Polymer Sci., 11, 2201 (1967).
37. H. Winn, J.R. Shelton and D. Turnbull, Ind. Eng. Chem., 38, 1052 (1946).
38. A.S. Kuzminskii, L.I. Lyubshchanskaya, L.I. Khitrana and S.I. Bass, Rubber Chem. Technol., 26, 858 (1953).
39. W.L. Hawkins and M.A. Warthington, J. Polym. Sci., 62, S 106 (1962).
40. G.J. van Amerongen, Rubber Chem. Technol., 28, 821 (1955).
41. J.R. Shelton and W.T. Wickham Jr., Ind. Eng. Chem., 49, 1277 (1957).
42. J.C. Ambelang, R.H. Klim, O.M. Lorenz, C.R. Parks, C. Wadelin and J.R. Shelton, Rubber Chem. Technol., 36, 1497 (1963).
43. G.M. Bristow and G.J. Lake and P.M. Lewis, Paper presented at a Conference on Weathering of Plastics and Rubber, Plastics and Rubber Institute, London, 1977.
44. G.J. Lake and A.G. Thomas, Kautsch. Gummi Kunstst., 20, 211 (1967).
45. L.L. Best and R.C.W. Moakes, Trans. Inst. Rubb. Ind., 27, 103 (1951).

46. M. Braden and A.N. Gent, J. Appl. Polymer Sci., 3, 90, 100 (1960).
47. A.N. Gent and J.E. McGrath, J. Polym. Sci., A3, 1473 (1965).
48. A.N. Gent and H. Hirakawa, J. Polym. Sci., A.2.5, 157 (1967).
49. J.C. McCool, Rubber Chem. Technol., 37, 583 (1964).
50. E. Cutts and M.A. Wheelans, NR Technology, 5, 58 (1974).
51. G.J. Lake, Rubber Chem. Technol., 43, 1230 (1970).
52. O. Lorenz and C.R. Parks, Rubber Chem. Technol., 34, 816 (1961).
53. D.C. Lloyd and J. Payne, Rubber News, 6(4), 26 (1967).
54. E.H. Andrews, J. Appl. Polym. Sci., 10, 47 (1966).
55. E.S. Dizon, A.E. Hicks and V.E. Chirico, Rubber Chem. Technol., 47, 231 (1974).
56. A.N. Gent, P.B. Lindley and A.G. Thomas, J. Appl. Polymer Sci., 8, 445 (1964).
57. A.G. Thomas, J. Polym. Sci., 31, 467 (1958).
58. G.J. Lake and P.B. Lindley, Rubb. J., 146(10), 24 (1964).
59. G.J. Lake and P.B. Lindley, J. Appl. Polymer Sci., 2, 1233 (1965).

60. H.W. Greensmith, J. Appl. Polymer Sci., 7, 923 (1963).
61. G.J. Lake and A.G. Thomas, Proc. Roy. Soc. A, 300, 103 (1967).
62. A. Schallamach, Trans. Inst. Rubb. Ind., 28, 75 (1952).
63. A. Schallamach, Proc. Phys. Soc. B, 67, 883 (1954).
64. A. Schallamach, Wear, 17, 301 (1971).
65. A. Schallamach, Rubber Chem. Technol., 41, 209 (1968).
66. M.M. Reznikovskii and G.I. Brodskii in 'Abrasion of Rubber', D.I. James Ed., MacLaren and Sons Ltd, London, 1967, p. 14.
67. G.I. Brodskii and M.M. Reznikovskii, Ibid., p. 1.
68. M.M. Reznikovskii, Ibid., p. 119.
69. G.I. Brodskii, N.L. Sakhnovskii, M.M. Reznikovskii and V.F. Evstratov, Soviet Rubber Technology, 12, 22 (1960).
70. A.P. Rudakov and Ye. V. Kumshinskii, Polymer Science (USSR), 4, 1081 (1963).
71. K.A. Grosch and L. Mullins, Rev. Gen. Caoutch., 39(11), 1781 (1962).
72. F.A. Greenwood and D. Tabor, Proc. Phys. Soc., 71, 989 (1958).

73. E. Southern and A.G. Thomas, Rubber Chem. Technol., 52, 1008 (1979).
74. K.T. Satake, T. Sone, M. Hamada and K. Hayakawa, Rubber Chem. Technol., 44, 1173 (1971).
75. H.J. Jahn and H.H. Bertman, Rubber Chem. Technol., 46, 305 (1973).
76. F.P. Baldwin, Rubber Chem. Technol., 43, 1040 (1970).
77. G.M. Bristow, J.I. Cunnane and L. Mullins, International Symposium on Isoprene Rubber, Moscow, November 20-24, 1972.
78. Gino Dall'Asta, Rubber Chem. Technol., 47, 511 (1974).
79. J.G. Curro and E.A. Salazar, J. Appl. Polymer Sci., 19, 2571 (1975).
80. B. Stenberg and J.F. Janson, Rubber Chem. Technol., 50, 906 (1977).
81. B. Stenberg and J.F. Janson, Rubber Chem. Technol., 50, 915 (1977).
82. Marton L. Studebaker, Rubber Chem. Technol., 39, 1359 (1966).
83. A.K. Bhowmick and S.K. De, Rubber Chem. Technol., 52, 985 (1979).
84. A.K. Bhowmick and S.K. De, Rubber Chem. Technol., 53, 960 (1980).

85. R. Mukhopadhyay, S.K. De and S.N. Chakraborty, *Polymer*, 18, 1243 (1977).
86. R. Mukhopadhyay, S.K. De, *Rubber Chem. Technol.*, 51, 704 (1978).
87. R. Mukhopadhyay A.K. Ghoshick and S.K. De, *Polymer*, 19, 1176 (1978).
88. G.B. Nando and S.K. De, *Polymer*, 21, 10 (1980).
89. G.B. Nando and S.K. De, *J. Polym. Sci.*, (Polymer Letters edition, 19, 5 (1981).
90. R. Bakshandeh, A.J. Gregory, A.J. Rigby and J.E. Stuckey, Paper presented at the International Conference on Structure-Property Relations of Rubber, Kharagpur, India, December, 29-31, 1980.
91. J.I. Cunneen and R.M. Russel, *J. Rubber Res. Inst. Malaya*, 22, 300 (1969); *Rubber Chem. Technol.*, 43, 1215 (1970).
92. W.S. Howard and G.R. Wilder, Paper presented at a meeting of the Division of Rubber Chemistry, American Chemical Society, Philadelphia, October 15-18, 1974.
93. M.M. Podkolzina, S.B. Petrova and T.V. Fedorova, *Kauchuk i Rezina*, 2, 16 (1978).
94. Wiesbadan, A. Wolk, *Kautsch. Gummi Kunstst.*, 33(11), 930 (1980).

95. Julius Kruse, Rubber Chem. Technol., 46, 653 (1973).
96. W.H. Smith and C.P. Saylov, Rubber Chem. Technol., 12, 18 (1939).
97. H.N. Campbell and M.D. Allen, Rubber Chem. Technol., 24, 550 (1951).
98. E.H. Merz, G.C. Claver and M. Baer, J. Polym. Sci., 22, 325 (1956).
99. D.H. Kay, Techniques for Electron Microscopy, 2nd edition, Blackwell Scientific Publications, London, 1965.
100. D.C. Pease, Histological Techniques for Electron Microscopy, Academic Press, New York, 1964.
101. J.E. Callan, B. Topcik and F.P. Ford, Rubber World, 151, 60 (1965).
102. P.A. Marsh, A. Voet and L.D. Price, Rubber Chem. Technol., 40, 359 (1967).
103. W.M. Hess, C.E. Scott and J.E. Callan, Rubber Chem. Technol., 40, 371 (1967).
104. P.A. Marsh, A. Voet, L.D. Price and T.J. Mullens, Rubber Chem. Technol., 41, 344 (1968).
105. F. Endter, Kautsch. Gummi Kunstst., 5, 17 (1952).
106. R.W. Smith, Rubber Chem. Technol., 40, 350 (1967).

107. E.H. Andrews and A. Walsh, J. Polymer Sci., 33, 39 (1958).
108. F.M. Hess and F.P. Ford, Rubber Chem. Technol., 36, 1175 (1963).
109. Truman L. Ward and Ruth R. Benerito, J. Appl. Polymer Sci., 21, 1933 (1977).
110. A. Munoz-Escalona and A. Parada, Polymer, 20, 474 (1979).
111. B.K. Garg, R.A.V. Raff and R.V. Subramanian, J. Appl. Polymer Sci., 22, 65 (1978).
112. Ronald J. Dennenberg, Rodney J. Bothast and Thomas P. Abbot, J. Appl. Polymer Sci., 22, 459 (1978).
113. Eng-Pi Chang and Eugene L. Slagowski, J. Appl. Polymer Sci., 22, 769 (1978).
114. Herman B. Wagner and Dallas G. Grenley, J. Appl. Polymer Sci., 22, 813 (1978).
115. S. Gogolewski and A.J. Pennings, Polymer, 18, 647 (1977).
116. J.E. Stamhuis and A.J. Pennings, Polymer, 18, 667 (1977).
117. J.R. White and J.W. Teh, Polymer, 20, 764 (1979).

118. Keith Smith and Robert N. Howard, *Polymer*, 20, 921 (1979).
119. Raymond R. Parent and Edward V. Thompson, *J. Polym. Sci., Polymer Phys. edition*, 16, 1829 (1978).
120. G.E. Sweet and J.P. Bell, *J. Polym. Sci., Polymer Phys. edition*, 16, 2057 (1978).
121. H.D. Wagner, F.R. Tuler and G. Marom, *Polymer*, 20, 653 (1979).
122. J. Krager-Kocsis, A. Kalló, A. Szafrer, G. Bodor and Zs. Sanyai, *Polymer*, 20, 37 (1979).
123. Roger R. Morgan and James E. O'Neal, *Polymer*, 20, 375 (1979).
124. C.J. Singleton, E. Roche and P.H. Geil, *J. Appl. Polymer Sci.*, 21, 2319 (1977).
125. E.M. Smoloy, *J. Appl. Polymer Sci.*, 20, 217 (1976).
126. R.C. Thamm, *Rubber Chem. Technol.*, 50, 24 (1977).
127. D.N. Schulz, L.E. Calihan and D.P. Tate, *Rubber Chem. Technol.*, 49, 126 (1976).
128. J.C. Andries, C.K. Rhee, R.W. Smith, D.B. Rose and H.E. Diem, *Rubber Chem. Technol.*, 52, 823 (1979).
129. H.E. Haxo Jr., and P.K. Mehta, *Rubber Chem. Technol.*, 48, 271 (1975).
130. A. Voet, J.C. Morawski and J.B. Donnet, *Rubber Chem. Technol.*, 50, 342 (1977).

131. J.E. O'Conner, Rubber Chem. Technol., 50, 945 (1977).
132. V.M. Murty, A.K. Bhowmick and S.K. De, J. Mater. Sci., 17, 709 (1982).
133. V.M. Murty and S.K. De, Rubber Chem. Technol., 55, 287 (1982).
134. S.K. Chakraborty, D.K. Setua and S.K. De, Rubber Chem. Technol., 55, 1370 (1982).
135. D.K. Setua and S.K. De, Rubber Chem. Technol., (in press).
136. V.M. Murty and S.K. De, J. Appl. Polymer Sci., 27, 4611 (1982).
137. W.D. Bascom, Rubber Chem. Technol., 50, 327, 875 (1977).
138. B.B. Boonstra, F.A. Heckman and A. Kabaya, Paper presented at the 99th meeting of the Rubber Division, American Chemical Society, Miami Beach, Florida, April 27-30, 1971.
139. Anil K. Bhowmick, Sanjay Basu and Sadhan K. De, J. Mater. Sci., 16, 1654 (1981).
140. A. Subramanyam, Proc. of the R.R.L.M. Planters' Conference, 1971, Kuala Lumpur, p. 255.
141. A. Subramanyam, Rubber Chem. Technol., 45, 346 (1972).

142. H.E. Adam and B.L. Johnson, Rubber Chem. Technol., 26, 741 (1953).
143. B. Ellis and G.N. Welding, Techniques of Polymer Science Soc. Chem. Ind., London, p. 46 (1964); Rubber Chem. Technol., 37, 571 (1964).
144. L. Mullins, J. Appl. Polymer Sci., 2, 1 (1959).
145. P.J. Flory and J. Rehner Jr., J. Chem. Phys., 11, 521 (1943).
146. H. Kraus, Rubber Chem. Technol., 30, 928 (1957).
147. G.M. Bristow and B.J. Wistall, J. Appl. Polymer Sci., 9, 495 (1965).
148. M. Porter, Rubber Chem. Technol., 40, 866 (1967).
149. D.S. Campbell, J. Appl. Polymer Sci., 13, 1201 (1969).
150. D.S. Campbell and B. Saville, Proc. Int. Rubber Conference, Brighton, p. 1 (1967).
151. M.B. Evans and B. Saville, Proc. Chem. Soc., 18 (1962).
152. G.M. Bristow, J. Appl. Polymer Sci., 7, 1023 (1963).
153. O. Johari and A.V. Samudra, in 'Characterization of Solid Surfaces', P.F. Kane and G.B. Larrabee Ed., Plenum Press, New York, 1974, Chapter 5.
154. J.R.M. Radok and C.L. Tai, J. Appl. Polymer Sci., 6, 518 (1962).

155. G. Kraus, in 'Science and Technology of Rubber',
F.R. Eirich Ed., Academic Press, New York, 1978, Ch.8.
156. R. Mukhopadhyay and S.K. De, Rubber Chem. Technol.,
52, 263 (1979).
157. S.K. Chakraborty, A.K. Bhowmick, S.K. De and B.K.
Dhindaw, Rubber Chem. Technol., 55, 41 (1982).
158. A. Kadir and A.G. Thomas, Rubber Chem. Technol.,
54, 15 (1981).
159. P.K. Pal, A.K. Bhowmick and S.K. De, Rubber Chem.
Technol., 55, 23 (1982).
160. A.N. Gent, in 'Science and Technology of Rubber'
F.R. Eirich Ed., Academic Press, New York, 1978, Ch. 1
161. G.M. Bartenev and Yu. S. Zuyev, in 'Strength and Failure
of Viscoelastic Materials', Pergamon Press, London,
1968, p. 96.
162. A.K. Bhowmick, S. Basu and S.K. De, Rubber Chem.
Technol., 53, 321 (1980).
163. A.K. Bhowmick, G.B. Nando, S. Basu and S.K. De,
Rubber Chem. Technol., 53, 327 (1980).
164. D.K. Setua, S.K. Chakraborty, B.K. Dhindaw and
S.K. De, J. Scanning Electron Microscopy, 3, 973 (1982)
165. L.J. Maisey and J. Scanlan, J. Appl. Polymer Sci.,
7, 1147 (1963).

166. A.N. Gent and P.B. Lindley, Proc. Roy Soc., London, A, 249, 195 (1959).
167. J.R. Beatty, Paper presented at the 110th meeting of the Rubber Division, American Chemical Society, San Francisco, Oct. 5-8, 1976.
168. W.L. Cox and C.R. Parks, Rubber Chem. Technol., 39, 785 (1977).
169. M.G. Bader and M. Johnson, Composites, 5, 58 (1974).
170. R. Prakash, Composites, 10, 174 (1979).
171. W.M. Saltman, in 'Encyclopedia of Polymer Science and Technology', H.F. Mark, N.G. Gaylord and N.M. Bikales Ed., Interscience Publishers, New York, 1965, Vol. 2, p. 678.
172. A. Schallamach, J. Appl. Polymer Sci., 12, 281 (1968).
173. K.A. Grosch and A. Schallamach, Rubber Chem. Technol., 49, 862 (1976).
174. Z.W. Wilchinsky and E.N. Kresge, Rubber Chem. Technol., 47, 895 (1974).
175. P.J. Corish, in 'Science and Technology of Rubber', F.R. Eirich Ed., Academic Press, New York, 1978, Ch. 12.
176. C.O. Johnson and K.G. Hornung, Paper presented at the 92nd Meeting of the Rubber Division, American Chemical Society, Chicago, September 13-15, 1967.

177. G. Vickery, P.V. Fullam and J.E. Snyder, Paper presented at the 111th Meeting of Rubber Division, American Chemical Society, May 6-7, 1977.
178. G. Walter, Rubber Chem. Technol., 49, 775 (1976).
179. W. Hofmann, Vulcanization and Vulcanizing agents' MacLaren and Sons Ltd., London, 1967, Chapter 1.
180. G.B. Nando and S.K. De, Kautsch. Gummi. Kunstst., 33(11), 920 (1980).

LIST OF PUBLICATIONS

The following research papers have been published from the present work.

1. Scanning electron microscopy studies on tear fracture of natural rubber, *Polymer*, 23, 632 (1982)
2. Scanning electron microscopy studies on tensile rupture of rubber, *J. Mater. Sci.*, 17, 2594 (1982)
3. Thermo-oxidative aging and its effect on network structure and fracture mode of natural rubber vulcanizates, *Polymer* (In press)
4. Chemical and scanning electron microscopic studies on fatigue failure of NR vulcanizates, *Rubber Chem. Technol* 55, 51 (1982)
5. Scanning electron microscopy studies on flexing and tension fatigue failure of rubber, *International Journal of Fatigue*, January (1983).
6. Scanning electron microscopy studies on abrasion of NR/BR blends under different test conditions, *J. Mater. Sci.*, 17 (1982)
7. Network changes in NR vulcanizates under compression, *J. Appl. Polymer Sci.*, 27, 1827 (1982)

RUBBER RESEARCH INSTITUTE OF INDIA

LIBRARY

Acc. No. : T/19

Date : 28/6/2000

Initial